INSPECTION & MODELLING OF CUSP GEOMETRY IN ADDITIVE MANUFACTURING TO PREDICT PRODUCT'S SURFACE ROUGHNESS

By

Farzaneh Kaji

Thesis submitted in partial fulfilment of the requirement for the degree of

Master of Applied science

In

Mechanical Engineering

Faculty of Engineering and Applied Science

University of Ontario Institute of Technology

APRIL 2015

Abstract

The final dimensional and geometric inaccuracies, and the resulting high surface roughness of the products have been the major problems in employing Additive Manufacturing (AM) technologies. Most of commonly used Additive manufacturing (AM) technologies are developed based on a layer-based manufacturing process to fabricate 3D models. However, a critical drawback that reduces the surface quality of the AM parts is the stair case effect as a direct result of the layered deposition of the material. In this thesis, a new approach to model surface roughness in Fused Deposition Modeling (FDM) is proposed. Based on actual observations and modeling of the cusp geometry under various setups and fabrication conditions, an empirical model to express the surface roughness distribution is presented. The developed methodology presents mathematical expressions for the profile of cusps classified based on two parameters of additive manufacturing layer thickness and the slope of the fabricated surface. Considering the fact that the cusp profile crucially affects the surface quality, the developed model is used directly to estimate surface roughness of the final product. The proposed expression is verified by implementation and comparison with the experimental case studies. The developed models can be used for optimum selection of the build direction or layer thickness when a certain surface roughness range is targeted. It can also be used as a tool for modification of the design to control the final surface roughness of the AM products.

Acknowledgment

I would like to express my gratitude to my supervisor Dr. Ahmad Barari. From the first day as his student, he was always supportive ,understanding and motivating me to do better .

Contents

Abstract i

Acknowledgment ii

List of Tables xii

List of Figures……vii

Notations xiii

Abbreviations xv

1 Chapter 1: Introduction 1

2 Chapter 2: Literature Review 4

2.1 Introduction 4

2.2 Classification of Additive Manufacturing Processes 4

2.2.1 Fused Deposition Modeling (FDM) 4

2.2.2 Streolithography Apparatus (SLA) 5

2.2.3 3 Dimensional Printing (3DP) 6

2.2.4 Pro-Metal 6

2.2.5 Selective Laser Sintering (SLS) 7

2.2.6 Laminated Object Manufacturing 7

2.3 Relationship between the Process Parameters and Surface Roughness 7

2.4 Modeling of Surface Roughness Based on Geometry of the Cusp 10

3 Chapter 3 Methodology 18

3.1 Introduction 18

3.2 Measurement of cusp profile 18

3.2.1 3D Profile Measurement 18
3.2.2 2D Profile Measurement 20
3.3 Cusp Modelling 25
3.3.1 Representing the cusp geometry with a cubic B-spline 26
3.4 B-spline Curve Modeling Using Total Least Square Fitting 40
3.4.1 Total Least Square Method 42
3.5 B-spline Curve Modeling Using Genetic Algorithm 47
3.6 Three Piece Curve Fitting Including a third Degree Polynomial Curve and Genetic Algorithm 48
3.7 Three Piece Curve Fitting Including second degree Polynomial Curve and Genetic Algorithm 49
3.8 Fitting Data Points Using Two Line Pieces and a Second Degree polynomial 52
3.9 Surface Roughness Measurement 54
3.10 Undetermined Region 56
3.11 Width Calculation 60
3.11.1 Width Correction 62
4 Implementation 70
4.1 Introduction 70
4.2 Design of The Specimen 70
5 Chapter 5: Results and discussion 75
5.1 Introduction 75
5.2 B-spline curve modeling using total least square fitting 75

5.2.1 Case study for B-spline curve modeling using total least square fitting 75

5.3 B-spline curve modeling using genetic algorithm 77

5.3.1 Case study for B-spline curve modeling using genetic algorithm.....78

5.4 Three Piece Curve Fitting Including a Third Degree Polynomial Curve and Genetic Algorithm.....79

5.4.1 Case Study For Three Piece Curve Fitting Including a Third Degree Polynomial Curve and Genetic Algorithm 80

5.5 Three Piece Curve Fitting Including Second degree Polynomial Curve and Genetic Algorithm.....82

5.5.1 Case Study For Three Piece Curve Fitting Including second degree Polynomial Curve and Genetic Algorithm 83

5.6 Surface Roughness Prediction 85

5.7 Width Calculation Results 91

5.8 Comparsion of Four Fitting Methods 91

5.9 Discussion 100

5.9.1 Effect of Layer Thickness on Surface Roughness 100

5.9.2 Effect of Surface Angle on Surface Roughness 101

5.9.3 Surface Roughness of Surface Angles Less Than Critical Surface Angle 101

6 Conclusion and Recommendations.....102

6.1 Conclusion 102

6.2 Using B-spline and NURBS to Represent The Cusp Geometry 103

6.3 Recommendation 104

7 References 104

List of Figures

Figure 1-1: Jeopardizing accuracy by approximating the cusp geometry by rectangle shapes. 2
Figure 2-1: FDM process schematics 5
Figure 2-2: Schematic of SLA process [1] 6
Figure 2-3: The geometry of the cusp for surface roughness model. 10
Figure 2-4: Edge profile of the layer....12
Figure 2-5: Elliptical profile of the layers 14
Figure 2-6:The rounded profile shape for FDM prototypes[32]. 15
Figure 3-1: 3D profile roughness measurement 19
Figure 3-2: Profile roughness measurement using 3D picture 20
Figure 3-3: Cusps side view of a specific slope (65 degrees)....21
Figure 3-4: An example of the black and white regions....22
Figure 3-5: The border of the white and black regions shows the actual profile of the cusps. 23
Figure 3-6: Width of the 1mm gauge....25
Figure 3-7: Linear and curve segments of the cusp profile 26
Figure 3-8: The position of control points on the B-spline 36
Figure 3-9: Dependency of first derivative of the curve on the location of $P4$....36
Figure 3-10: Position of control points on the curve and dependency of first derivative continuity on position of $P4$ 37
Figure 3-11: Dynamic change of location of $P4$ based on incremental change in y coordinate of $P1$....38
Figure 3-12: Dynamic change of location of $P4$ based on incremental change in x coordinate of $P1$....38

Figure 3-13: Dynamic change of location of $P4$ based on incremental change in y coordinate of $P5$ 39
Figure 3-14: Dynamic change of location of $P4$ based on incremental change in x coordinate of $P5$ 40
Figure 3-15: Euclidian distance of actual points from the B-spline 41
Figure 3-16: Total Least squares versus Least Squares 43
Figure 3-17: Minimizing the distance between $P4$ and $P4'$ 47
Figure 3-18: Initial four points for starting the genetic algorithm 49
Figure 3-19: An example of fitted curve using third degree polynomial and 2 line pieces 52
Figure 3-20: Schematic of surface roughness measurement 54
Figure 3-21: Total least squares centre line and the profile roughness measurement 56
Figure 3-22: Undetermined region for surface angle of 5° and layer thickness of 250 microns 57
Figure 3-23: Undetermined region disappears for upper surface angles (25°), layer thickness of 250 microns 58
Figure 3-24: Non-undetermined region and undetermined region 58
Figure 3-25: The horizontal distance of cusps 59
Figure 3-26: Mechanism of filament extrusion in FDM process 61
Figure 3-27: Cross section of extruded material 62
Figure 3-28: Width correction in FDM process 63
Figure 3-29: Positive ε and extended profile 65
Figure 3-30: Negative ε and profile shortening 66
Figure 3-31: Actual cross section of extruded material 66

Figure 3-32: Example of $S1$ and $S2$for surface angle of 25° and layer thickness of 250 microns.....68
Figure 3-33: Example of $S1$ and $S2$ for surface angle of 90° and layer thickness of 250 microns.....69
Figure 4-1: The designed specimen including all surface angles from 0° to 90°....70
Figure 4-2: Roughness measurement setup 74
Figure 5-1: An example of fitted curve using NURBS and TLS for the surface angle of 25° and layer thickness of 250 microns.....76
Figure 5-2: An example of fitted curve using NURBS and TLS for the surface angle of 90° and layer thickness of 250 microns.....77
Figure 5-3: An example of fitted curve using NURBS and GA for the surface angle of 25° and layer thickness of 250 microns.....78
Figure 5-4: An example of fitted curve using NURBS and GA for the surface angle of 90° and layer thickness of 250 microns.....79
Figure 5-5: An example of fitted curve using 3-piece third degree polynomial and GA for the surface angle of 25° and layer thickness of 250 microns.....80
Figure 5-6: An example of fitted curve using 3-piece third degree polynomial and GA for the surface angle of 90° and layer thickness of 250 microns.....82
Figure 5-7: An example of fitted curve using 3-piece second degree polynomial and GA for the surface angle of 25° and layer thickness of 250 microns 83
Figure 5-8: An example of fitted curve using 3-piece second degreepolynomial and GA for the surface angle of 90° and layer thickness of 250 microns.....85
Figure 5-9: Distribution of the predicted and actual surface roughness and by variation of the surface angle – 125 micron Layer thickness 86
Figure 5-10: General shape of the cusp for surface angle from 5° to 90° and layer thickness of 125 microns 87

Figure 5-11: Distribution of the predicted and actual surface roughness by variation of the surface angle – 250 micron Layer thickness 87
Figure 5-12: General shape of the cusp for surface angle from 5° to 90° and layer thickness of 250 microns 88
Figure 5-13: Distribution of the predicted and actual surface roughness by variation of the surface angle – 500 micron Layer thickness 89
Figure 5-14: General shape of the cusp for surface angle from 5° to 90° and layer thickness of 500 microns 90
Figure 5-15: Distribution of the predicted surface roughness by variation of the surface angle 90
Figure 5-16: Distribution of fitting error using TLS method for layer thickness of 250 microns.....92
Figure 5-17: Distribution of fitting error using TLS and genetic algorithm method for layer thickness of 250 microns.....92
Figure 5-18: Distribution of fitting error using third degree polynomial and genetic algorithm method for layer thickness of 250 microns 93
Figure 5-19: Distribution of fitting error using second degree polynomial and genetic algorithm method for layer thickness of 250 microns 93
Figure 5-20: Comparison of fitting error using all developed fitting models 94
Figure 5-21: Distribution of fitting error using TLS method for layer thickness of 125 microns.....95
Figure 5-22: Distribution of fitting error using TLS and genetic algorithm method for layer thickness of 125 microns.....96
Figure 5-23: Distribution of fitting error using third degree polynomial and genetic algorithm method for layer thickness of 125 microns 96
Figure 5-24: Distribution of fitting error using second degree polynomial and genetic algorithm method for layer thickness of 125 microns 96

Figure 5-25: Comparison of fitting error using all developed fitting models for layer thickness of 125 microns 97
Figure 5-26: Distribution of fitting error using TLS method for layer thickness of 500 microns.....98
Figure 5-27: Distribution of fitting error using TLS and genetic algorithm method for layer thickness of 500 microns.....99
Figure 5-28: Distribution of fitting error using third degree polynomial method for layer thickness of 500 microns 99
Figure 5-29: Distribution of fitting error using second degree polynomial method for layer thickness of 500 microns.....99
Figure 5-30: Comparison of fitting error using all developed fitting models for layer thickness of 500 microns 100

List of Tables

Table 3-1: Details of measurement process. 24

Table 3-2: Nominal extrusion width for every specific layer thickness 60

Table 3-3: Machine parameters 67

Table 4-1: Information of cups for layer thickness of 500 microns 71

Table 4-2: Information of pictures for layer thickness of 250 microns 72

Table 4-3: Information of pictures for layer thickness of 125 microns 73

Notations

R_a	Profile roughness
R_{a_w}	Weighted profile roughness
u_i	Knot value
$A_{cross-sectional}$	Area of the cross section of extruded filament
A_{nozzle}	Area of the nozzle tip
A	Mixed basis function
ω	Angular velocity
R	Radius of the screw
A	Polynomial coefficient
B	Polynomial coefficient
C	Polynomial coefficient
C	Polynomial coefficient
D	Polynomial coefficient
E	Polynomial coefficient
F	Polynomial coefficient
G	Polynomial coefficient
H	Polynomial coefficient

N_{mixed}	Mixed basis functions
CData	Actual points
CP	Measured control points
$N_{i,p}$	Basis function of *i*-th control point of degree p
l_t	Layer thickness
α_t	Critical surface angle
α	Surface angle
M	Number of knots
N	Number of control points
P	Degree of the B-spline
C(u)	B-spline representation
e_i	Euclidian distance
ΔA	Error in Total least square
$\Delta CData$	Error in Total least square
H	Height of the layer
l	Layer thickness
d	Diameter of filament
S_{total}	Experimental area of the cross section of filament
I	Identity matrix

V	Unitary matrix factor of singular value decomposition
U	Unitary matrix factor of singular value decomposition
Σ	Rectangular diagonal matrix factor of singular value decomposition

Abbreviations

ANOVA	Analysis of variance
3DP	3 dimensional printing
ABS	Acrylonitrile butadiene styrene
PLA	Polylactic acid
NURBS	Non-uniform rational B-spline
B-spline	Basis spline
TLS	Total least square
LOM	Laminated object manufacturing
FDM	Fused deposition modelling
SLA	Stereo-lithography Apparatus

SLS	Selective Laser Sintering
AM	Additive manufacturing
CCD	Central rotatable Composite Design
3D	3 dimensional
2D	2 dimensional

1 Chapter 1: Introduction

Additive manufacturing (AM) has introduced a new group of technologies to support design of more complex and more efficient products. Developing products, producing prototypes and evaluating the customer specifications have significantly shorter time span using AM technologies. However, the functionality of AM parts is highly related to their dimensional accuracy and surface integrity. The surface integrity is a very critical issue for the AM products because they are inherently affected by the staircase effect phenomenon resulting from the layer by layer manufacturing nature of the AM processes. The staircase effect greatly influences the surface texture of the parts manufactured by AM technologies. A comprehensive understanding of the surface roughness in AM will lead us to find the ways to model the staircase effect. The main feature created due to staircase effect affecting the surface roughness is called ”Cusp”. Therefore, one can expect using a model of the cusps based on the manufacturing parameters to predict the surface roughness and surface integrity of the AM products.

In most applications of Additive manufacturing such as adaptive slicing, post processing of the products and optimizing the process parameters, the cusp profile is approximated as a rectangle with sharp edges as shown in Figure 1-1 with red lines.

In this research, a mathematical model for exact cusp geometry shown in Figure 1-1(blue curve) based on two important parameters of layer thickness and surface angle of the products needs to be developed

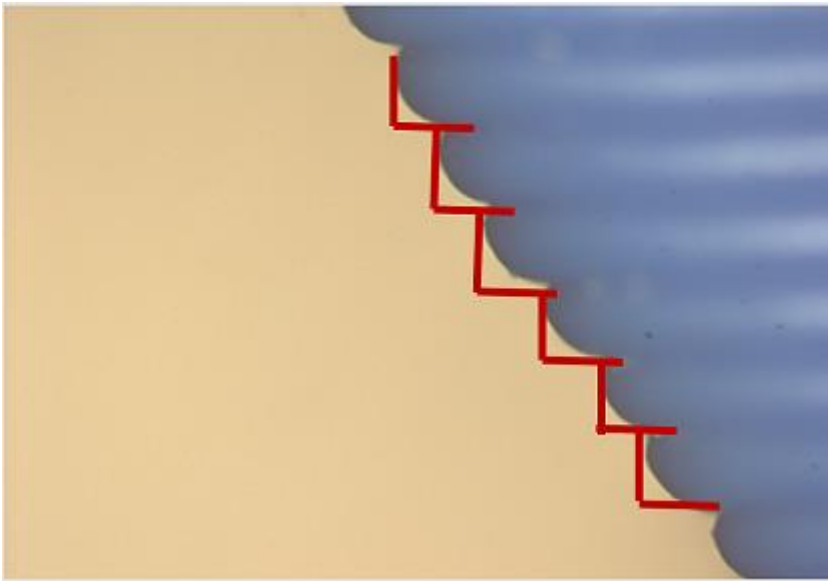

Figure 1-1: Jeopardizing accuracy by approximating the cusp geometry by rectangle shapes.

The additive manufacturing technologies have been developed significantly within the past 35 years. In first years, they were known as technologies to only build prototypes. But the industries today consider it as a substitution to the traditional manufacturing technologies. AM products are also used directly or indirectly to develop manufacturing tools including the fixtures, molds, and casts. For a final product in manufacturing, functionality is the most important metric and the surface roughness of AM parts, directly affects the functionality of the product.

Many Researchers developed the models for surface roughness but available models have their c and simplification that limits their practicality. The developed models typically are based on the experimental studies of the surface roughness or purely theoretical concepts about the shape and form of the cusps. In this work a combination of the experimental and theoretical study is presented to predict the surface roughness of AM parts based on an accurate modelling of the cusps.

There are many additive manufacturing technologies commercially available today. Many new processes have been developed in past 10 years to reduce the cost, improve surface integrity, and increase the applications of additive manufacturing. Also, the technology is becoming more accessible to a variety of industries. All of these developments make the need to improve the surface integrity of the AM much more crucial than before. Prediction, monitoring, and control of the surface roughness in the AM products create some unique opportunities to take a step forward toward implementing these technologies as some reliable and advanced manufacturing processes. The structure of this thesis is as follows. After this introduction, Chapter 2 presents the literature review on different processes of additive manufacturing, effect of process parameters on surface roughness of the parts and the last section of chapter two presents the geometrical, theoretical, statistical and experimental models for surface roughness of AM products. Chapter 3 provides the methodology developed using experimental and theoretical investigation. It includes the geometric modelling of the cusp, 3D roughness measurement, 2D profile measurement, and extraction of cusp profile data by image processing. Chapter 4 provides the implementation process including the information required to design the specimen and number of observations for each picture and cusp. In this chapter the implementation of the developed methodologies to measure the cusp geometry is presented.Chapter 5 presents the result of implementation of the approaches that were presented in chapter 3 and discussion about the results. Chapter 6 presents the conclusion and the recommendations for future work.

2 Chapter 2: Literature Review

2.1 Introduction

The literature review of this work covers a range of topics to assist a better understanding of the surface roughness and its controlling parameters in additive manufacturing and particularly in the process of Fused Deposition Modeling (FDM). The literature review is divided into 3 parts: Classification of the additive manufacturing processes; relationship of the process parameter and surface roughness in additive manufacturing, and modeling of the surface roughness based on the geometry of the cusp.

2.2 Classification of Additive Manufacturing Processes

2.2.1 Fused Deposition Modeling (FDM)

FDM is an additive manufacturing process in which a filament of thermoplastic polymer is feed to the extruder. The material is melted in the extruder and then is extruded on a bed. After each layer being built, the bed is lowered in z axis direction to allow the upper layers of the prototype to be built. The most used material in FDM process are Polylactic Acid (PLA) and Acrylonitrile Butadiene Styrene (ABS). Printing with PLA is easier to lower melting point [1, 2]. The main advantage of FDM process is that the machine and the material are less expensive in compare to other AM processes. The main disadvantage of this process is low surface quality in z direction due to staircase effect [3]. Figure 2-1 shows the basics of the fused deposition modeling process schematically.

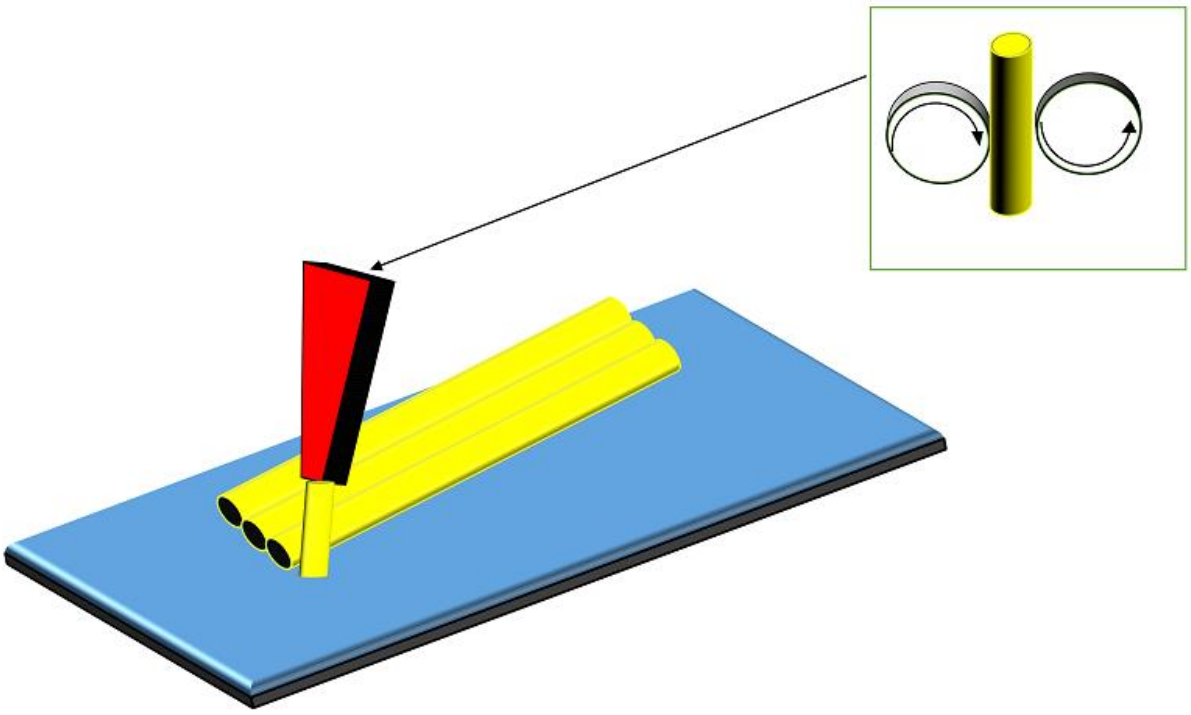

Figure 2-1: FDM process schematics

2.2.2 Streolithography Apparatus (SLA)

Stereo-lithography Apparatus (SLA) is the first and the most used process among the additive manufacturing technologies. SLA is a liquid-based process that includes curing or solidification of a polymer when an ultraviolet laser makes contact with the resin. The layer thickness in SLA processes depends on the equipment used. A platform is built to anchor the piece and support the overhanging structures. Then the UV laser is applied to the resin solidifying specific locations of each layer. When the layer is finished, the platform is lowered and the new layer will be built on top of the previous layer. Layer thickness in this process is less than 10 μm and the quality of the surface achieved in this process is higher than one using the FDM process because of this reason. **Error! Reference source not found.** shows the basic parts of a stereo-lithography apparatus [1, 2]

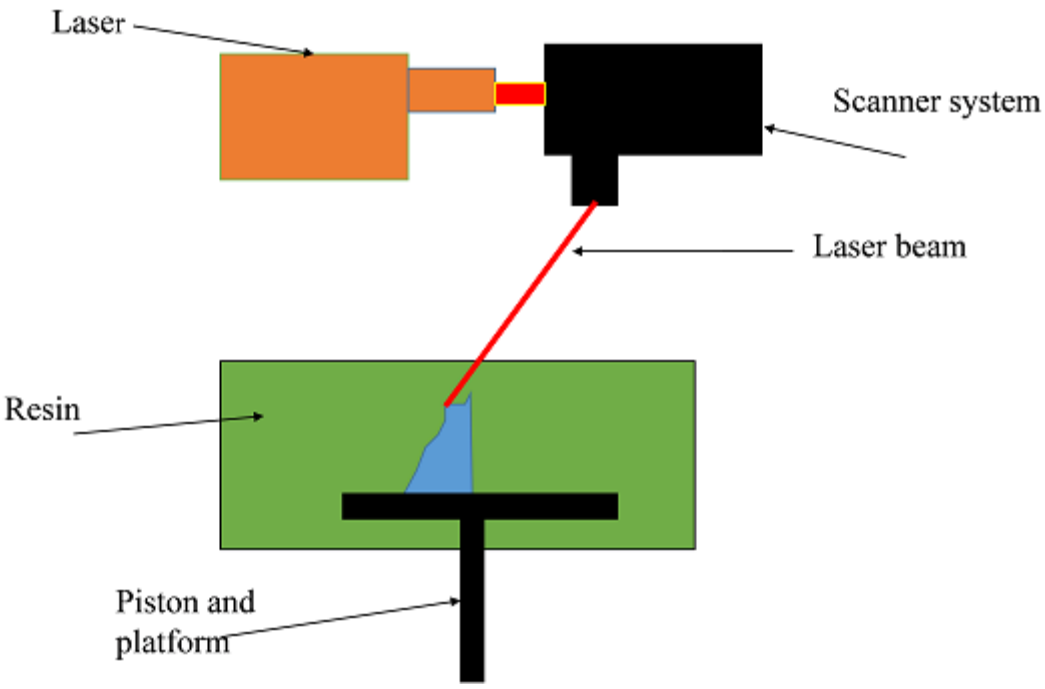

Figure 2-2: Schematic of SLA process [1]

2.2.3 3 Dimensional Printing (3DP)

3DP process is a processes that was implemented by a group of researchers in MIT. In this process a liquid binder is injected into a jet onto a powder to print the prototype directly from the CAD model. The particles for every layer, are spread in a surface and glued together after the liquid binder is jetted. The main advantage of 3DP is that it can build parts from any material including ceramics, plastic, metal powders [3-5].

2.2.4 Pro-Metal

Pro-metal is an additive manufacturing process to build dies and injection tools. The process is powder-based and the main material to print is stainless steel. The printing process happens when a liquid binder is sprayed out in jets to steel powder. The bed consists of steel powder and it is lowered when each layer is printed [4, 5].

2.2.5 Selective Laser Sintering (SLS)

Selective Laser Sintering (SLS) is an additive manufacturing process in which a powder is sintered for a laser beam. The chamber is heated to the melting point of the material that is supposed to be printed. The laser heats the powder at a specific point for each layer. The bed is then lowered to let the next layer to be printed. This process can be used to print a wide range of materials including plastics, metal, combination of polymer and combination of metals and ceramics. [6-8].

2.2.6 Laminated Object Manufacturing

Laminated Object Manufacturing (LOM) is an AM technology which is a combination of additive and subtractive manufacturing to make parts layer by layer. The material is used in sheets form in LOM process and the layers are glued together by heat and pressure. A laser beam cuts the sheets to the shape of each layer which is given by a CAD file. The main advantage of LOM process is that no post processing is needed and the cost is low in compare to other AM technologies.. The main disadvantage of LOM process is due to material subtraction, internal surface features are hard to be built. LOM can be used for building parts and products with papers, composites and metals. [9, 11, 12].

2.3 Relationship between the Process Parameters and Surface Roughness

Chryssolouris et al. [13] used a full factorial experiment to investigate the effect of the process parameter such as layer thickness, heated roller temperature, heated roller speed and platform retraction on the surface roughness of LOM products. They proposed a statistical model for surface roughness of the LOM prototypes using Analysis of Means and as a function of that process parameters and validated the statistical model by performing two additional sets of experiments using different

levels of process parameters and observed that the predicted values for the surface roughness and the measured values are in good agreement.

Vasudevaro et al. [14] studied the effect of some process parameters such as surface angle, layer thickness, raster width, and air gap and model temperature on the surface roughness of FDM products. They performed fractional factorial experiments to investigate the effect of each parameter on the surface roughness in different levels of each parameter. Using statistical model, they concluded that the layer thickness and surface angle has the most significant effect on the surface roughness of the products and the air gap, model temperature and road width have less effect on the surface roughness of the prototypes.

Anahita et al. [15] performed a set of experiments based on Taguchi method to study the effect of process parameter on surface roughness of FDM prototypes. They studied the effect of layer thickness, road width and speed of material deposition on the surface roughness using three levels for each parameters and studying the effect of each parameter on the final surface roughness. The surface roughness was measured using Surtronic surface roughness measurement tester. Using analysis of variance (ANOVA) and regression analysis they concluded that the layer thickness has the most significant effect on the surface roughness and the road width and speed of deposition of material doesn't have significant effect on surface roughness.

Bacchewar.,et al [16] predicted the surface roughness of SLS products using statistical model. They investigated the effect of process parameter of SLS printing such as laser power, beam speed, building orientation, layer thickness and hatch spacing on the surface roughness of SLS prototypes. They carried out the experiments using Central rotatable Composite Design (CCD) of experiments. They measured the surface roughness by changing the levels of each process parameter to observe the effect of each parameter on surface roughness. Using analysis of

variance (ANOVA) they found out that in upward surfaces, the layer thickness and the build orientation have the most significant effect on the surface roughness where rather than layer thickness and build orientation, the laser power is another significant factor to predict the surface roughness of SLS prototypes in downward surfaces. They validated their model for the building orientations from 10° to 70° but they stated that for building orientation between 0° and 10° and from 70° to 90° the model doesn't predict the accurate values for surface roughness and needs correction.

Galantucci et al. [17] investigated the effect of process parameter such as raster width, layer thickness and tip diameter on the surface roughness of the FDM parts. They only studied the surface roughness of surface angle of 0° and 90°. Using full factorial experiments, they observed that the layer thickness and raster width strongly affect the surface roughness when the tip diameter doesn't affect the surface roughness significantly. It was also observed that the raster width affect the surface roughness of the 0°surface angle more than 90° surface angle. The surface roughness was measured with contact device and optical device and the results of the measurements were in good agreement with predicted ones. They used the acetone vapor to make the surface of the prototypes smooth and they showed that they decreased the surface roughness of the FDM prototypes significantly by chemical treatment.

Sikder et al. [18-20] studied the effect of staircase effect on dimensional accuracy and the surface roughness of the final products to use it as a criteria for input of a global adaptive slicing algorithm.

Jamioalahmadi and Barari, studied the distribution of the surface roughness on the AM surfaces and presented an algorithmic approach based on the properties of Laplace equation to estimate the surface roughness [19].

2.4 Modeling of Surface Roughness Based on Geometry of the Cusp

Reeves and Cobb [21] proposed a mathematical model of surface roughness of additive manufactured parts using parameters such as layer thickness, surface angle and layer profile and quoted values of surface roughness. They assumed the profile edges as sharp triangular edges with an inclination to the normal direction. They also predicted the surface roughness for downward surface planes. They used the center line method for calculating the average surface roughness value. They validated their model using the additive manufactured parts with different surface angles and the results were compatible with the mathematical model. The schematic for the model is shown in Figure 2-3.

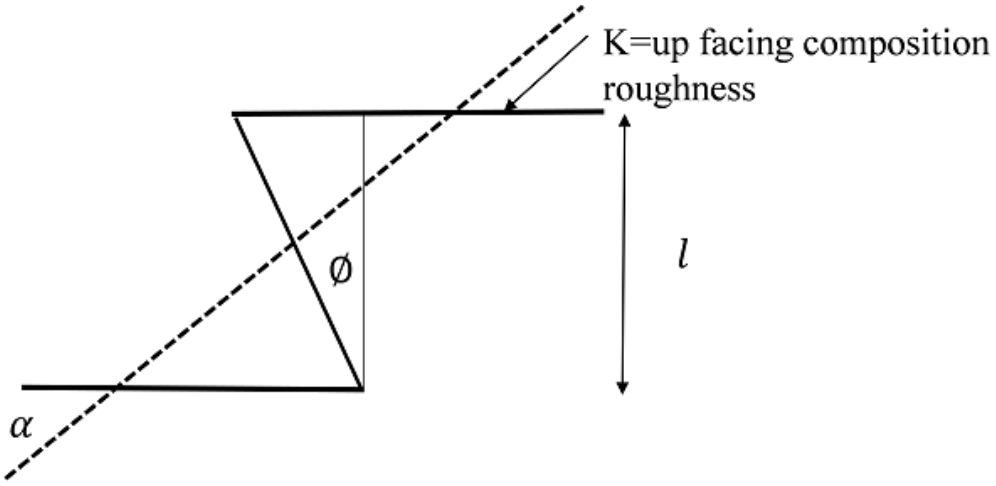

Figure 2-3: The geometry of the cusp for surface roughness model.

$$R_a = \frac{l * (tan\,\emptyset * sin\,\alpha + cos\,\alpha)}{4} + K \qquad (2\text{-}1)$$

Paul and Voorakarnam [22]considered staircase error as the most effective error in surface roughness of the layer by layer manufacturing prototypes. They developed a model for predicting surface roughness of the additive manufactured parts based on centerline average roughness calculation method. They verified their model with running a full-factorial experiment and studied the effect of surface angle and layer thickness on the surface roughness of the specimens which was measured using a Mitutoyo SurfTest Model 212 contact surface topography. The general result of the experimental study showed that the surface roughness model achieved by centerline average roughness method has predicted the surface roughness of the specimens good where the layer thickness doesn't exceed a certain amount but it's poor to predict the roughness for thicker layer thicknesses. They also found that the smaller surface angles in prototypes show the minimized surface roughness [22].

Perez et al. [23] presented a geometrical model of surface roughness. The model defines the surface roughness as a function of layer thickness and horizontal space between layers. They defined the distance between layer as a function of layer thickness and surface angle, then the surface roughness is a function of surface angle and layer thickness. They also considered rounded shape of the edge profiles. They manufactured several prototypes with different surfaces angles to validate their model for surface angles between 0° and 90°. They performed an experimental plan to measure the surface roughness of prototypes and they observed that the measured surface roughness is in a good agreement with the geometrical model results however the experimental results revealed that the geometrical model need correction close to surface angle 0° and 90°.

Pandey et al. [24-26] considered the profile edges of layers as a parabolic curve as shown in Figure 2-4.They modeled the surface roughness using center line average method. Using the stochastic model they estimated the profile height as a function

of the base of the profile. They showed that for surface angles from 70° to 90° a gap is observed between the roads of the filament and it changes the general model of the surface roughness. The final model predicts the surface roughness for surface angles from 0°to 70°, 70°to 90° and a special value for 90°. they also predicted the surface roughness for downward surfaces with support material and concluded that for the same surface angle, the downward surface has a greater surface roughness. They carried out a fraction factorial experiments to verify their approach. The result of the experiment were in good agreement with the proposed model for the surface roughness.

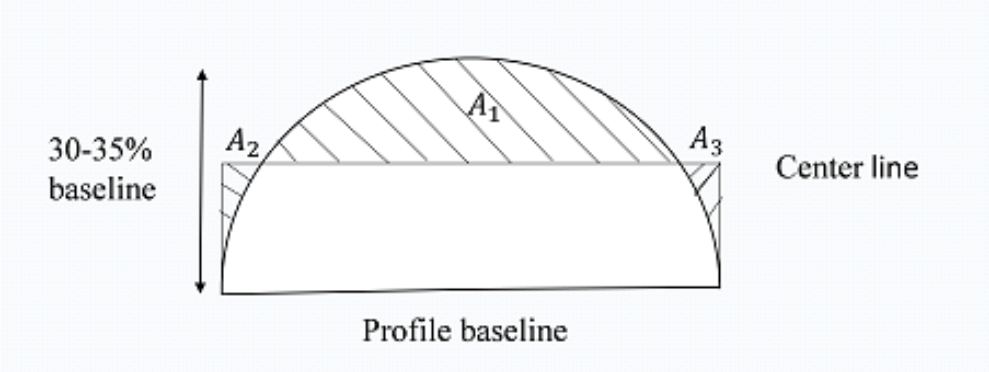

Figure 2-4: Edge profile of the layer

Ahn et al. [27] proposed a theoretical model for prediction of surface roughness based on experimental measurement of the surface roughness of a prototype having all surface angle from 0° to 180° by increment of 3°. The models has been developed based on interpolation of the measured surface roughness to predict the roughness at non-measured surface angles. This gives a distribution of surface roughness from 0° to 180°. Using the normal vector of the facet of the triangle in CAD model and picking the corresponding surface roughness based on roughness distribution, the model predicts the surface roughness at the specified surface angle. The accuracy of the model was tested by measuring surface roughness by different increment of

angles. They verified the model by comparing the predicted roughness with the surface roughness of two complex geometries.

Ahn et al. [28] proposed a model for surface roughness based on elliptical edge profile of the layers. The profile edge is shown in Figure 2-4. Using center line method for measuring the surface roughness, they calculated the surface roughness. They also assumed the overlap between layers and calculated the surface roughness for three levels of overlaps. They showed that the overlap of the layers doesn't affect the surface roughness significantly. They verified their model by manufacturing and measuring the surface roughness of a prototype having all surface angles from 0° to 90° for two different layer thicknesses. They concluded that their model is in a good agreement with the experimental results. They showed that for angles close to 90° , layer thickness doesn't affect the surface roughness significantly. Figure 2-5 shows the schematic of the present model for surface roughness.

Campbell et al. [29]designed a methodology to visualize the surface roughness of the additive manufactured prototypes. Their model for surface roughness was a function of layer thickness and the surface angle. They designed a part having all surface angle from 0° to 180° with increment of 2° and measured the surface roughness of each surface angle using a contact measurement device. They verified their theoretical model with the measurement of roughness of the specimen. They used the surface roughness model to visualize the surface roughness of the Additive manufactured prototype as shaded colours on the 3D CAD image of the prototype.

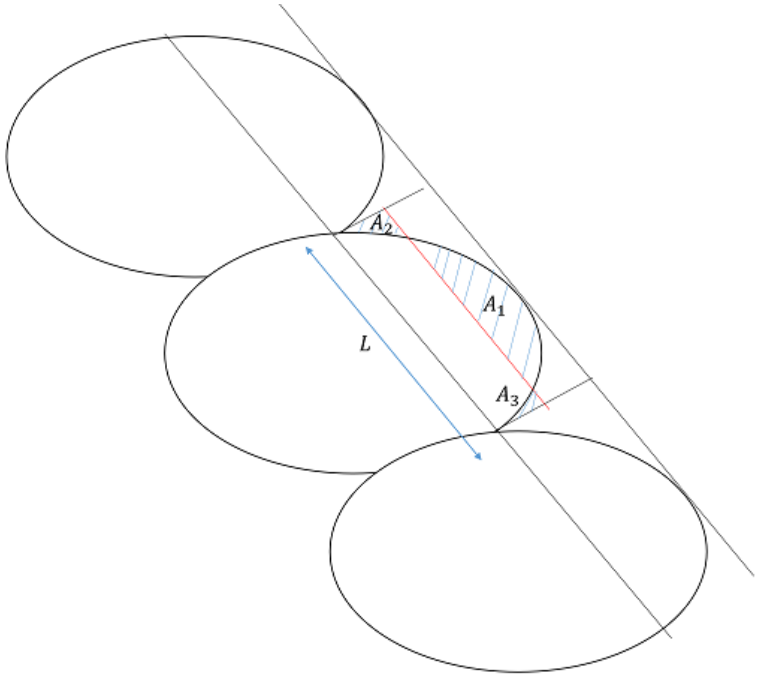

Figure 2-5: Elliptical profile of the layers

$$R_a = \frac{A_1 + A_2 + A_3}{L} \qquad 2\text{-}2$$

Ahn et al. [30]approximated the edge profile of the layers in LOM process as a parabolic curve. Using center line average method for computing surface roughness, they predicted the surface roughness of LOM prototypes. They also predicted the surface roughness for different coefficients of the parabolic shape. They validated the model using manufacturing two prototypes by two different layer thicknesses and measuring their surface roughness at different surface angles. The results of the measurement were in good agreement with the predicted values.

Kechagias [31] studied the effect of process parameters on the surface roughness of the LOM prototypes. He used Taguchi method for performing the experiments and

then modeled the results by regression method. He showed that the heater temperature, layer thickness and laser speed are the most important factors affecting the surface roughness. He verified the results of the experiment by comparison of the predicted values of surface roughness of a cube with actual surface roughness of it.

Byun and Lee [32] predicted the model for surface roughness of FDM prototypes based on round and fillet corner for each profile of the filament. Using STL file of the CAD model, the normal vector and area of the facet is found. Since the greater area of the facet makes the roughness value greater, they used the weight for the area of the facet as a weight factor. They also avoid the effect of support material on surface roughness of FDM parts for downward surface angles because they are removed from the FDM prototypes. They used the surface roughness model to find the optimal build orientation of the FDM prototypes. Figure 2-6 shows the profile model.

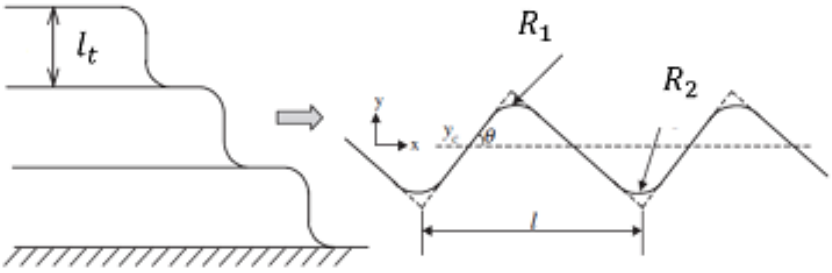

Figure 2-6:The rounded profile shape for FDM prototypes[32].

$$R_a = \frac{l_t}{4}\cos\theta - \frac{(R_1^2 + R_2^2)(1 - \frac{\pi}{4})\sin\theta}{l_t} + \frac{\left((R_1^2 - R_2^2)\left(1 - \frac{\pi}{4}\right)\right)^2}{l_t^3}\tan\theta \sin\theta \quad 2\text{-}3$$

$$R_{a_w} = \sum_{i=1}^{N_f} R_{a_i} A_i \quad 2\text{-}4$$

Boschetto et al. [33] performed a full factorial experiment to study the effects of process parameters on the surface roughness of FDM prototypes. They designed a part having 5 levels of surface angles and using roughness profilometer, the surface roughness was measured. They carried out statistical analysis and concluded that the edge profile of the layer can be expressed by rounded curve. They presented a model for edge profile using rounded geometry and based on layer thickness and surface angle. They validated their model by measuring the surface roughness of a tube having all surface angle from 0° to 180° with increment of 5° using reconstructing the profile and then it was compared to the geometric specifications of the predicted geometry (rounded curve) and observed a very good agreement between the experimental and theoretical results. The model needed correction for angles close to 0° and 180°.

Ali et al. [34] conducted Taguchi design of experiments to study the effect of process parameters such as air gap, raster angle and road width on the surface

roughness of FDM parts. They concluded that the positive air gap will lead to a greater surface roughness than negative air gap and as the raster angle increases to 90° the surface roughness decreases. They also observed that increasing the road width of the deposited filament, increases the surface roughness.

Boschetto et al. [33, 35] proposed a theoretical model of the edge profile of the FDM parts. They predicted the profile of the layer as an ellipse and measured the roughness of each profile using least square center line. The roughness model was a function of layer thickness and build orientation. They validated the predicted model by measuring a suitable geometry using profilometer and the results of experiment were in good agreement with the predicted model.

Jin et al. [36] proposed 3 geometrical model for the cross section of the filament in FDM process based on tractrix, parabola, and catenary curves. They compared the result of the predicted model with the actual cross section of the profile and they concluded that the tractrix model has the best agreement with the experimental results.

Sreedhar et al. [37] proposed a theoretical model for predicting the surface roughness of FDM parts. They found the surface angle from 20 ° to 30° as the optimum surface angle in order to minimize the surface roughness. They verified their model by measuring the surface roughness of a specimen and comparing the result with the predicted values [38].

3 Chapter 3 Methodology

3.1 Introduction

This chapter presents the methodologies developed in this research for geometric modelling of the cusp, 3D roughness measurement, 2D profile measurement, and extraction of cusp profile data by image processing. The developed methodologies in this research are presented in this chapter. Four methodologies are developed to find the best mathematical representation of the fitted curves to the captured data points including B-spline curve modeling using total least square fitting, B-spline curve modeling by genetic algorithm, three piece curve fitting including second degree polynomial curve and genetic algorithm, three piece curve fitting including a third degree polynomial curve and genetic algorithm. The method that gives the minimum residual error of fitting is then chosen as the model of the cusp. The surface roughness is calculated using total least square center line. An experimental methodology for calculating the actual width of extrusion using cusp geometry is presented at the end of this chapter.

3.2 Measurement of cusp profile

3.2.1 3D Profile Measurement

3D surface roughness measurement is a useful approach to estimate the surface roughness, profile roughness and surface integrity of the AM products. The 3D surface topography device takes stacked images from the surface of the parts and reconstructs the 3D topographic surface data using those images.

3D surface roughness measurement will give us useful information as shown in Figure 3-1, but it doesn't give enough information about exact geometry of the cusp as shown in Figure 3-2.

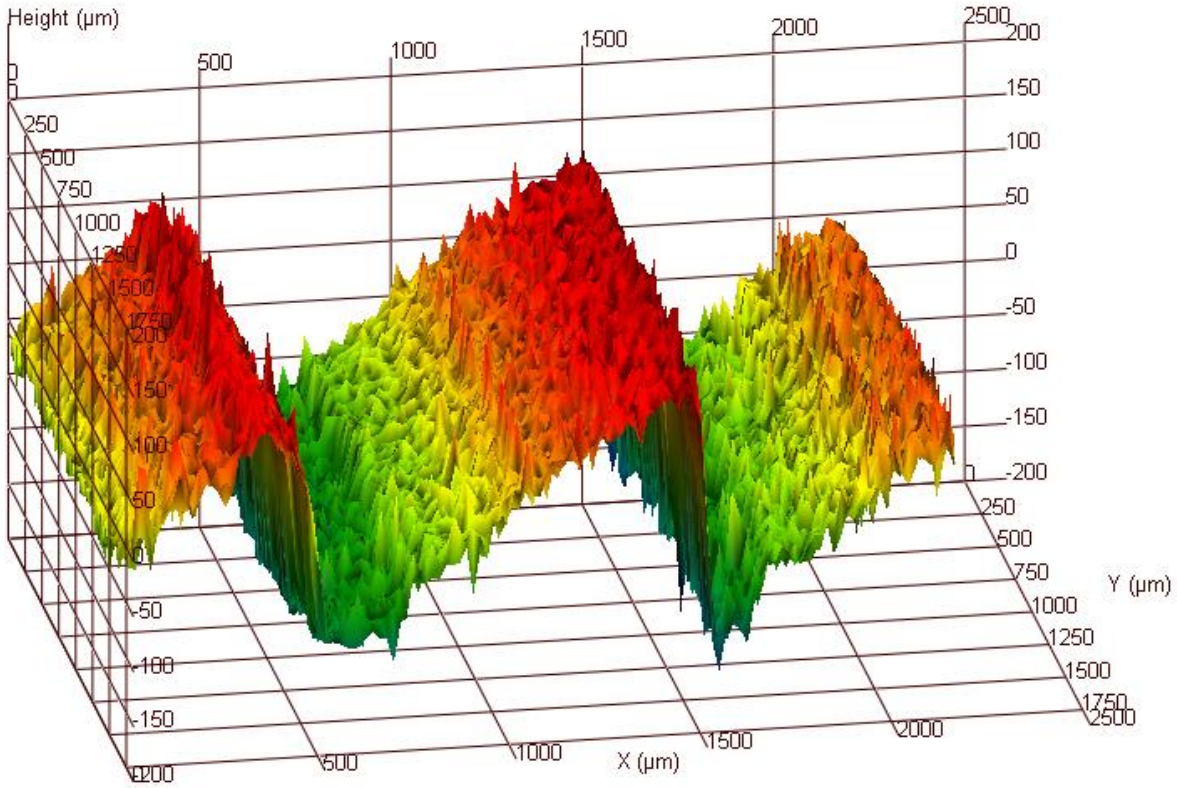

Figure 3-1: 3D profile roughness measurement

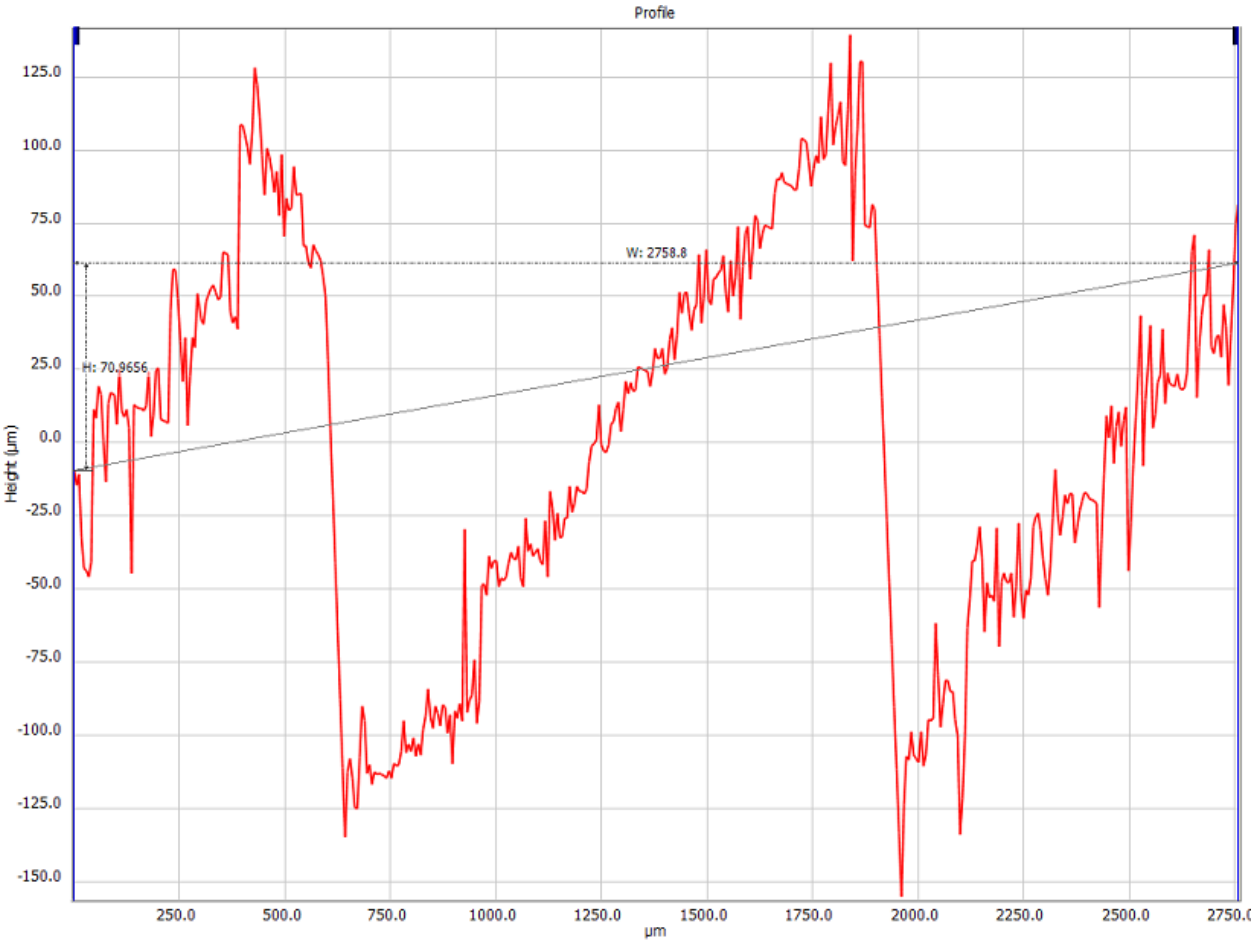

Figure 3-2: Profile roughness measurement using 3D picture

3.2.2 2D Profile Measurement

3.2.2.1 Extraction of cusp profile using 3D surface topography device

The 2D measurement of the cusp has been conducted using side view picture of the cusp as shown in Figure 3-3.

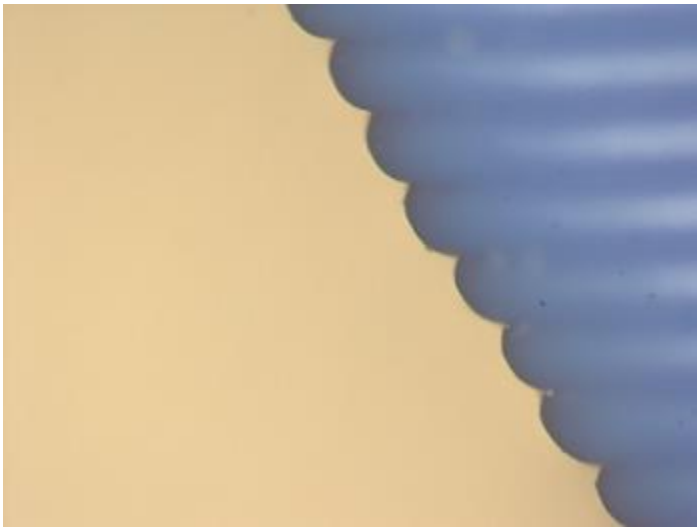

Figure 3-3: Cusps side view of a specific slope (65 degrees)

According to the distribution of the colour intensity in each specific image a threshold value has been defined to clearly define the material and void portions of the images by the black and white colours. The pixels with greater value than the threshold value are considered as black pixels and the pixels with values less than the threshold value are considered as white. An example of the processed black and white picture is shown in Figure 3-4. It is not difficult to use this black and white image to extract the border of the material region.

Figure 3-4: An example of the black and white regions

Using the black and white representation the borders of the white and black regions is extracted and is used to capture the data of the profile cusp geometry as it is shown in Figure 3-5.

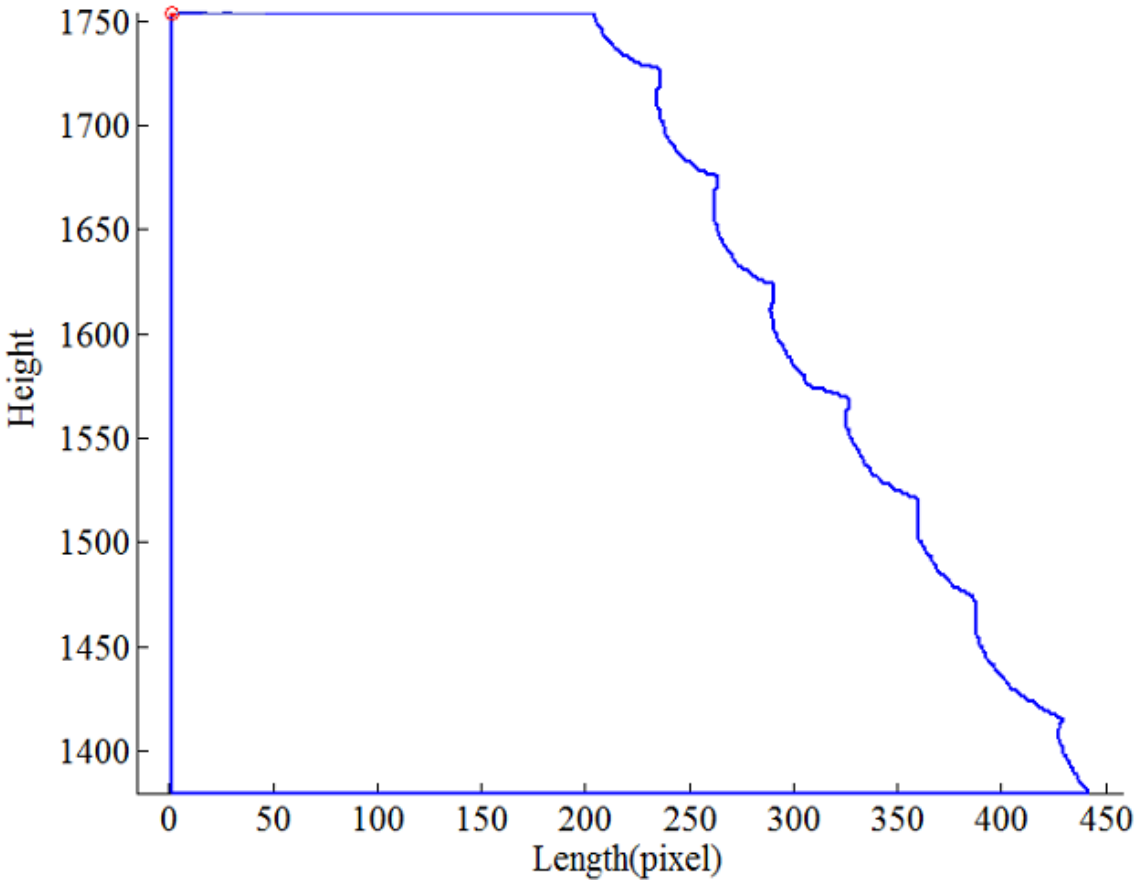

Figure 3-5: The border of the white and black regions shows the actual profile of the cusps.

It is very important to calibrate the microscope accurately and use the proper dimensional scale of the image pixels. Also it was crucial in this work to validate the threshold approach employed in the image processing stage when the black and white region are recognized. A validation test was conducted as follows. The test validates the microscope scaling factor based on its image resolution and also the threshold approach in the image processing. A standard 1-mm gauge is measure with the microscope (Figure 3-6) and its image has been processed by the threshold approach to specify the black and white regions. The size of the image that was taken by 5X lens is 1611 pixel×1211pixel and the scope of the 5X is 2322×1755. The

picture of the gauge has 647 pixels in the width, then Width in x-y coordinate system is as follows:

$$674 * \frac{1755(\mu m)}{1211(x - size - pixel)} = 976.77 \mu m$$

Then the error of measurement could be represented as:

$$\frac{1000 - 976.77}{1000} * 100 = 2.32\%$$

Measurement process was conducted with the following details:

Table 3-1: Details of measurement process.

Magnification	5x
Numerical Aperture	0.15
Acquisition System	Micro Phase
Adapter Magnification	0.63x
Overall Magnification	3.05x
X Scale	1.443 μm/pixel
Y Scale	1.443 μm/pixel

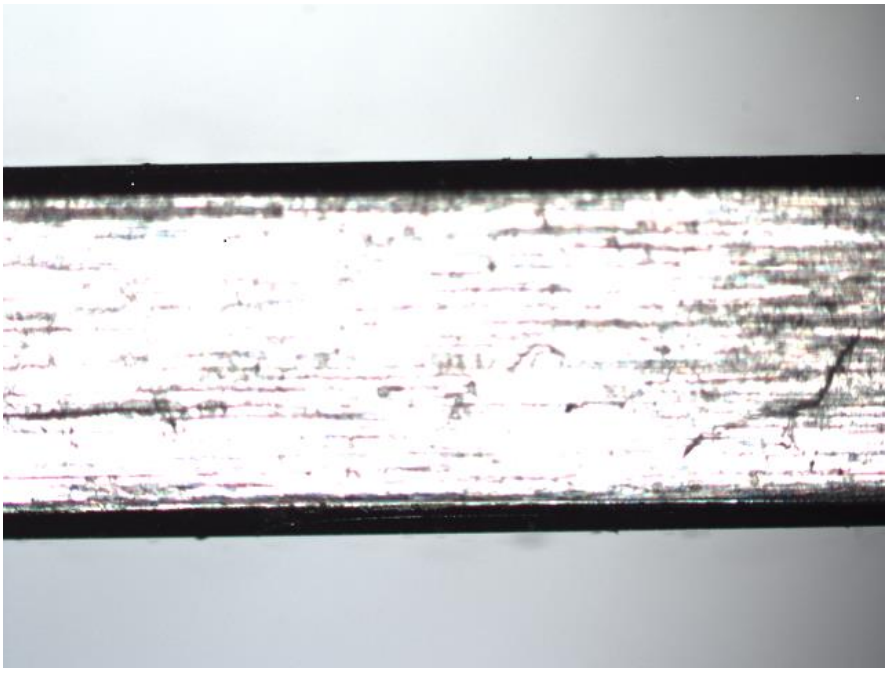

Figure 3-6: Width of the 1mm gauge

3.3 Cusp Modelling

The observations show that three regions can be recognized in the general cusp profile. Variety of analyses were contacted and from what has been reviewed it's more likely accurate enough to model each cusp with two pieces of the straight lines at the two ends and a degree two (or three) polynomial as the middle piece. Three following methodologies are presented to find the best approximation for the cusp geometry considering the whole cusp profile as:

1- A single cubic B-spline with two line segments. The entire data points belonging to a cusp is defined by the user.

2- Two straight lines at the two ends and a second degree polynomial as the middle piece.

3- Two e straight lines at the two ends and a third degree polynomial as the middle piece.

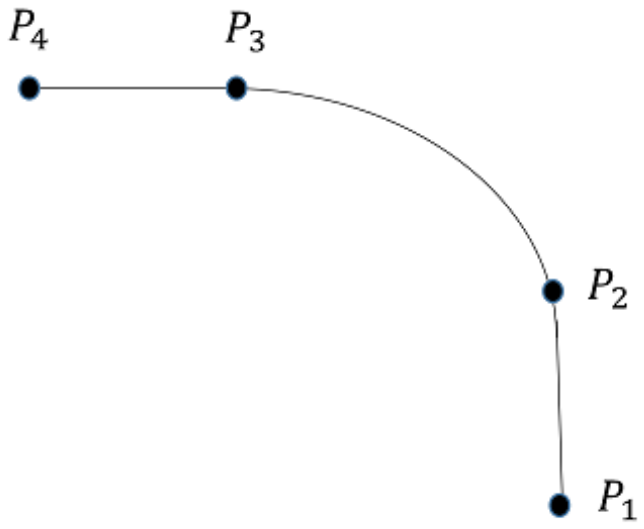

Figure 3-7: Linear and curve segments of the cusp profile

3.3.1 Representing the cusp geometry with a cubic B-spline

3.3.1.1 The introduction and properties of B-spline Curves

A B-spline is a piecewise polynomial which is defined based on a variable "*u*" and in domain of "*u*". Corresponding to each *u*, the *B*-spline returns a point on the curve based on *u* [39].

A *p*th-degree *B*-spline curve is represented as follows:

$$C(u) = \sum_{i=0}^{n} N_{i,p}(u) P_i \qquad 3\text{-}1$$

P_i is the ith control point and $N_{i,p}$ is the pth-degree *B*-spline basis function which is recursively defined by:

$$N_{i,0}(u) = \begin{cases} 1 & if\ u_i < u < u_{i+1} \\ 0 & otherwise \end{cases} \qquad 3\text{-}2$$

$$N_{i,p}(u) = \frac{u - u_i}{u_{i+p} - u_i} N_{i,p-1}(u) + \frac{u_{i+p+1} - u}{u_{i+p+1} - u_{i+1}} N_{i+1,p-1}(u) \qquad 3\text{-}3$$

For modeling the cusp geometry as shown in Figure 3-7 it is assumed that the whole profile is made by three polynomial segments. Considering the cubic *B*-spline determines that the degree of the curve is 3. Equation 3-4 represents the relation between the degree of the B-spline and the number of the control points with the number of knots.

$$m = n + p + 1 \qquad 3\text{-}4$$

Where p is the degree of the curve, *m* is the number of knots and *n* is the number Of the control points.

3.3.1.2 Knot Vector Selection

Choosing the proper knot vector is one of the important steps for defining a B-spline. The knot vector affects the shape and parameterization of the curve. Three common methods of selecting the knot vector are as follows:

1- Equally spaced.
2- Chord length.
3- Centripetal method.

We choose the knot vector based on the equally spaced method.

Considering that *u* lies in the range of $[0,1]$, for equally spaced method we have:

$$\overline{u_0} = 0$$

$$\overline{u_n} = 1$$

$$\overline{u_k} = \frac{k}{n}$$

Where $k = 1, \dots, n-1$.

The multiplicity of the first knot has to be equal to the degree of the curve plus one ($p+1$).

The knot vector has to end with the same number of multiplicity of knots for the last knot span. Based on above discussion the knot vector is defined as follows:

$$\textit{Knot vector} = [0,0,0,0,1/4,1/4,1/2,3/4,3/4,1,1,1,1]$$

Multiplications of the 0 and 1 are equal to ($p+1$) =4 since the curve is degree 3($p=3$). The knot multiplications at the beginning and the end of the curve make the curve pass from the first and last control points.

3.3.1.3 Basis Functions

The first linear part of the curve lie between *u=0* and *u=1/4*. The basis function for the curve are calculated according to Equation 3-2 and Equation 3-3. Zero degree basis functions are as follows:

$$N_{0,0} = 0 \qquad \text{3-5}$$

$$N_{1,0} = 0$$

$$N_{2,0} = 0$$

$$N_{3,0} = \begin{cases} 1 & 0 \le u < 1/4 \\ 0 & otherwise \end{cases}$$

$$N_{4,0} = 0$$

$$N_{5,0} = \begin{cases} 1 & 1/4 \le u < 1/2 \\ 0 & otherwise \end{cases}$$

$$N_{6,0} = \begin{cases} 1 & 1/2 \le u < 3/4 \\ 0 & otherwise \end{cases}$$

$$N_{7,0} = 0$$

$$N_{8,0} = \begin{cases} 1 & 3/4 \le u < 1 \\ 0 & otherwise \end{cases}$$

$$N_{9,0} = 0$$

$$N_{10,0} = 0$$

$$N_{11,0} = 0$$

First degree basis functions are as follows:

$$N_{0,1} = 0$$

$$N_{1,1} = 0 \qquad \text{3-6}$$

$$N_{2,1} = \frac{u-u_2}{u_3-u_2}N_{2,0} + \frac{u_4-u}{u_4-u_2}N_{3,0} = \begin{cases} 1-4u & 0 \le u < 1/4 \\ 0 & otherwise \end{cases}$$

$$N_{3,1} = \frac{u-u_3}{u_4-u_3}N_{3,0} + \frac{u_5-u}{u_5-u_3}N_{4,0} = \begin{cases} 4u & 0 \le u < 1/4 \\ 0 & otherwise \end{cases}$$

$$N_{4,1} = \frac{u-u_4}{u_5-u_4}N_{4,0} + \frac{u_6-u}{u_6-u_4}N_{5,0} = \begin{cases} 2-4u & 1/4 \le u < 1/2 \\ 0 & otherwise \end{cases}$$

$$N_{5,1} = \frac{u-u_5}{u_6-u_5}N_{5,0} + \frac{u_7-u}{u_7-u_6}N_{6,0}$$

$$= \begin{cases} 4u-1 & 1/4 \le u < 1/2 \\ 3-4u & 1/2 \le u < 3/4 \\ 0 & otherwise \end{cases}$$

$$N_{6,1} = \frac{u-u_6}{u_7-u_6}N_{6,0} + \frac{u_8-u}{u_8-u_7}N_{7,0} = \begin{cases} 4u-2 & 1/2 \le u < 3/4 \\ 0 & otherwise \end{cases}$$

$$N_{7,1} = \frac{u-u_7}{u_8-u_7}N_{7,0} + \frac{u_9-u}{u_9-u_8}N_{8,0} = \begin{cases} 4-4u & 3/4 \le u < 1 \\ 0 & otherwise \end{cases}$$

$$N_{8,1} = \frac{u-u_8}{u_9-u_8}N_{8,0} + \frac{u_{10}-u}{u_{10}-u_9}N_{9,0} = \begin{cases} 4u-3 & 3/4 \le u < 1 \\ 0 & otherwise \end{cases}$$

$$N_{9,1} = 0$$

$$N_{10,1} = 0$$

Second degree basis functions are as follows:

$$N_{0,2} = 0 \qquad \text{3-7}$$

$$N_{1,2} = \frac{u-u_1}{u_3-u_1}N_{1,1} + \frac{u_4-u}{u_4-u_2}N_{2,1} = \begin{cases} (1-4u)^2 & 0 \le u < 1/4 \\ 0 & otherwise \end{cases}$$

$$N_{2,2} = \frac{u-u_2}{u_4-u_2}N_{2,1} + \frac{u_5-u}{u_5-u_3}N_{3,1} = \begin{cases} 8u(1-4u) & 0 \le u < 1/4 \\ 0 & otherwise \end{cases}$$

$$N_{3,2} = \frac{u-u_3}{u_5-u_3}N_{3,1} + \frac{u_6-u}{u_6-u_4}N_{4,1} = \begin{cases} 16u^2 & 0 \le u < 1/4 \\ (2-4u)^2 & 1/4 \le u < 1/2 \\ 0 & otherwise \end{cases}$$

$$N_{4,2} = \frac{u-u_4}{u_6-u_4}N_{4,1} + \frac{u_7-u}{u_7-u_5}N_{5,1}$$

$$= \begin{cases} -24u^2 + 20u - \frac{7}{2} & \frac{1}{4} \le u < 1/2 \\ 8u^2 - 12u + \frac{9}{2} & \frac{1}{2} \le u < 3/4 \\ 0 & othrwise \end{cases}$$

$$N_{5,2} = \frac{u-u_5}{u_7-u_5}N_{5,1} + \frac{u_8-u}{u_8-u_6}N_{6,1}$$

$$= \begin{cases} 8u^2 - 4u + \frac{1}{2} & \frac{1}{4} \le u < 1/2 \\ -24u^2 + 24u - \frac{15}{2} & \frac{1}{2} \le u < 3/4 \\ 0 & othrwise \end{cases}$$

$$N_{6,2} = \frac{u-u_6}{u_8-u_6}N_{6,1} + \frac{u_9-u}{u_9-u_7}N_{7,1} = \begin{cases} (4u-2)^2 & 1/2 \le u < 3/4 \\ (4-4u)^2 & 3/4 \le u < 1 \\ 0 & otherwise \end{cases}$$

$$N_{7,2} = \frac{u-u_7}{u_9-u_7}N_{7,1} + \frac{u_{10}-u}{u_{10}-u_8}N_{8,1}$$

$$= \begin{cases} -32u^2 + 56u - 24 & 3/4 \le u < 1 \\ 0 & otherwise \end{cases}$$

$$N_{8,2} = \frac{u-u_8}{u_{10}-u_8}N_{8,1} + \frac{u_{11}-u}{u_{11}-u_9}N_{9,1}$$

$$= \begin{cases} (4u-3)^2 & 3/4 \le u < 1 \\ 0 & otherwise \end{cases}$$

$N_{9,2}$=0

Third degree basis functions are as follows:

$$N_{0,3} = \frac{u-u_0}{u_3-u_0}N_{0,2} + \frac{u_4-u}{u_4-u_1}N_{1,2} = \begin{cases} (1-4u)^3 & 0 \le u < 1/4 \\ 0 & otherwise \end{cases} \quad 3\text{-}8$$

$$N_{1,3} = \frac{u-u_1}{u_4-u_1}N_{1,2} + \frac{u_5-u}{u_5-u_2}N_{2,2} = \begin{cases} 192u^3 - 96u^2 + 12u & 0 \le u < 1/4 \\ 0 & otherwise \end{cases}$$

$$N_{2,3} = \frac{u-u_2}{u_5-u_2}N_{2,2} + \frac{u_6-u}{u_6-u_3}N_{3,2}$$

$$= \begin{cases} -160u^3 + 48u^2 & 0 \le u < 1/4 \\ -32u^3 + 48u^2 - 24u + 4 & \frac{1}{4} \le u < 1/2 \\ 0 & otherwise \end{cases}$$

$$N_{3,3} = \frac{u-u_3}{u_6-u_3}N_{3,2} + \frac{u_7-u}{u_7-u_4}N_{4,2}$$

$$= \begin{cases} 32u^3 & 0 \le u < \frac{1}{4} \\ 80u^3 - 108u^2 + 45u - \frac{21}{4} & \frac{1}{4} \le u < \frac{1}{2} \\ -16u^3 + 36u^2 - 27u + \frac{27}{4} & \frac{1}{2} \le u < \frac{3}{4} \\ 0 & otherwise \end{cases}$$

$$N_{4,3} = \frac{u-u_4}{u_7-u_4}N_{4,2} + \frac{u_8-u}{u_8-u_5}N_{5,2}$$

$$= \begin{cases} -64u^3 + 72u^2 - 24u + \frac{5}{2} & \frac{1}{4} \le u < \frac{1}{2} \\ 64u^3 - 120u^2 + 72u - \frac{27}{2} & \frac{1}{2} \le u < \frac{3}{4} \\ 0 & otherwise \end{cases}$$

$$N_{5,3} = \frac{u-u_5}{u_8-u_5}N_{5,2} + \frac{u_9-u}{u_9-u_6}N_{6,2}$$

$$= \begin{cases} 16u^3 - 12u^2 + 3u - \frac{1}{4} & \frac{1}{4} < u < \frac{1}{2} \\ -80u^3 + 132u^2 - 69u + \frac{47}{4} & \frac{1}{2} \le u < \frac{3}{4} \\ -32u^3 + 96u^2 - 96u + 32 & \frac{3}{4} \le u < 1 \\ 0 & otherwise \end{cases}$$

$$N_{6,3} = \frac{u-u_6}{u_9-u_6}N_{6,2} + \frac{u_{10}-u}{u_{10}-u_7}N_{7,2}$$

$$= \begin{cases} 32u^3 - 48u^2 + 24u - 4 & \frac{1}{2} \le u < \frac{3}{4} \\ 160u^3 - 432u^2 + 384u - 112 & \frac{3}{4} \le u < 1 \\ 0 & otherwise \end{cases}$$

$$N_{7,3} = \frac{u-u_7}{u_{10}-u_7}N_{7,2} + \frac{u_{11}-u}{u_{11}-u_8}N_{8,2}$$

$$= \begin{cases} -192u^3 + 480u^2 - 396u + 108 & 3/4 \le u < 1 \\ 0 & otherwise \end{cases}$$

$$N_{8,3} = \frac{u-u_8}{u_{11}-u_8}N_{8,2} + \frac{u_{12}-u}{u_{12}-u_9}N_{9,2} = \begin{cases} (4u-3)^3 & 3/4 \le u < 1 \\ 0 & otherwise \end{cases}$$

Combining all the basis functions corresponding to each interval, the general form of the curve is achieved. The general representation of the curve is defined as follows:

$$c(u) = \begin{cases} N_{0,3}P_0 + N_{1,3}P_1 + N_{2,3}P_2 + N_{3,3}P_3 & 0 \le u < \frac{1}{4} \\ N_{2,3}P_2 + N_{3,3}P_3 + N_{4,3}P_4 + N_{5,3}P_5 & \frac{1}{4} \le u < \frac{1}{2} \\ N_{3,3}P_3 + N_{4,3}P_4 + N_{5,3}P_5 + N_{6,3}P_6 & \frac{1}{2} \le u < \frac{3}{4} \\ N_{5,3}P_5 + N_{6,3}P_6 + N_{7,3}P_7 + N_{8,3}P_8 & \frac{3}{4} \le u < 1 \end{cases} \quad \text{3-9}$$

N_{mixed} is defined as follows:

$$\begin{bmatrix} N_{0,3} & N_{1,3} + N_{2,3} + N_{3,3} & 0 & 0 & 0 \\ 0 & N_{2,3} + N_{3,3} & N_{4,3} & N_{5,3} & 0 \\ 0 & N_{3,3} & N_{4,3} & N_{5,3} + N_{6,3} & 0 \\ 0 & 0 & N_{5,3} + N_{6,3} + N_{7,3} & N_{8,3} & 0 \end{bmatrix} \quad \text{3-10}$$

A set of the control points has to be defined in a way that makes the first segment of the curve linear. In order to do that, using strong convex hull property of the B-splines proves that multiplication of control points make the segment linear.

3.3.1.3.1 Strong convex hull property

The curve is contained in the convex hull of its control polygon If $u \in [u_i, u_{i+1})$ and $p \leq i < m - p - 1$, then $C(u)$ is in the convex hull of the control points $P_{i-p}, \ldots\ldots, P_i$. For the case that has been discussed above it's been shown:

$$p(=3) \leq i = 3 < m(=13) - p(=3) - 1$$

$$3 \leq 3 < 9$$

Therefor $u \in [u_3, u_4)$ and it means $u \in \left[0, \frac{1}{4}\right)$.

Using strong convex hull property the curve when $u \in \left[0, \frac{1}{4}\right)$ should be contained in the convex hull of its control polygon. $P_0, P_1, P_2 \; and \; P_3$ Are making the control polygon and as long as $P_1, P_2 \; and \; P_3$ are the same points, the curve is subjected to be a straight line for $u \in [u_3, u_4)[40]$.

By choosing the control points as:

$$P = \{(0,0), (2,-2), (2,-2), (2,-2), (3,-3), (4,-2), (4,-2), (4,-2), (6,0)\}$$

The curve becomes as shown in Figure 3-8:

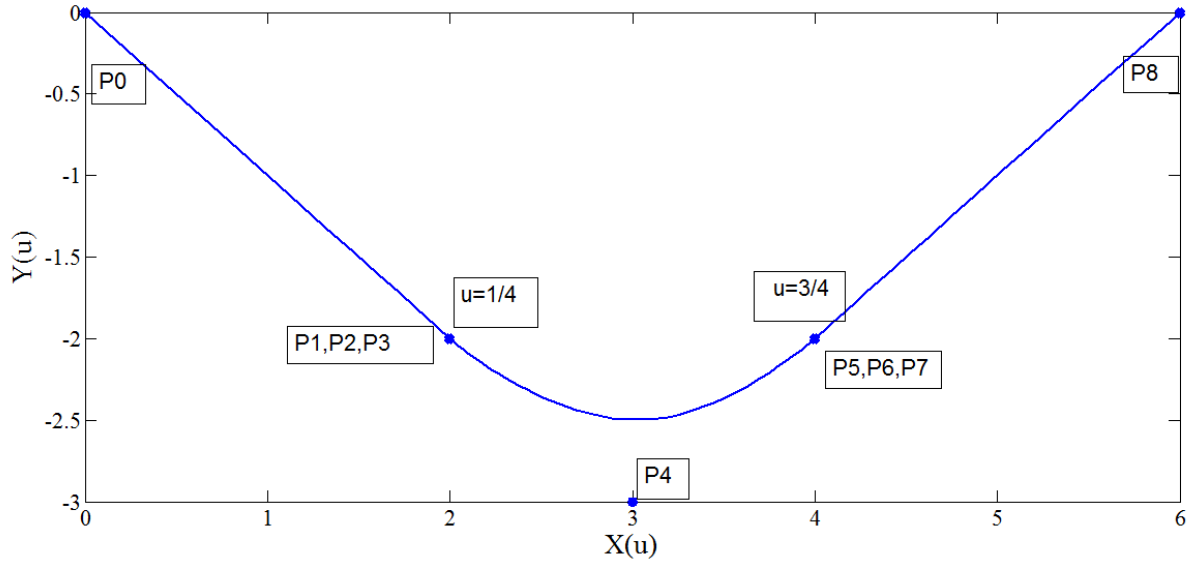

Figure 3-8: The position of control points on the B-spline

Multiplicity of the knots at *u=1/4* and *u=3/4* makes the first derivative of the B-spline P_1 and P_6 non continuous at It means choosing another set of control points which doesn't make the curve symmetric may make the first derivative of the curve at *u=1/4* and *u=3/4* non continuous as shown in Figure 3-9.

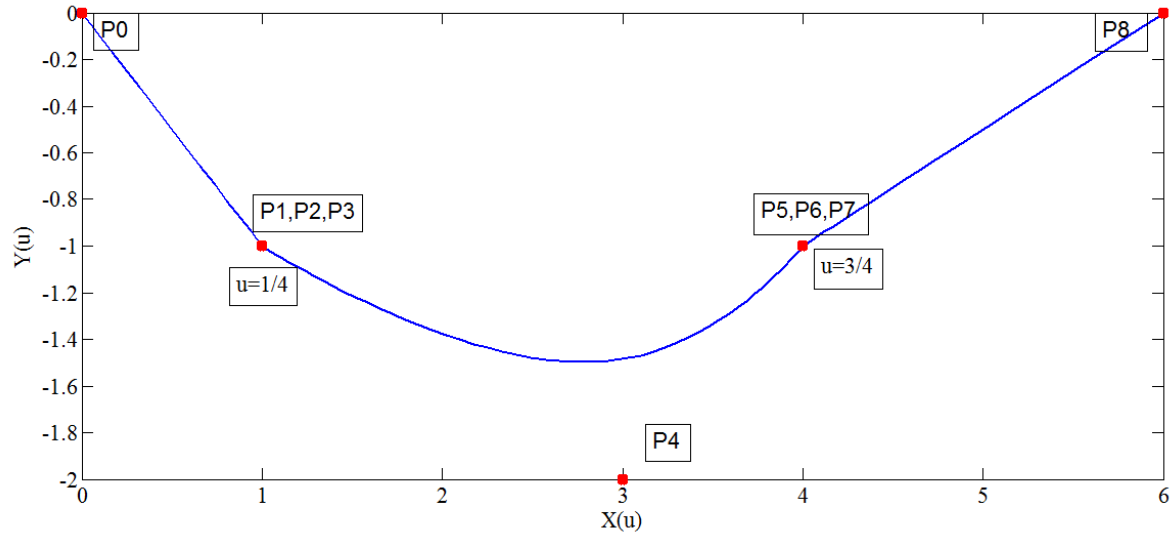

Figure 3-9: Dependency of first derivative of the curve on the location of P_4

The position of P_4 plays an important role on continuity of the first derivative at indicated knots.

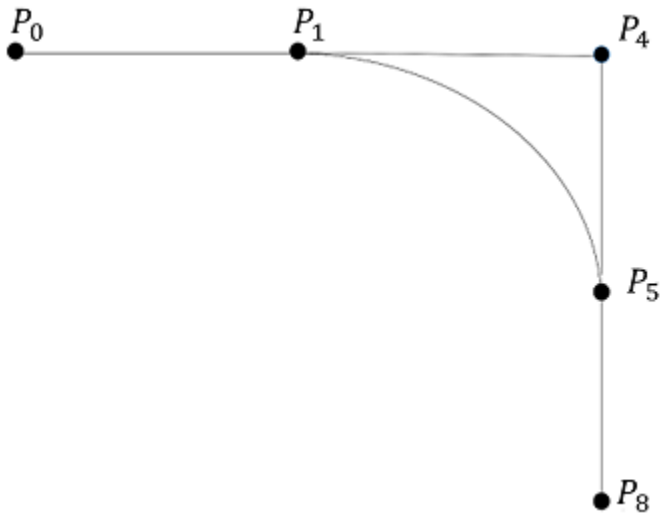

Figure 3-10: Position of control points on the curve and dependency of first derivative continuity on position of P_4

As shown in Figure 3-10, If the slope of P_0P_1 is equal to the slope of P_1P_4 and the slope of P_5P_8 is equal to the slope ofP_4P_5, the first derivative of the curve at the indicated knots is continuous. Applying the above condition, the coordinate of P_4 is a function of P_0, P_1, P_5 and P_8 :

$$m_{\overline{P_0P_1}} = m_{\overline{P_1P_4}} \qquad 3\text{-}11$$

$$m_{\overline{P_4P_5}} = m_{\overline{P_5P_8}} \qquad 3\text{-}12$$

The following conditions lead to find the position of the P_4 as a function of P_0, P_1, P_5 and P_8.

Figure 3-11 and Figure 3-12 Show the incrementally changing the position of the P_1 in x and y direction and dynamically changing P_4 to keep the first derivative of the curve continuous.

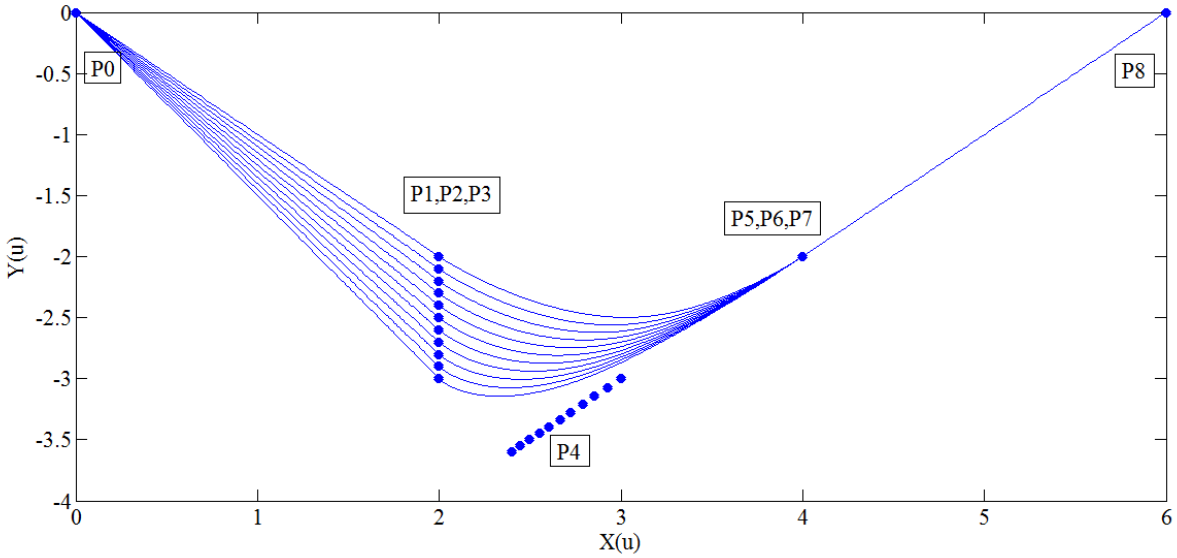

Figure 3-11: Dynamic change of location of P_4 based on incremental change in y coordinate of P_1

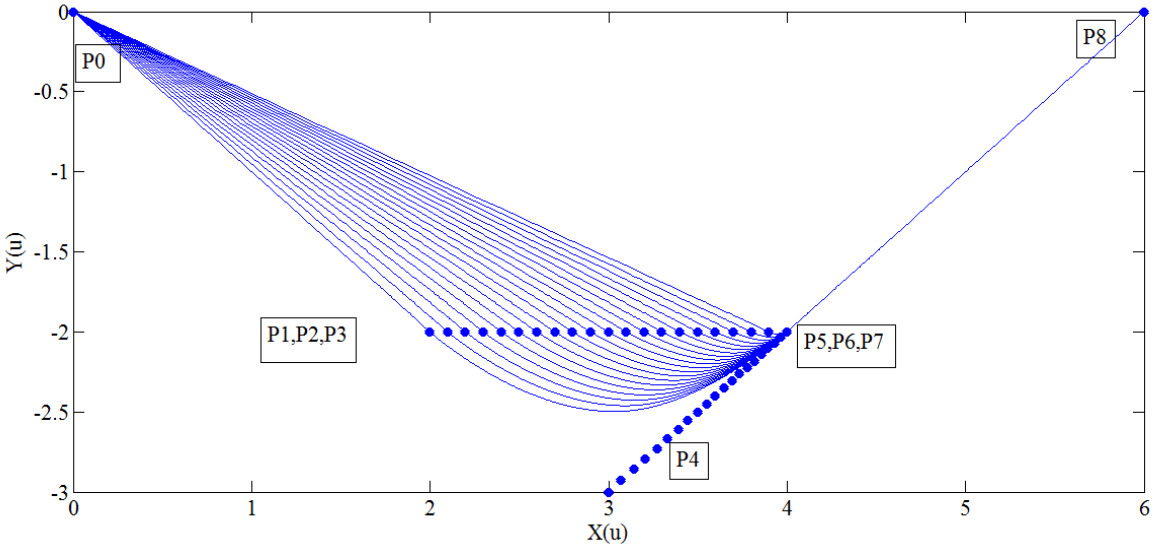

Figure 3-12: Dynamic change of location of P_4 based on incremental change in x coordinate of P_1

Figure 3-13 and Figure 3-14 Show the incrementally changing the position of the P_5 in x and y direction and dynamically changing P_4 to keep the first derivative of the curve continuous.

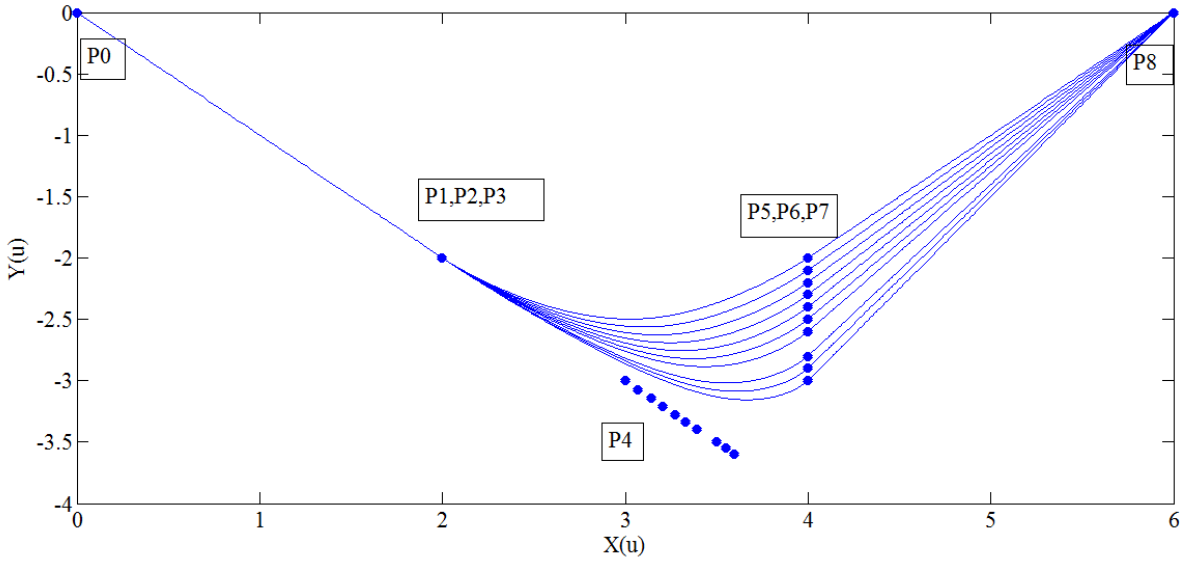

Figure 3-13: Dynamic change of location of P_4 based on incremental change in y coordinate of P_5

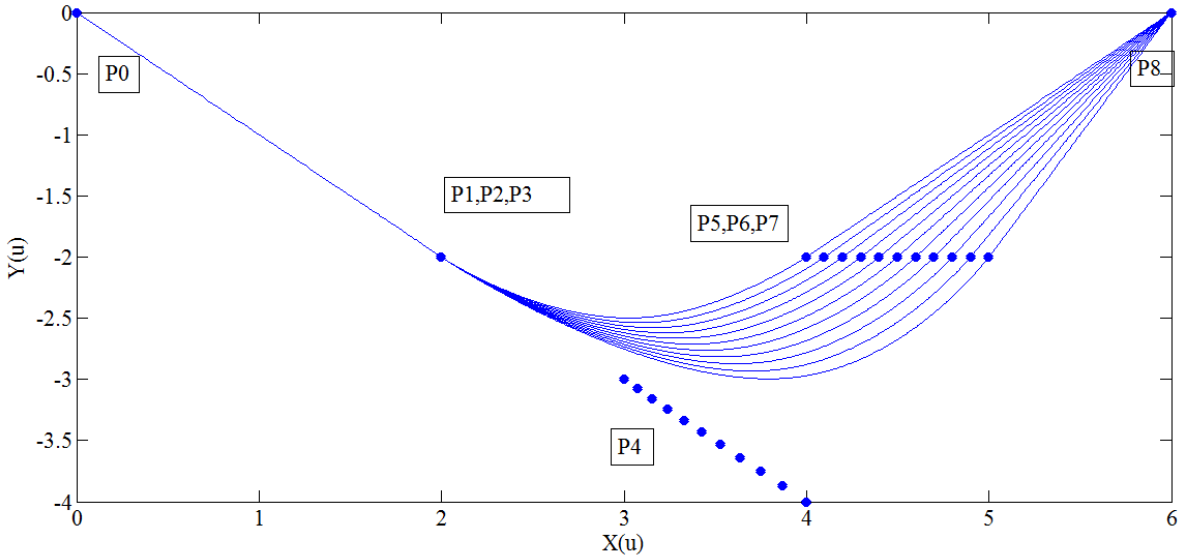

Figure 3-14: Dynamic change of location of P_4 based on incremental change in x coordinate of P_5

3.4 B-spline Curve Modeling Using Total Least Square Fitting

If we want to interpolate the points with the p-th degree B-Spline curve, we can set a value of $\bar{u}_k$ to each $CData_k$ .Choosing a proper knot vector as it was explained in the previous section we can set up the $(n+1)\times(n+1)$ system of linear equations as follows:

$$CData_k = C(\bar{u}_k) = \sum_{i=0}^{n} N_{i,p}(\bar{u}_k)P_i \qquad 3\text{-}13$$

The number of control points are $(n+1)$ and all of them are unknown. Choosing the knot vector has been done in previous section. Substitution of $CData_k$ in the above formula will lead to the following system of linear equation:

$$[N_{mixed}][P] = [CData] \qquad 3\text{-}14$$

Where $CData$'s are the data points and the P's are the control points and $[N_{mixed}]$ is the mixed basis function from equation 3-10.

Processing every picture of the cusps will approximately give around 15000-20000 points on the profile border. Considering that, the number of the points on the B-spline could be determined. The number of the points on the B-spline are more than the number of the captured points due using small steps for u . The closest points of the B-spline to the actual points are found using minimum Euclidian distance as shown in Figure 3-15. Using this approach the closest point on the B-spline to each actual point is found.

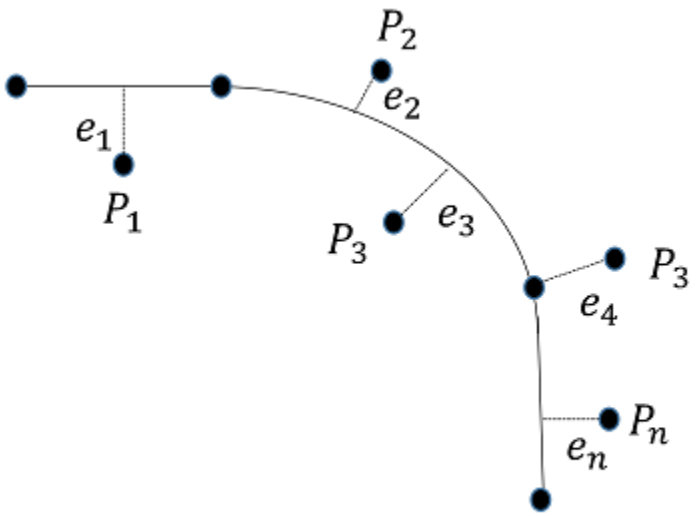

Figure 3-15: Euclidian distance of actual points from the B-spline

The fitting error can be calculated as follows:

$$Fitting\ error = \sqrt{\sum_{i=1}^{n} e_i^2} \qquad 3\text{-}15$$

After finding the closest points on the B-spline to the actual points the actual points are fitted to the B-spine using total least square method.

3.4.1 Total Least Square Method

Total least square is a fitting method that is proper to use when errors exist in the both of measured vectors(x direction and y direction) [40-42]. Figure 3-16 illustrates the difference between a typical least square fitting and total least square fitting. As it can be seen, least square fitting of a line segment to data points only minimizes the sum of square of the distances of all the data points along the Y-axis to the fitted line, while, the total least square fitting of a line segment to data points minimizes the sum of square of Euclidean distances of all the data points to the fitted line.

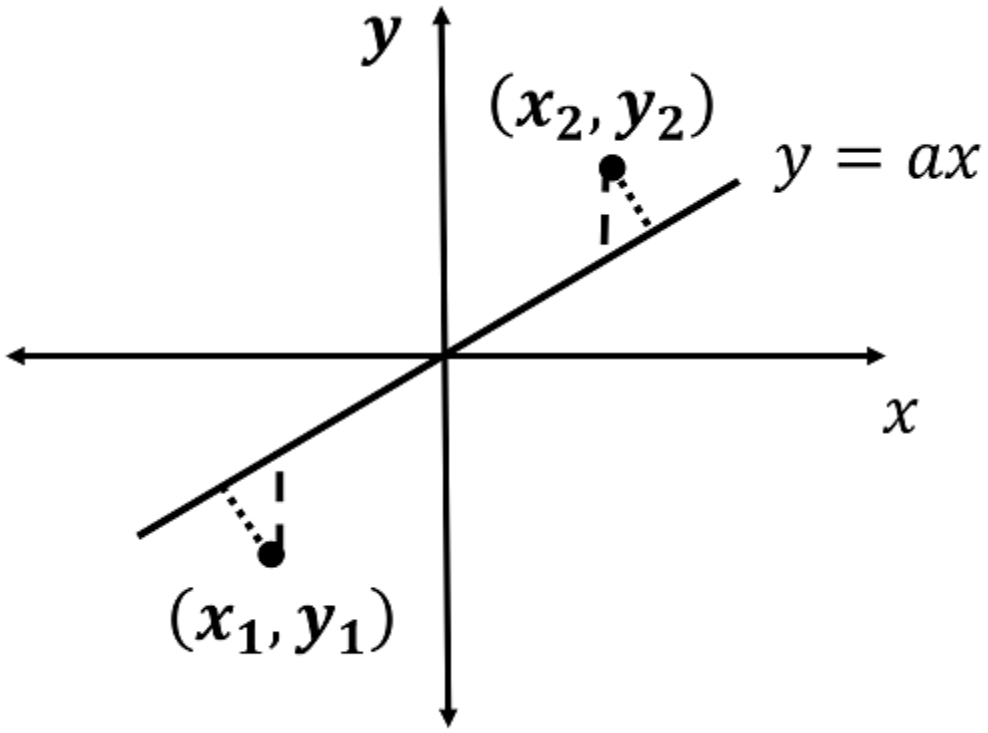

Figure 3-16: Total Least squares versus Least Squares

If we have:

$$N_{mixed} \times [CP] \approx [CData] \qquad 3\text{-}16$$

Where N_{mixed} is the mixed basis functions for the closest points to the actual points, CP's are the answers for the total least squares problem and CData is the x and y components of the actual points. N_{mixed} is a $m \times 5$ matix since there are 5 main control points to determine the B-spline main shape and the 5th point is a function of other control points. m is the number of points that is given by the surface topography measurement device.

3.4.1.1 Computation of the Total Least Squares Using Singular Value Decomposition

The total least square is an approximation to the 3-16 and the objective is to find the CPs that minimizes the error matrices ΔN_{mixed} and $\Delta CData$ for N_{mixed} and CData respectively, where $\Delta N_{mixed}$and $\Delta CData$ are defined as follows [43]:

$$[N_{mixed} + \Delta N_{mixed}]X = CData + \Delta CData \qquad 3\text{-}17$$

N_{mixed} is a m× k matrix and $CData$ is a m× n matrix.

Total least square problem is looking for the minimum ΔN_{mixed} and $\Delta CData$ (in the Frobenius form[40, 44])which makes the equation 3-17 solvable.

$$\arg\ min_{\Delta CData, \Delta N_{mixed}} \|[\Delta N_{mixed}\ \Delta CData]\|_F \qquad 3\text{-}18$$

Equation 3-17 can be written as follows:

$$[(N_{mixed} + \Delta N_{mixed})(CData + \Delta CData)] \begin{bmatrix} X \\ -I_n \end{bmatrix} = 0 \qquad 3\text{-}19$$

Where I_n is the identity matrix with size of n.

The Purpose is to find $[\Delta N_{mixed},\ \Delta CData]$ that reduces the rank of $[N_{mixed} \quad CData]$ by n. The singular value decomposition of the augmented matrix $[N_{mixed} \quad CData]$ is defined as follows:

$$[N_{mixed} \quad CData] = [U][\Sigma][V^*]$$

Where U is a unitary matrix, Σ is a rectangular diagonal matrix which has non-negative numbers on diagonal and $V^*$is transpose of V when V is a unitary matrix.

Based on definition of Singular Value Decomposition, we have:

$$[N_{mixed} \quad CData] = [U_x \quad U_y]\begin{bmatrix}\Sigma_X & 0\\ 0 & \Sigma_Y\end{bmatrix}\begin{bmatrix}V_{XX} & V_{XY}\\ V_{YX} & V_{YY}\end{bmatrix}^* \qquad 3\text{-}20$$
$$= [U_X \quad U_Y]\begin{bmatrix}\Sigma_X & 0\\ 0 & \Sigma_Y\end{bmatrix}\begin{bmatrix}V_{XX}^* & V_{YX}^*\\ V_{XY}^* & V_{YY}^*\end{bmatrix}$$

Where *V* is partitioned into blocks corresponding to the shape of *X* and *Y*.

Using the Eckart-Young theorem, the approximation minimising the norm of the error is such that matrices *U* and *V* are unchanged, while the *n*-smallest singular values is substituted with zeroes [45] :

$$[(N_{mixed} + \Delta N_{mixed})(CData + \Delta CData)] \qquad 3\text{-}21$$
$$= [U_X \quad U_Y]\begin{bmatrix}\Sigma_X & 0\\ 0 & 0_{n\times n}\end{bmatrix}\begin{bmatrix}V_{XX} & V_{XY}\\ V_{YX} & V_{YY}\end{bmatrix}^*$$

Therefore, based on linearity we have:

$$[\Delta N_{mixed} \quad \Delta CData] = -[U_X \quad U_Y]\begin{bmatrix}0_{k\times k} & 0\\ 0 & \Sigma_Y\end{bmatrix}\begin{bmatrix}V_{XX} & V_{XY}\\ V_{YX} & V_{YY}\end{bmatrix}^* \qquad 3\text{-}22$$

Removing blocks from *U* and Σ matrices and simplifying equation 3-22 will lead to:

$$[\Delta N_{mixed} \quad \Delta CData] = -U_Y \Sigma_Y \begin{bmatrix} V_{XY} \\ V_{YY} \end{bmatrix}^* \qquad \text{3-23}$$

$$= -[N_{mixed} \quad CData] \begin{bmatrix} V_{XY} \\ V_{YY} \end{bmatrix} \begin{bmatrix} V_{XY} \\ V_{YY} \end{bmatrix}^*$$

From the above equation, we have:

$$[(N_{mixed} + \Delta N_{mixed})(CData + \Delta CData)] \begin{bmatrix} V_{XY} \\ V_{YY} \end{bmatrix} = 0 \qquad \text{3-24}$$

Based on above equation, it's obvious that if V_{YY} is non-singular, the both sides of above equation could be multiplied by $-V_{YY}^{-1}$ as follows:

$$[(N_{mixed} + \Delta N_{mixed})(CData + \Delta CData)] \begin{bmatrix} -V_{XY}V_{YY}^{-1} \\ V_{YY}V_{YY}^{-1} \end{bmatrix} \qquad \text{3-25}$$

$$= [(N_{mixed} + \Delta N_{mixed})(CData + \Delta CData)] \begin{bmatrix} X \\ -I_n \end{bmatrix}$$

$$= 0$$

The X is solution to the total least square problem and finding X means the CPs are found and it basically means the 5th control point for making the appropriate B-spline is found. The observations shows that the coordinates of the 5th control point is not a function of $m_{\overline{P_0P_4}}$ and $m_{\overline{P_5P_8}}$ and it means that the B-spline is C^0continuous but not C^1 continues. This issue is being resolved by calculating P_4 based on Equation 3-11 and Equation 3-12 and then switching that new point with the point that has been calculated using Total least squares till the error (d) is the minimized. The process is shown in Figure 3-17.

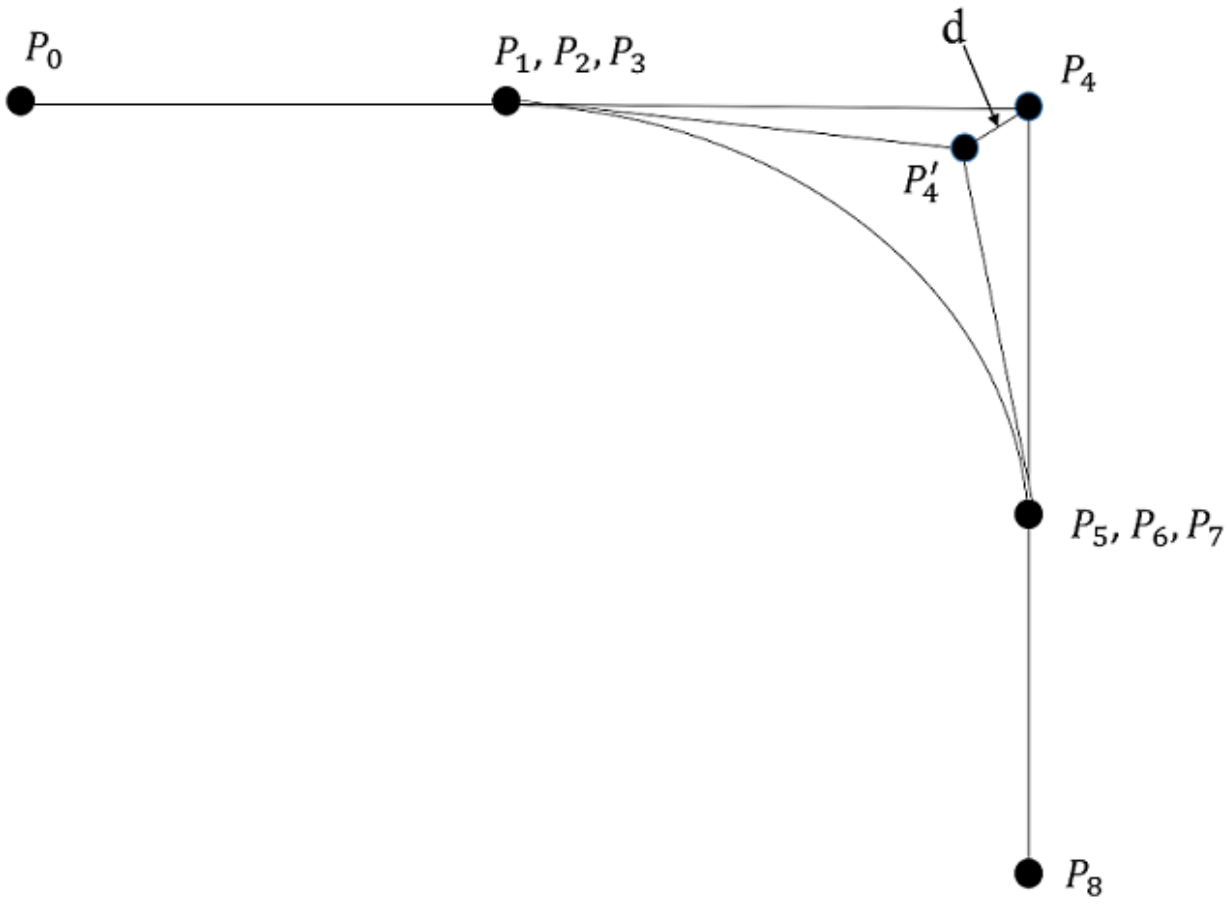

Figure 3-17: Minimizing the distance between P_4 and P_4'

3.5 B-spline Curve Modeling Using Genetic Algorithm

The fitting method presented in the previous section can find the best possible model if the associated *u*-values of the data points are estimated adequately. The method presented in this section uses genetic algorithm to find the best three portions of the data points suitable for the three segments of the curve. The result of the previous section is used as the initial guess for the genetic algorithm. The genetic algorithm uses the five output points of the total least squares method.

Based on the empirical observation, increasing the number of generations don't make the error less significant and the going to 10^{th} generation gives a very less fitting error comparing to total least squares results. The objective function for the genetic algorithm is the euclidean distance of the measured points to the fitted points:

$$Objective\ function = \sqrt{\sum_{i=1}^{n} e_i^2} \qquad 3\text{-}26$$

3.6 Three Piece Curve Fitting Including a third Degree Polynomial Curve and Genetic Algorithm

Variety of analyses were contacted and from what has been reviewed it's more likely accurate enough to model each cusp with two straight lines at the two ends and a second or third degree polynomial as the middle piece. This assumption could be implemented by dividing the entire set of data points into three groups and use each group to fit the best three representative pieces of curves. The entire data points belonging to a cusp is defined by the user. User picks the first and the last data points belonging to the profile. An algorithm is developed for best grouping of the data points and to fit each group to the best possible polynomial model. The algorithm finds the best point number two and point number three and also the best coefficients of the three polynomials. Nested in this algorithm two optimization process are conducted to optimally find the three groups and fit the best curves to them. Their objective function is to minimize the total fitting error of the three pieces to the actual measured data points.

The entire set of data points is constant during the optimization process. They are defined by the user at the beginning of the process by selecting the first and the last

points belonging to the profile. Also it can be shown that the minor changes in the range of data do not significantly affect the optimization result. The two middle data points separating the three groups are dynamically changed during the process according to the evaluated fitting in its smallest possible value.

Figure 3-18 shows a schematic representation of the initial four indexed points specifying the three groups and their upper and lower boundary points specifying the search constrains.

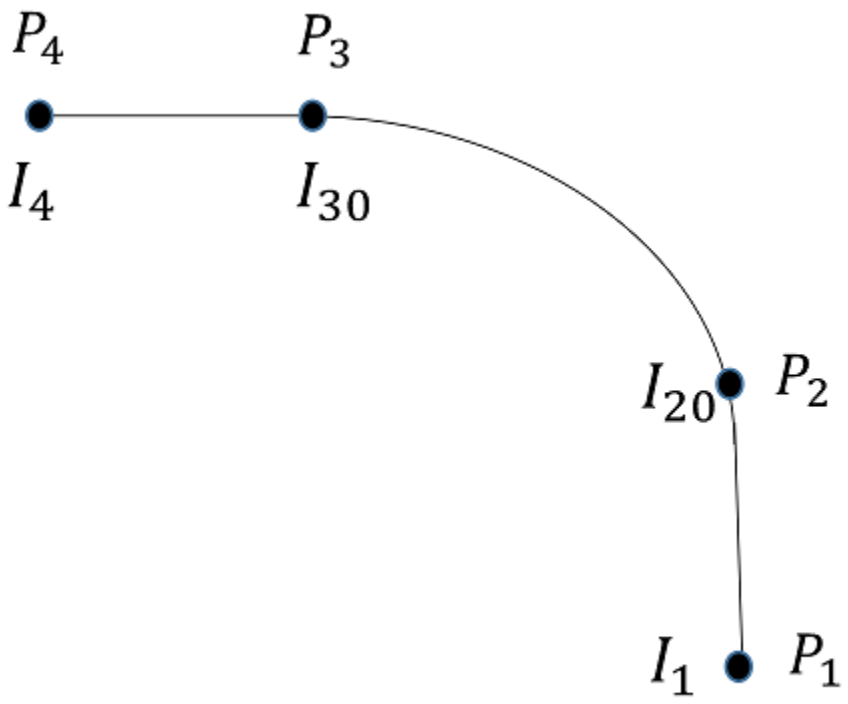

Figure 3-18: Initial four points for starting the genetic algorithm

3.7 Three Piece Curve Fitting Including second degree Polynomial Curve and Genetic Algorithm

A system of equations is made based on the specific geometry as follows:

For the first line segment we have:

$$\begin{cases} ax_1 + b = y_1 \\ ax_2 + b = y_2 \end{cases} \quad \text{3-27}$$

For the third degree polynomial section we have:

$$\begin{cases} cx_2^3 + dx_2^2 + ex_2 + f = y_2 \\ 3cx_2^2 + 2dx_2 + e - a = 0 \\ 3cx_3^2 + 2dx_3 + e - g = 0 \\ cx_3^3 + dx_3^2 + f = y_3 \end{cases} \quad \text{3-28}$$

The second and the third equations in 3-27 are to satisfy the continuity of the first derivatives of the three curves at their intersection points. However, their effect can be enhance by applying a weight factor to these equations. A weight factor equal to 20% of the number of data points typically produced a good fitting result in our experiments.

For the second linear piece we have:

$$\begin{cases} gx_3 + h = y_3 \\ gx_4 + h = y_4 \end{cases} \quad \text{3-29}$$

Combining all three systems of equations leads to the following matrix:

$$\begin{bmatrix} x_1 & 1 & 0 & 0 & 0 & 0 & 0 & 0 \\ x_2 & 1 & 0 & 0 & 0 & 0 & 0 & 0 \\ 0 & 0 & x_2^3 & x_2^2 & x_2 & 1 & 0 & 0 \\ -1 & 0 & 3x_2^2 & 2x_2 & 1 & 0 & 0 & 0 \\ 0 & 0 & 3x_3^2 & 2x_3 & 1 & 0 & -1 & 0 \\ 0 & 0 & 0 & 0 & 0 & 0 & x_3 & 1 \\ 0 & 0 & 0 & 0 & 0 & 0 & x_4 & 1 \end{bmatrix} \begin{bmatrix} a \\ b \\ c \\ d \\ e \\ f \\ g \\ h \end{bmatrix} = \begin{bmatrix} y_1 \\ y_2 \\ y_2 \\ \emptyset \\ \emptyset \\ y_3 \\ y_3 \\ y_4 \end{bmatrix} \quad \text{3-30}$$

The above system could be written as follows:

$$AC = B \qquad 3\text{-}31$$

And using Total Least Squares the Matric C is achieved.

After finding the coefficients matrix, the genetic algorithm is implemented and starts searching between I_1 to I_{20} , I_{20} to I_{30} and I_{30} to I_4 to find the optimal solution using minimizing the following objective function:

$$Objective\ function = \sqrt{\sum_{i=1}^{n} e_i^2} \qquad 3\text{-}32$$

Where e_i is the deviation of each actual point from its corresponding point on the fitted curve. Figure 3-19 shows the fitted curve using third degree polynomial and 2 line pieces.

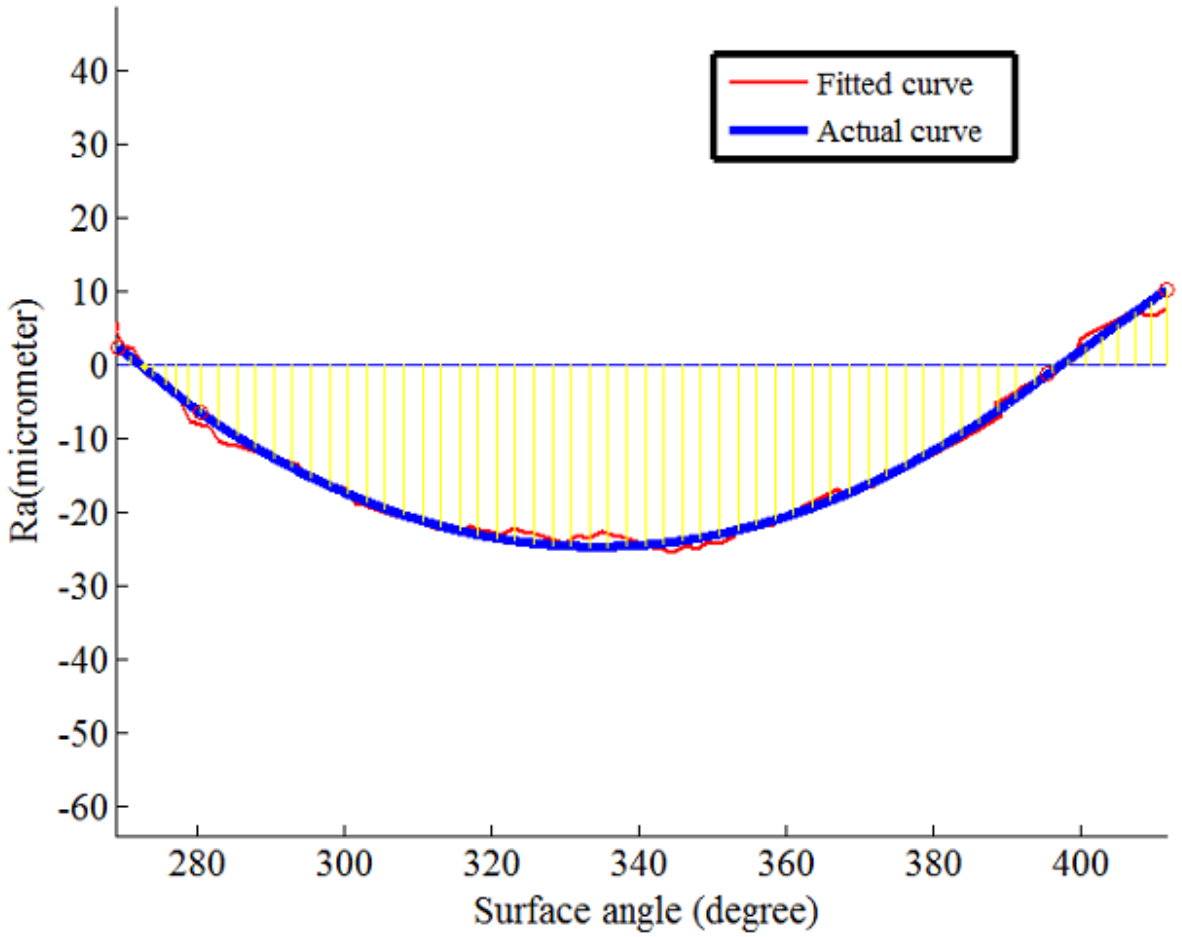

Figure 3-19: An example of fitted curve using third degree polynomial and 2 line pieces

3.8 Fitting Data Points Using Two Line Pieces and a Second Degree polynomial

For a better understanding of the exact geometry of the cusp, the last assumption for the cusp geometry is 2 line pieced at two ends and a second degree polynomial in the middle. This geometry can be modeled as follows:

For the first line segment we have:

$$\begin{cases} ax_1 + b = y_1 \\ ax_2 + b = y_2 \end{cases}$$

For thesecond degree polynomial section we have:

$$\begin{cases} cx_2^2 + dx_2 + e = y_2 \\ 2cx_2 + d - a = 0 \\ 2cx_3 + d - f = 0 \\ x_3^2 + dx_3 + e = y_3 \end{cases}$$

For the second linear piece we have:

$$\begin{cases} fx_3 + g = y_3 \\ fx_4 + g = y_4 \end{cases}$$

$$\begin{bmatrix} x_1 & 1 & 0 & 0 & 0 & 0 & 0 \\ x_2 & 1 & 0 & 0 & 0 & 0 & 0 \\ 0 & 0 & x_2^2 & x_2 & 1 & 0 & 0 \\ 0 & 0 & x_3^2 & x_3 & 1 & 0 & 0 \\ -1 & 0 & 2x_2 & 0 & 1 & 0 & 0 \\ 0 & 0 & 2x_3 & 1 & 0 & -1 & 0 \\ 0 & 0 & 0 & 0 & 0 & x_3 & 1 \\ 0 & 0 & 0 & 0 & 0 & x_4 & 1 \end{bmatrix} \begin{bmatrix} a \\ b \\ c \\ d \\ e \\ f \\ g \end{bmatrix} = \begin{bmatrix} y_1 \\ y_2 \\ y_2 \\ \emptyset \\ \emptyset \\ y_3 \\ y_3 \\ y_4 \end{bmatrix} \qquad 3\text{-}33$$

The above system could be written as follows:

$$AC = B \qquad 3\text{-}34$$

And using total least squares the matric C is achieved.

After finding the coefficients matrix, the genetic algorithm is implemented and starts searching between I_1 to I_{20} , I_{20} to I_{30} and I_{30} to I_4 to find the optimal solution using minimizing the following objective function:

$$Objective\ function = \sqrt{\sum_{i=1}^{n} e_i^2} \quad \text{3-35}$$

Where $e_i$is the deviation of each actual point from its corresponding point on the fitted curve.

3.9 Surface Roughness Measurement

The average surface roughness (Ra) is calculated based on its standard definition using the definition of the total least squares centre line[46]. Figure 3-20 presents a schematic of the profile and the way that the surface roughness is calculated using three areas of A_1, A_2, and A_3.

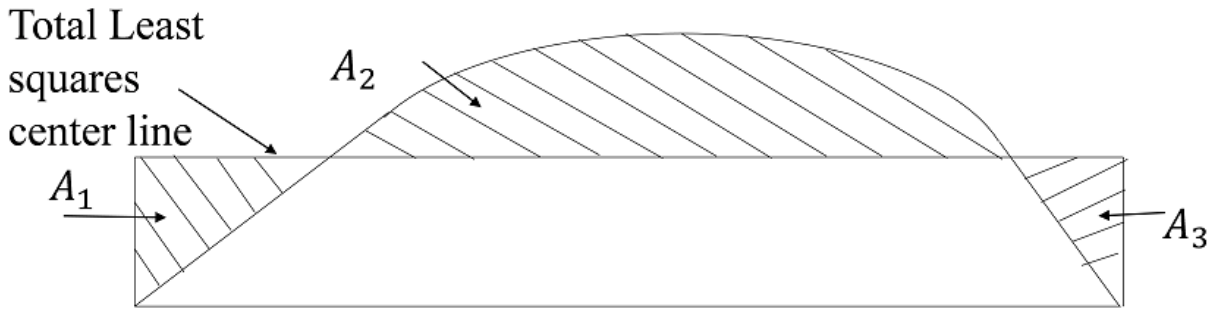

Figure 3-20: Schematic of surface roughness measurement

The measured surface roughness is calculated as follows:

$$R_a = \frac{1}{l}\int |f(x)dx| \qquad 3\text{-}36$$

$$|f(x)dx| = A_1 + A_2 + A_3 \qquad 3\text{-}37$$

$$l = \overline{P_1 P_4} \qquad 3\text{-}38$$

Where P_1 is the start point of the curve and P_4 is the end point of the curve.

Based on the conducted surface profile investigation a schematic was constructed to show the model of surface roughness of the part processes in FDM as shown in Figure 3-20

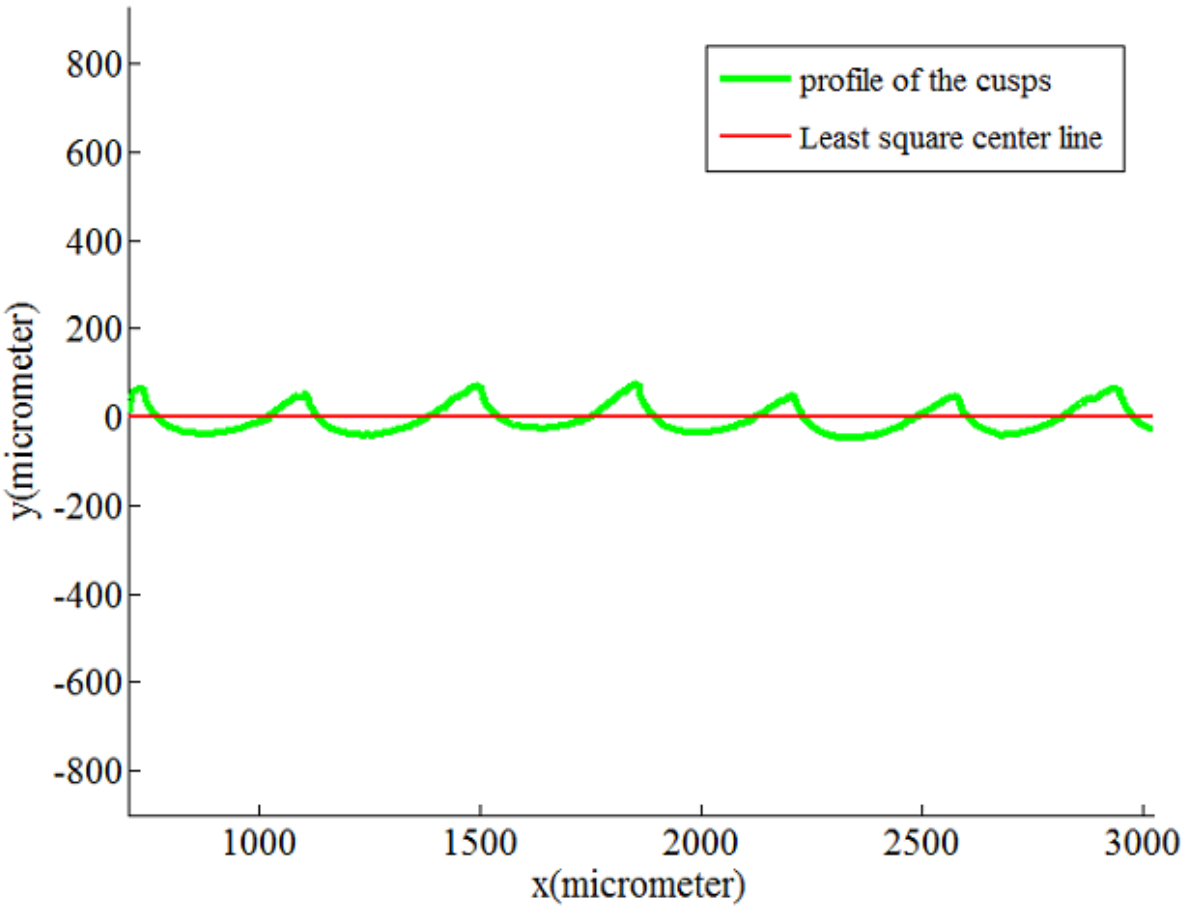

Figure 3-21: Total least squares centre line and the profile roughness measurement

3.10 Undetermined Region

As the surface angle decreases, two adjacent cusp profiles separate and this separation unveils the sub-layer of the current profile as shown in Figure 3-22. As the surface angle increases the undetermined region disappears. The surface angle in which the undetermined region disappears is called critical surface angel [28]. Figure 3-22 shows the undetermined region for a FDM surface with 5 degrees slope.

Figure 3-23 shows how the undetermined regions disappear for a 25 degrees FDM surface.

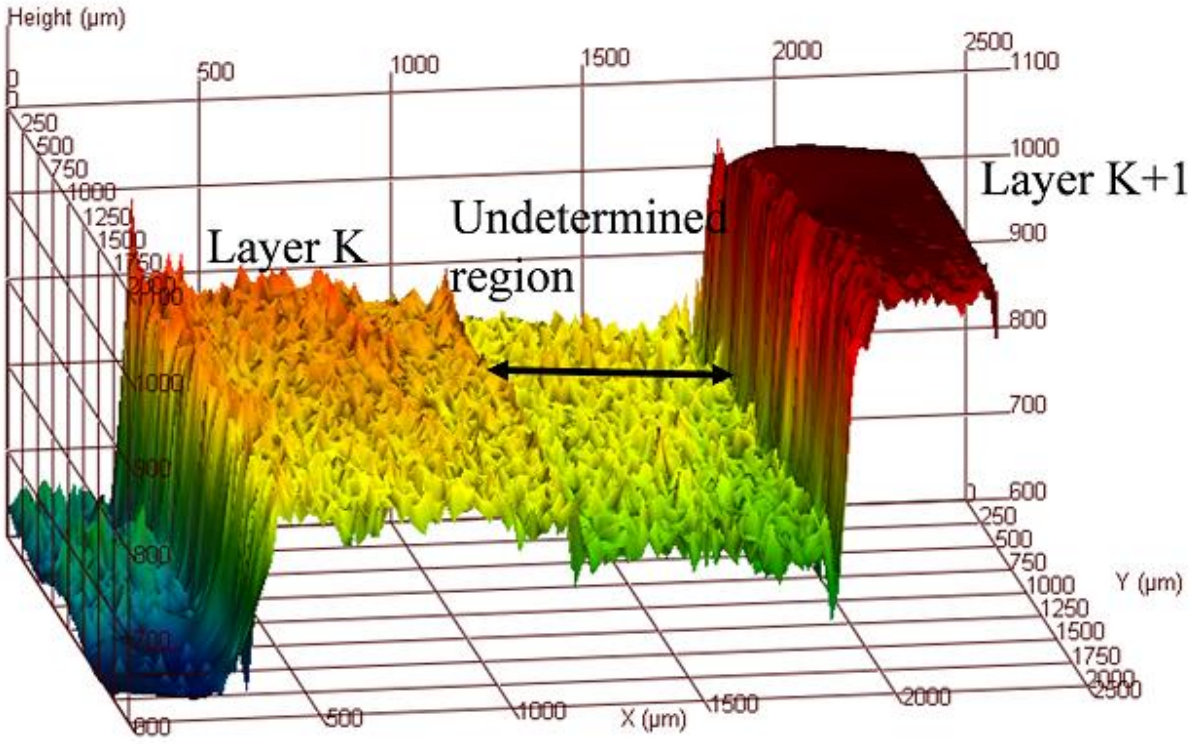

Figure 3-22: Undetermined region for surface angle of 5° and layer thickness of 250 microns

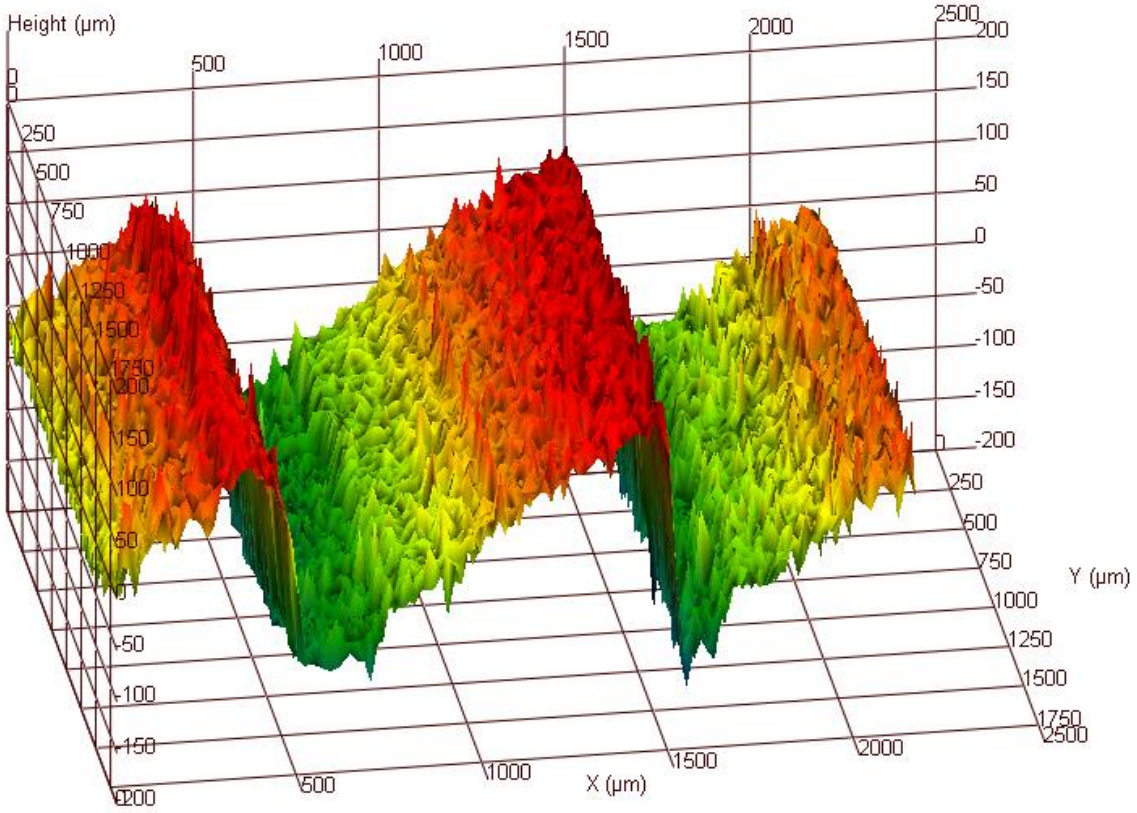

Figure 3-23: Undetermined region disappears for upper surface angles (25°), layer thickness of 250 microns

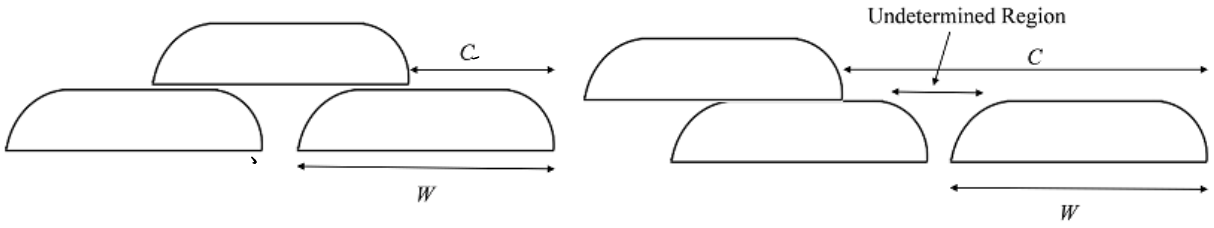

Figure 3-24: Non-undetermined region and undetermined region

If the horizontal distance of a cusp in layer k from the cusp in layer k+1 is C, using the basic trigonometry presented in Figure 3-24 C can be calculated as follows:

$$C = \frac{Layer\ thickness}{\tan(\alpha)} = \frac{l}{\tan(\alpha)} \quad 3\text{-}39$$

Where, α is the desired slope of the fabricated surface.

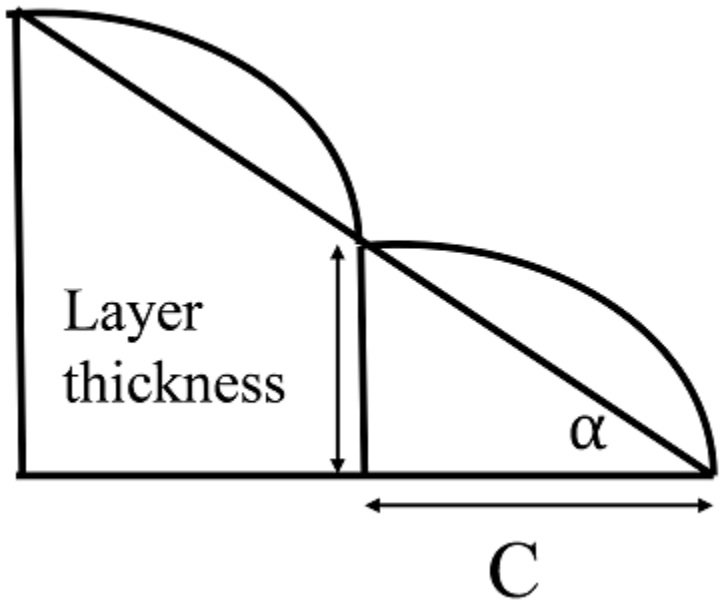

Figure 3-25: The horizontal distance of cusps

According to Figure 3-24, if $W < C$, the undetermined region is unveiled. α_t , critical angle for the given layer thickness, t, can be calculated as follows:

$$\alpha_t = tan^{-1}(\frac{t}{W}) \quad 3\text{-}40$$

Substituting the nominal width of the machine in Equation 3-1 will give us critical angle for any specific layer thickness.

Figure 3-25 shows the horizontal distance of the cusps in a FDM product.

Table 3-2: Nominal extrusion width for every specific layer thickness

Layer thickness(micrometer)	Extrusion width (micrometer)
125	490
250	600
500	675

The critical angle for three layer thicknesses of 125, 250 and 500 micrometers are:

$$\alpha_{125} = 14.31°$$

$$\alpha_{250} = 22.61°$$

$$\alpha_{500} = 36.25°$$

3.11 Width Calculation

Most of Slicing algorithms and 3D printer assumes that the cross-sectional shape of the extruded material is a rectangle with 2 semicircular at both ends as shown in Figure 3-27. Considering the radius of the roller which is leading the filament to the nozzle head, we have:

$$Flow\ rate = r\omega A \qquad 3\text{-}41$$

Where *r* is the radius of the roller, ω is the angular velocity of the roller and *A* is the surface area of the filament which is calculated as follows:

$$A_{filament} = \frac{\pi d^2}{4} \qquad 3\text{-}42$$

Where *d* is the diameter of the filament. For the extruded filament we have:

3-43

$$Flow\ rate = Feed\ rate \times S$$

Where feed rate is a linear velocity of the nozzle head and S is the cross-sectional area of the extruded filament.

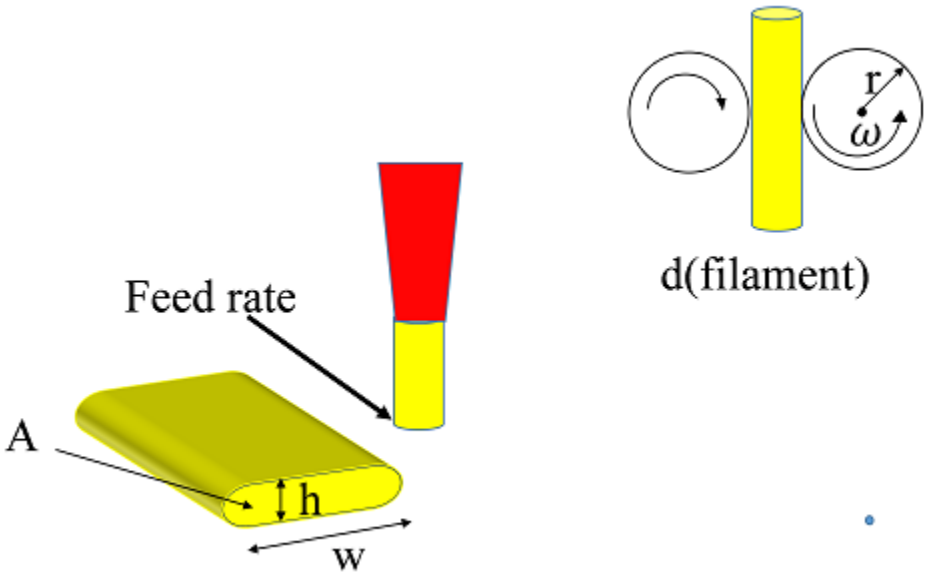

Figure 3-26: Mechanism of filament extrusion in FDM process

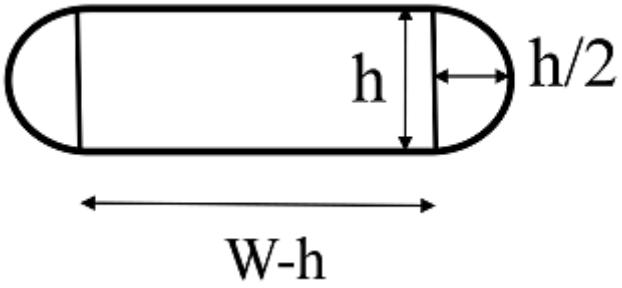

Figure 3-27: Cross section of extruded material

In order to simplify the problem the extrudued filament cross section is considered as a rectangle and two oval shapes, which is the assumption used in the common practice and many industrial applications. The area S is calculated as follows:

$$S_{cross-sectional} = (w - h) \times h + \frac{\pi h^2}{4} \qquad 3\text{-}44$$

3.11.1 Width Correction

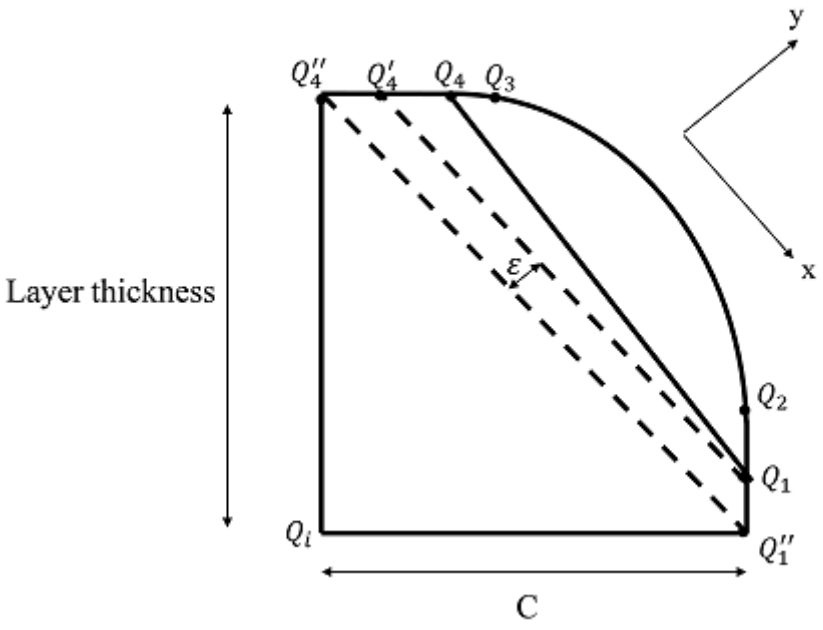

Figure 3-28: Width correction in FDM process

The measured data points by the microscope not necessarily captured from the entire cusp profile uniformly. Also, considering the fact that the developed system relies on the user to define the start and end points of the cusp profile, it is possible that some data points corresponding to two ends of the cusp profile are missed or some points that belong to the other cusps are added to the end of data points processed.

Since the start and end segments of the fitted profile models are linear, it is very easy to interpolate and/or extrapolate the two ends of the model to correct for the missing data or to eliminate the points that do not belong to the current cusp. In order to do that, the known information of the process, i.e., the Horizontal distance of the cusps in two consecutive layers and the layer thickness are used. The interpolation/extrapolation procedure is as follows:

Assuming the base of the cusp is $\overline{Q_1Q_4}$. $\overline{Q_1Q_4'}$ is defined in a way that Q_4' is on the line $\overline{Q_3Q_4}$ and the angle between the Q_1Q_4' and the x axis is exactly equal to α. The interpolation or extrapolation points on the two ends of the profile are found by a positive or negative offset, ε, of the line $\overline{Q_1Q_4'}$ as follows:

$$\overline{Q_1''Q_4''} = \frac{layer\ thickness}{\sin(\alpha)} \qquad 3\text{-}45$$

ε is then defined as follows:

$$m_{\overline{Q_1Q_2}} = m_{\overline{Q_1Q_1''}} \quad 3\text{-}46$$

$$m_{\overline{Q_4'Q_4''}} = m_{\overline{Q_4Q_3}} \quad 3\text{-}47$$

Then we have:

$$\frac{x_{Q_4''} - x_{Q_4'}}{y_{Q_4''} - y_{Q_4'}} = \frac{x_{Q_4} - x_{Q_3}}{y_{Q_4} - y_{Q_3}} \quad 3\text{-}48$$

$$\frac{x_{Q_1''} - x_{Q_1}}{y_{Q_1''} - y_{Q_1}} = \frac{x_{Q_1} - x_{Q_2}}{y_{Q_1} - y_{Q_2}} \quad 3\text{-}49$$

Where

$$y_{Q_4''} - y_{Q_4'} = y_{Q_1''} - y_{Q_1} = \varepsilon \quad 3\text{-}50$$

Substituting d into equation 3-48 and equation 3-49will lead to:

$$\varepsilon = \frac{(x_{Q_4''} - x_{Q_4'}) - (x_{Q_1''} - x_{Q_1})}{(\frac{x_{Q_1} - x_{Q_2}}{y_{Q_1} - y_{Q_2}}) - (\frac{x_{Q_4} - x_{Q_3}}{y_{Q_4} - y_{Q_3}})} \quad 3\text{-}51$$

And ε is found.

Depending on negative or positive values of ε we have two possible scenarios:

1-Positive ε:

The both line ended segments of the profile are extended to produce the nominal layer thickness as shown in Figure 3-29.

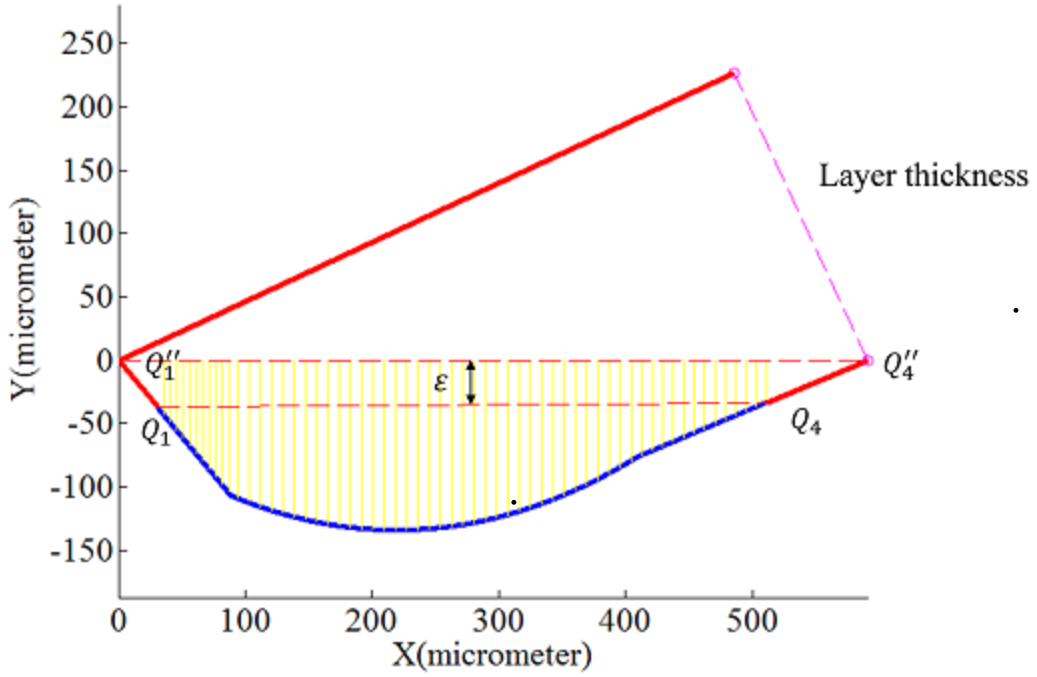

Figure 3-29: Positive ε and extended profile

2-Negative ε:

In case of negative ε, it's obvious that the profile has to be shortened as shown in Figure 3-30.

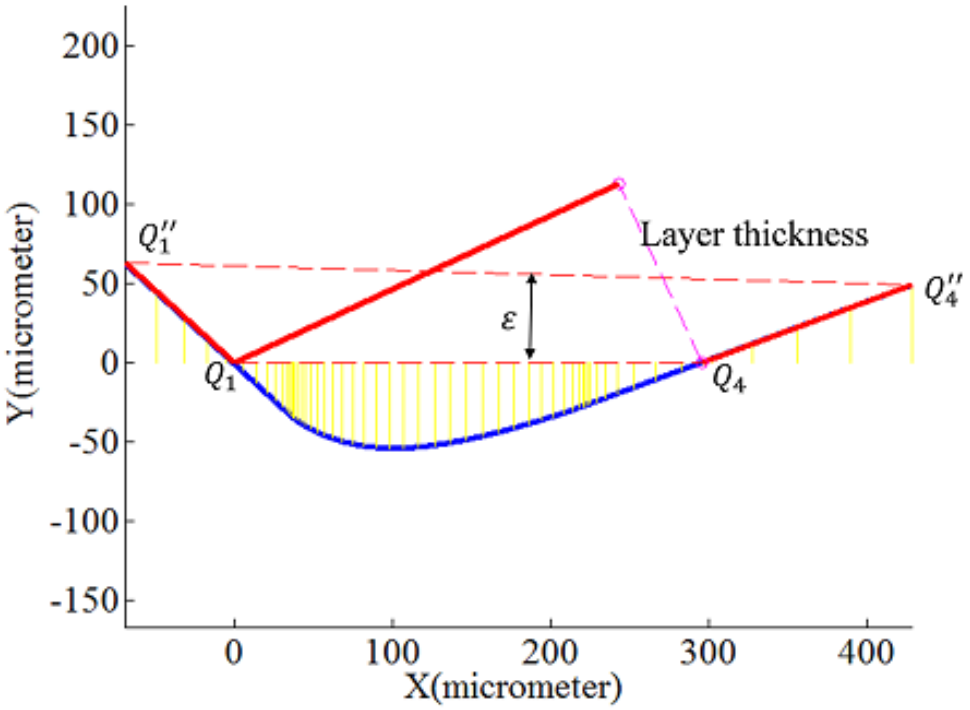

Figure 3-30

Figure 3-30

Figure 3-30: Negative ε and profile shortening

Using the developed solution the actual cross-sectional area of the extruded material (parameter Sin material can be calculated more accurately.

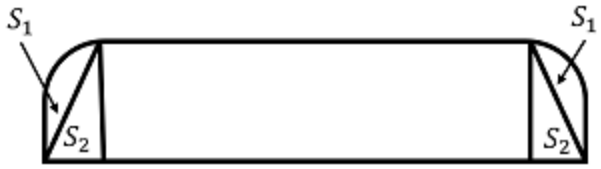

Figure 3-31: Actual cross section of extruded material

Then S_1 and S_2 are calculated numerically.

Due to symmetry we have:

$$S_{total} = (w - 2c)l + 2S_1 + 2S_2 \quad \text{3-52}$$

And then w is calculated as follows:

$$w = \frac{\frac{flow\ rate \times A(filament)}{feed\ rate} - 2S_1 - 2S_2}{l} + 2c \quad \text{3-53}$$

Where flow rate and *A* (filament) and feed rate are machine specification and can be found in Table 3-3.

Table 3-3: Machine parameters

Layer thickness(mm)	Flow rate(rpm)	Feed rate(mm/s)	A(filament)(mm^2)
0.125	8	16	2.27
0.25	20	16	2.27
0.5	40	16	2.27

Figure 3-32 shows an example of numerical calculation to find S_1 and S_2 for layer thickness of 250 microns and surface angle of 25°.

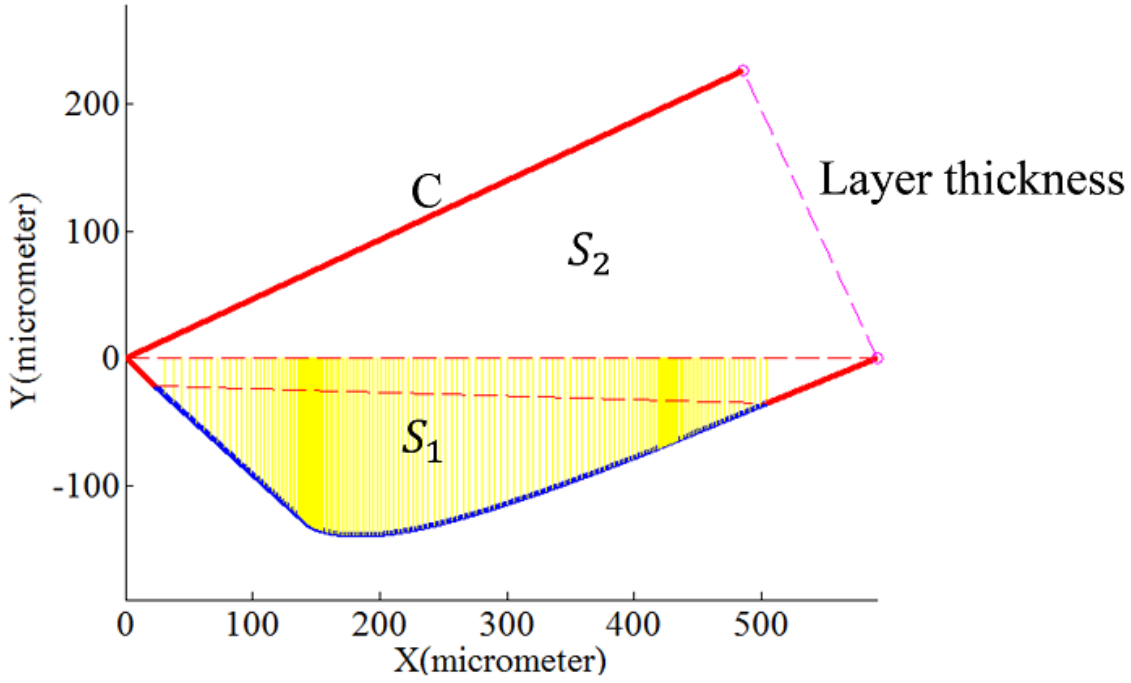

Figure 3-32: Example of S_1 and S_2 for surface angle of 25° and layer thickness of 250 microns

Figure 3-33 shows an example of numerical calculation to find S_1 and S_2 for layer thickness of 250 microns and surface angle of 90°. as shown in the Figure 3-33, S_2 is equal to zero for vertical surface angles.

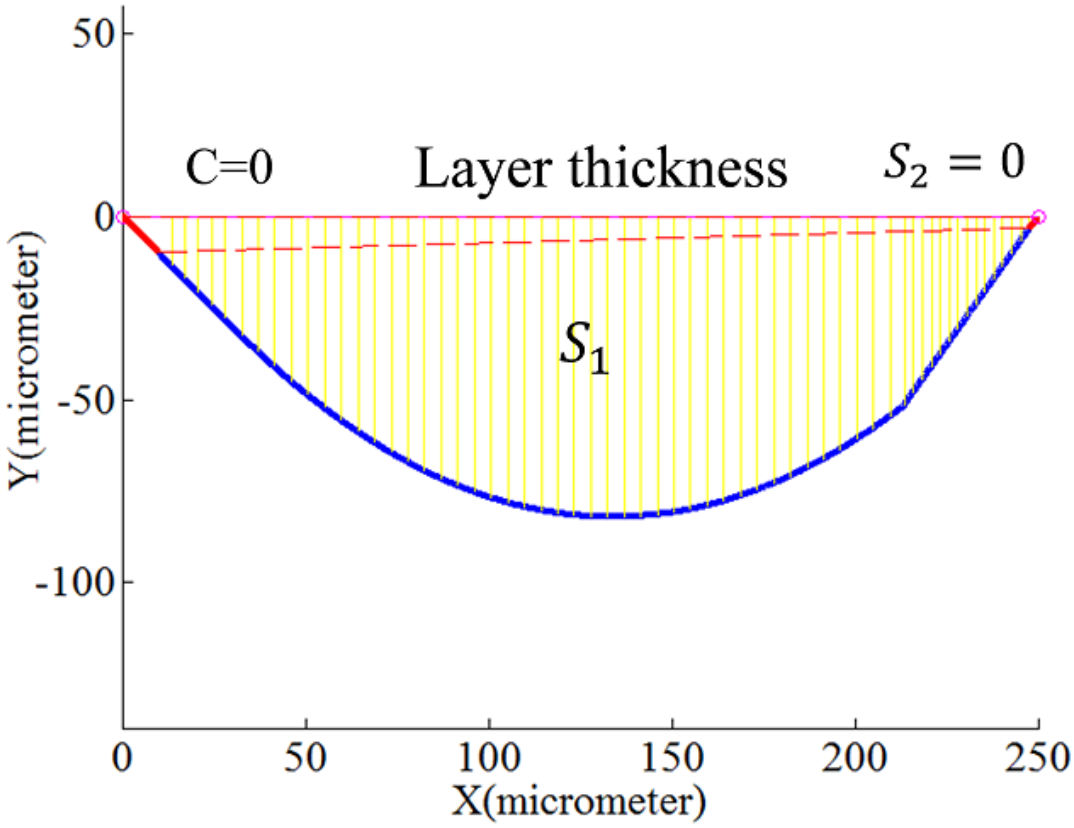

Figure 3-33: Example of S_1 and S_2 for surface angle of 90° and layer thickness of 250 microns

4 Implementation

4.1 Introduction

This chapter provides the implementation process. It is explained how the specimens are designed, fabricated, and inspected.

4.2 Design of the Specimen

The specimens designed for the experiments have a unique design with surface angles between 0 to 90 degrees with increment of 5 degrees. The specimens are printed with three different layer thicknesses: 0.15, 0.25 and 0.50 mm. Figure 4-1 shows one of the fabricated specimens.

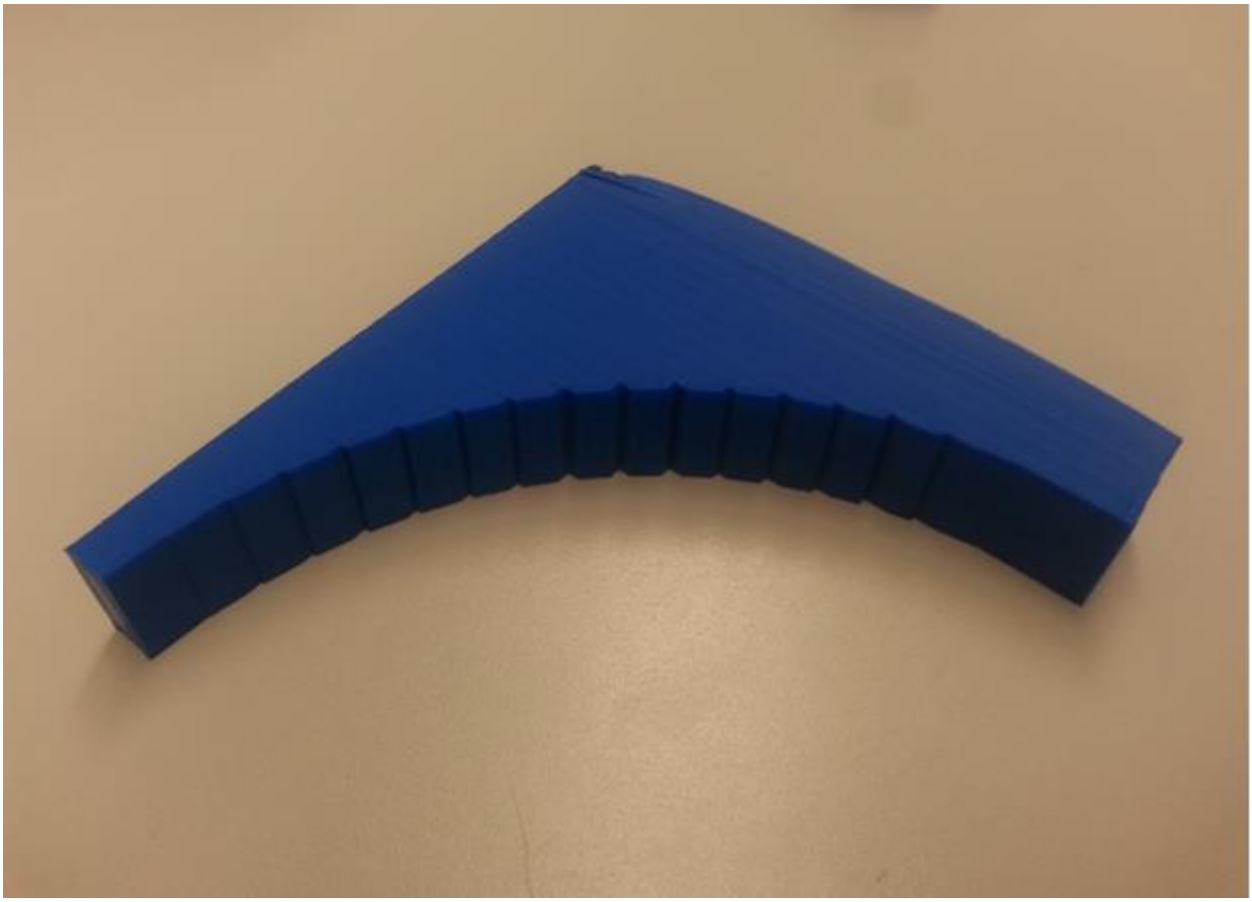

Figure 4-1: The designed specimen including all surface angles from 0° to 90°

Measurements of the part has been conducted using high resolution topography microscope. Each specific angle of each specimen were measure at each cusp by capturing its side view.

For each picture, a set of measurements were conducted. Number of pictures, number of cusps and average number of points on each cusp's profile are shown in Table 4-1Table 4-2Table 4-3.

Table 4-1: Information of cusps for layer thickness of 500 microns

Surface Angle	Number of pictures	Number of cusps	Average number of the points on each cusp
5	1	1	1532
10	1	1	1525
15	3	6	958
20	2	4	988
25	2	3	850
30	2	5	518
35	2	6	319
40	2	6	306
45	1	3	584
50	2	6	359
55	1	4	459
60	1	4	548
65	2	8	488
70	2	8	466
75	1	4	451
80	1	4	446
90	1	4	369

Table 4-2: Information of pictures for layer thickness of 250 microns

Surface angle	Number of pictures	Number of cusps	Average number of the points on each cusp
5	3	3	535
10	1	2	556
15	1	2	556
20	1	4	405
25	1	5	569
30	1	5	340
35	1	6	278
40	1	6	281
45	1	7	250
50	1	8	264
55	1	7	266
60	1	9	220
65	1	9	218
70	1	9	217
75	1	8	226
80	1	8	213
90	1	8	200

Table 4-3: Information of pictures for layer thickness of 125 microns

Surface angle	Number of pictures	Number of cusps	Average number of the points on each cusp
5	1	3	561
10	1	5	432
15	1	6	321
20	1	7	226
25	1	6	281
30	1	5	335
35	1	11	234
40	1	10	172
45	1	6	298
50	1	10	170
55	1	5	354
60	1	9	192
65	1	8	186
70	1	7	242
75	1	6	293
80	1	11	160
90	1	13	139

All four methods that were mentioned in chapter 3 were implemented in MATLAB and for each cusp, all four method were used to find the best method for fitting. The method that gives the minimum residual error was chosen then as the best approach for the fitting of every single cusp. It was observed that when the surface angles approaches to 90° the forth method will give the minimum residual fitting error. The results were validated using a microscope with camera and sensor provided

by Phaseview^{TM}. The setup can be seen in Figure 4-2. GetPhase software was used for taking images from the surface.

Figure 4-2: Roughness measurement setup

5 Chapter 5: Results and discussion

5.1 Introduction

This chapter presents the result of implementation of the approaches that were presented in chapter 3 and discussion about the results. Firstly, the Results of all the fittings are presented. The surface roughness models are presented for each layer thickness and as a function of surface angle. In the discussion section, the effect of layer thickness and surface angle on surface roughness of FDM products is discussed.

5.2 B-spline curve modeling using total least square fitting

Examples of the fitted curves using NURBS and TLS method for the surface angle of 25° and 90° are shown in Figure 5-1 and Figure 5-2. The difference between the actual curve and fitted curve is also shown.

5.2.1 Case study for B-spline curve modeling using total least square fitting

The Final curve fitted to the points of a cusp using TLS and B-spline at surface angle of 25° and layer thickness of 250 microns is like 5-1 and the control points for the specific surface angle of 20° and layer thickness of 250 microns are as follows:

$$c(u) = \begin{cases} N_{0,3}P_0 + N_{1,3}P_1 + N_{2,3}P_2 + N_{3,3}P_3 & 0 \le u < \frac{1}{4} \\ N_{2,3}P_2 + N_{3,3}P_3 + N_{4,3}P_4 + N_{5,3}P_5 & \frac{1}{4} \le u < \frac{1}{2} \\ N_{3,3}P_3 + N_{4,3}P_4 + N_{5,3}P_5 + N_{6,3}P_6 & \frac{1}{2} \le u < \frac{3}{4} \\ N_{5,3}P_5 + N_{6,3}P_6 + N_{9,3}P_9 + N_{10,3}P_{10} & \frac{3}{4} \le u < 1 \end{cases} \quad 5\text{-}1$$

Where P_0=$(-9.32729, 16.18248)\ \mu m$

, $P_1 = P_2 = P_3 = (17.7415, -2.28281)\mu m$

$P_4 = (322.5666, -126.4563)$, $P_5 = P_6 = P_7 = (661.466, 735.7438)\mu m$ and $P_8 = (846.806, 880.2964)\mu m$

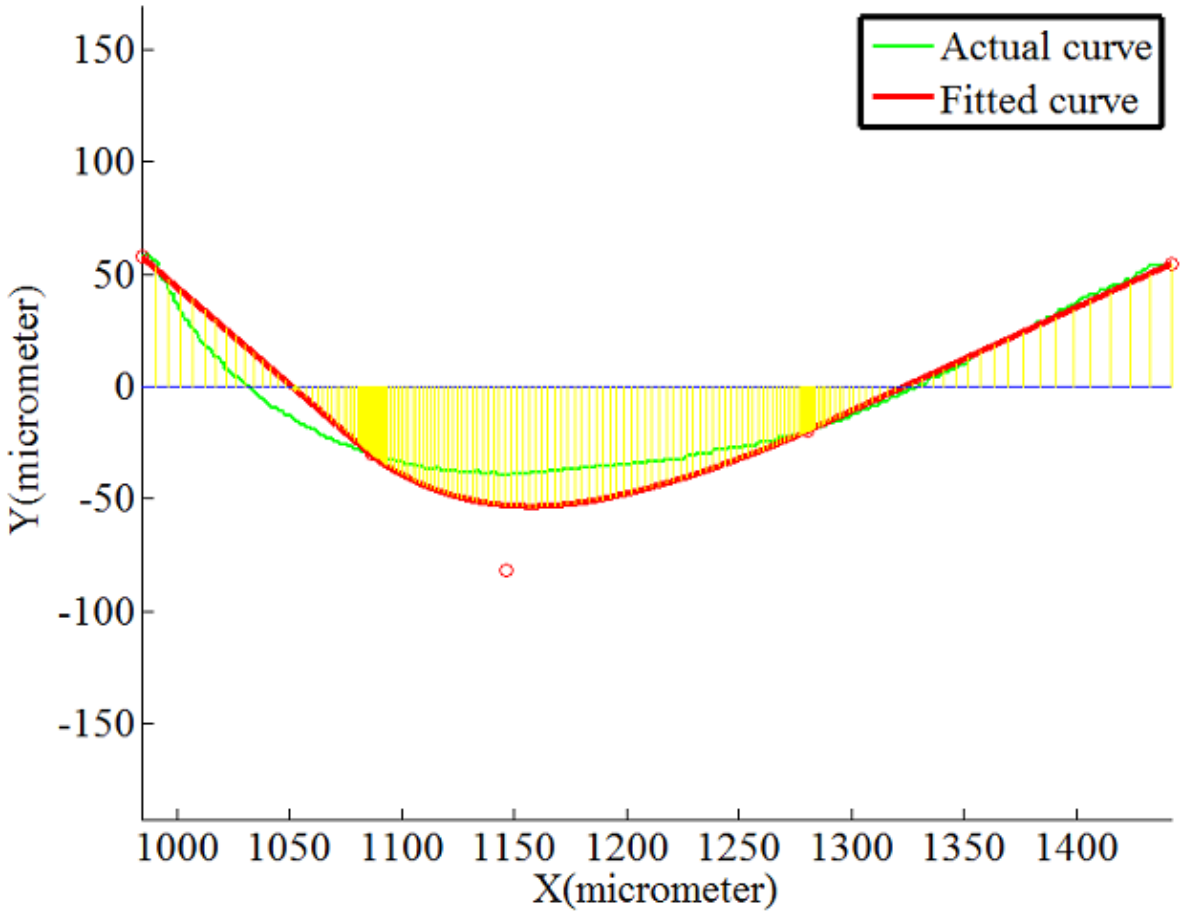

Figure 5-1: An example of fitted curve using NURBS and TLS for the surface angle of 25° and layer thickness of 250 microns

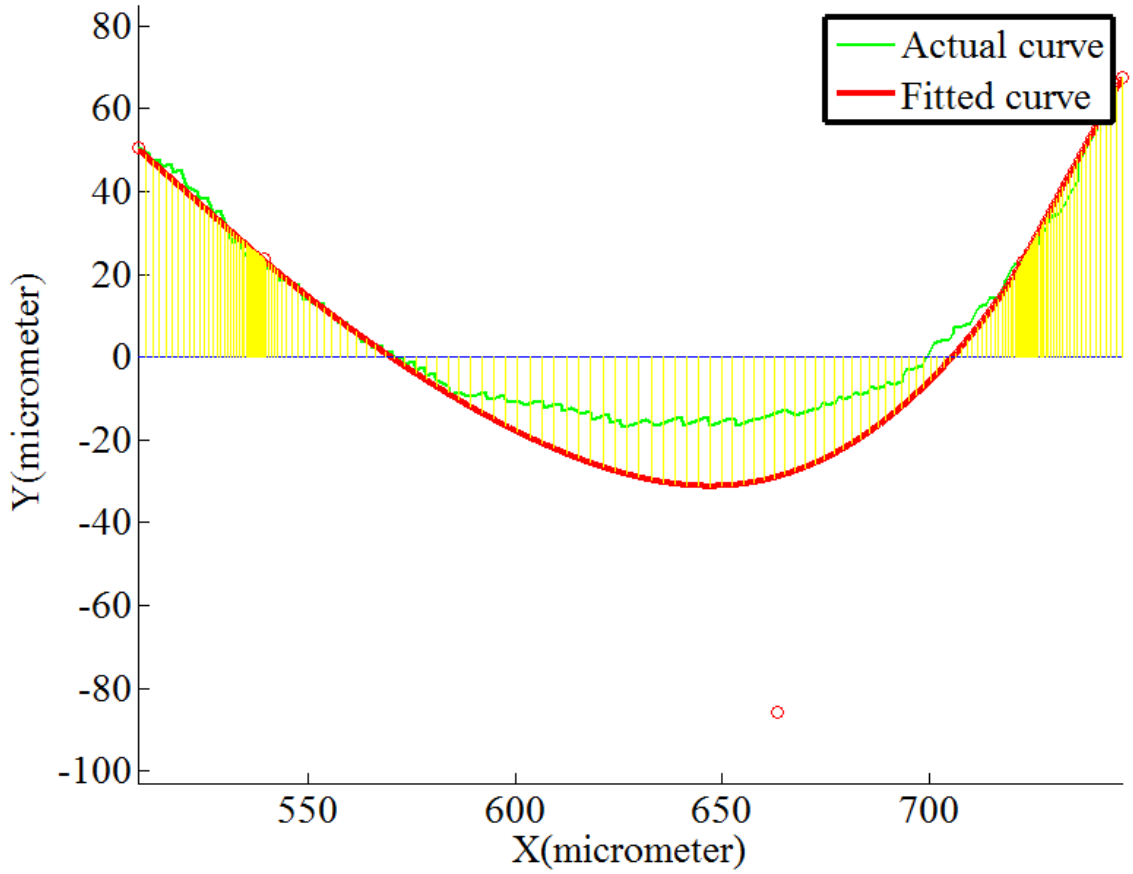

Figure 5-2: An example of fitted curve using NURBS and TLS for the surface angle of 90° and layer thickness of 250 microns

5.3 B-spline curve modeling using genetic algorithm

Examples of fitted curve using NURBS and genetic algorithm method for the surface angle of 25° and 90° are shown in Figure 5-3 and Figure 5-4.

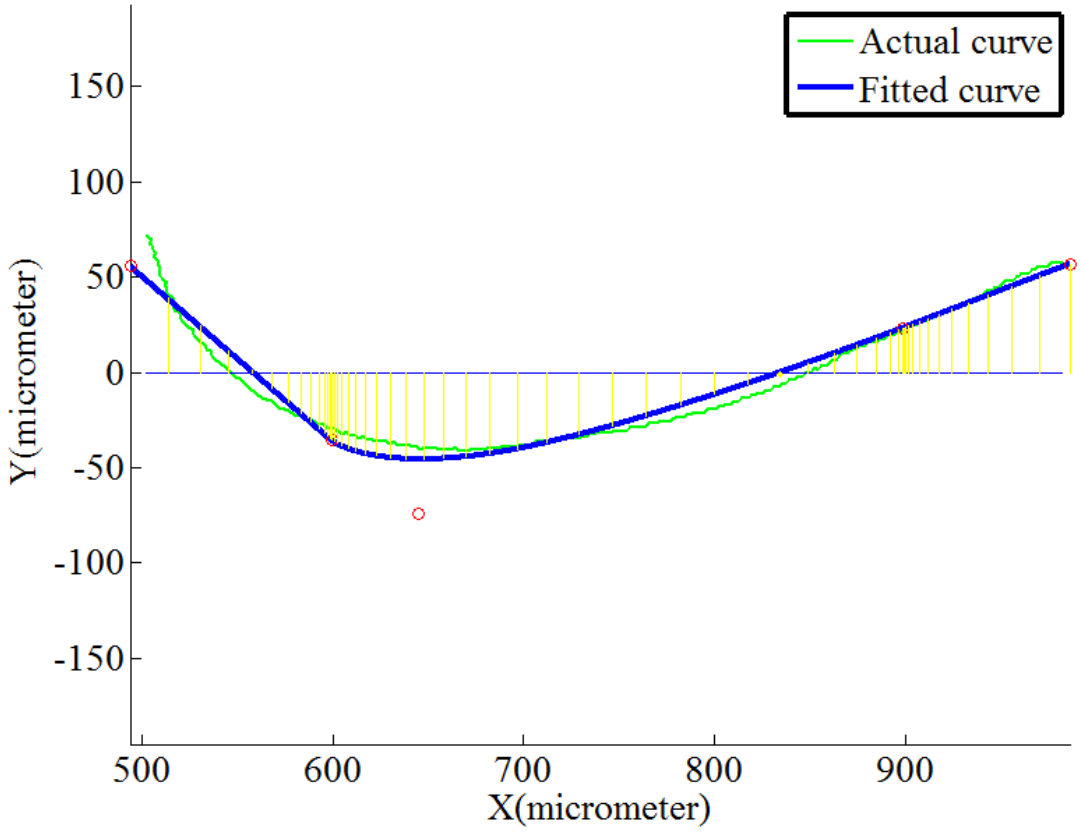

Figure 5-3: An example of fitted curve using NURBS and GA for the surface angle of 25° and layer thickness of 250 microns

5.3.1 Case study for B-spline curve modeling using genetic algorithm

The Final curve fitted to the points of a cusp using B-spline and GA at surface angle of 25° and layer thickness of 250 microns is like 5-1 and the control points for the specific surface angle of 20° and layer thickness of 250 microns are as follows:

P_0== $(-8.36541, 16.18248)\ \mu m$, $P_1 = P_2 = P_3 = (17.7415, -2.28281)\mu m$

$P_4 = (324.5666, -123.4563)\ \mu m$, $P_5 = P_6 = P_7 = (661.466, 735.7438)\mu m$ and $P_8 = (846.806, 880.2964)\ \mu m$

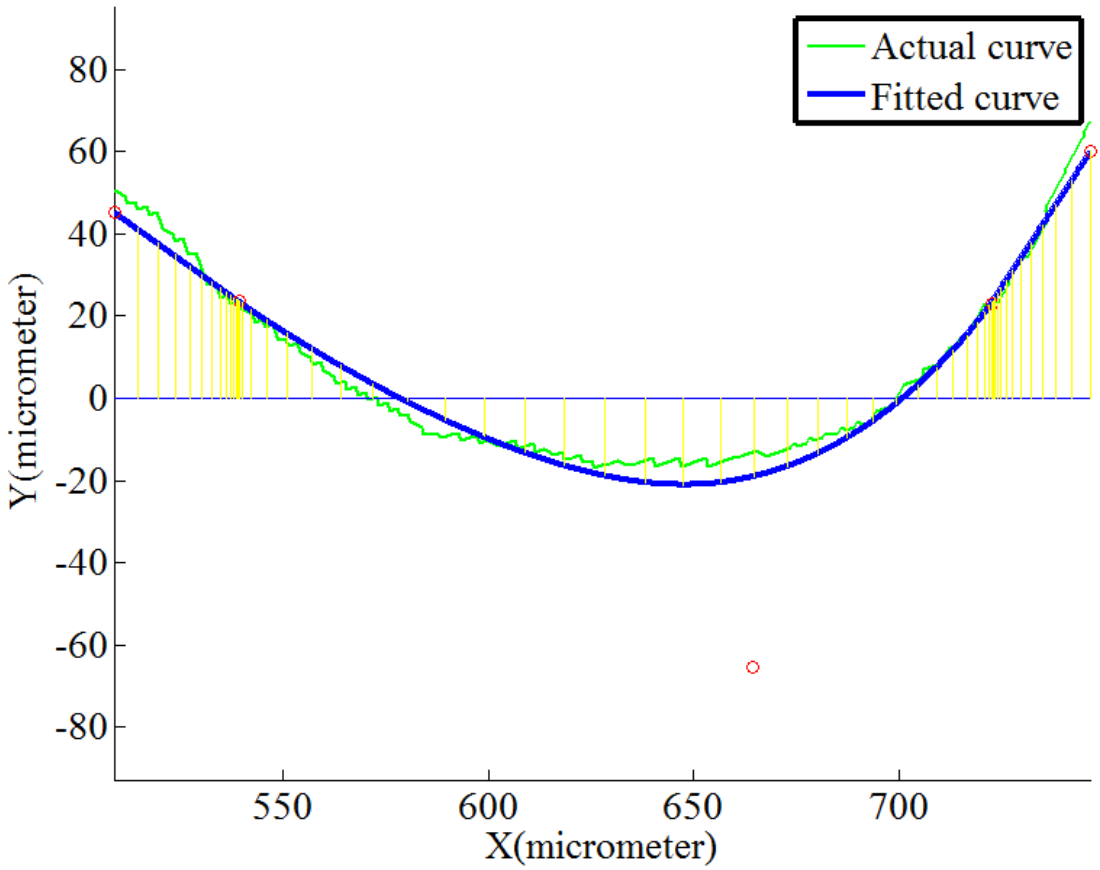

Figure 5-4: An example of fitted curve using NURBS and GA for the surface angle of 90° and layer thickness of 250 microns

5.4 Three Piece Curve Fitting Including a Third Degree Polynomial Curve and Genetic Algorithm

The fitted curves using degree 3 polynomial, 2 pieces of line and genetic algorithm are shown in Figure 5-5 and Figure 5-6.

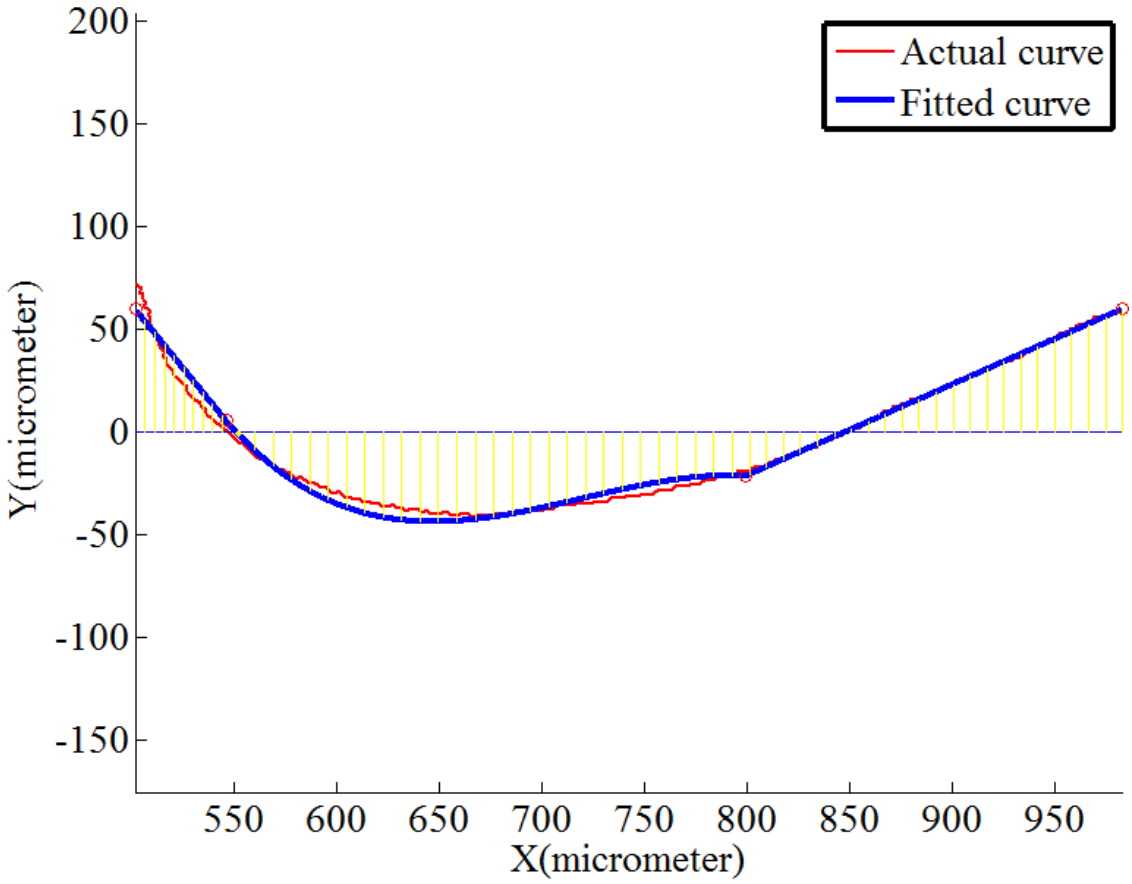

Figure 5-5: An example of fitted curve using 3-piece third degree polynomial and GA for the surface angle of 25° and layer thickness of 250 microns

5.4.1 Case Study For Three Piece Curve Fitting Including a Third Degree Polynomial Curve and Genetic Algorithm

The Final curve fitted to the points of a cusp using third degreepolynomial and 2 line segments and GA at surface angle of 25° and layer thickness of 250 microns is like 5-2 and the coefficients are as follows:

$$\begin{bmatrix} x_1 & 1 & 0 & 0 & 0 & 0 & 0 & 0 \\ x_2 & 1 & 0 & 0 & 0 & 0 & 0 & 0 \\ 0 & 0 & x_2^3 & x_2^2 & x_2 & 1 & 0 & 0 \\ -1 & 0 & 3x_2^2 & 2x_2 & 1 & 0 & 0 & 0 \\ 0 & 0 & 3x_3^2 & 2x_3 & 1 & 0 & -1 & 0 \\ 0 & 0 & 0 & 0 & 0 & 0 & x_3 & 1 \\ 0 & 0 & 0 & 0 & 0 & 0 & x_4 & 1 \end{bmatrix} \begin{bmatrix} a \\ b \\ c \\ d \\ e \\ f \\ g \\ h \end{bmatrix} = \begin{bmatrix} y_1 \\ y_2 \\ y_2 \\ \emptyset \\ \emptyset \\ y_3 \\ y_3 \\ y_4 \end{bmatrix} \qquad 5\text{-}2$$

Where $a = 0.22308, b = 164.572, c = 0.002236, d = 3.56769, e = 1410.545, f = 0.592436\ and\ g = -509.238$ for the specific surface angle of 20°

And layer thickness of 250 microns.

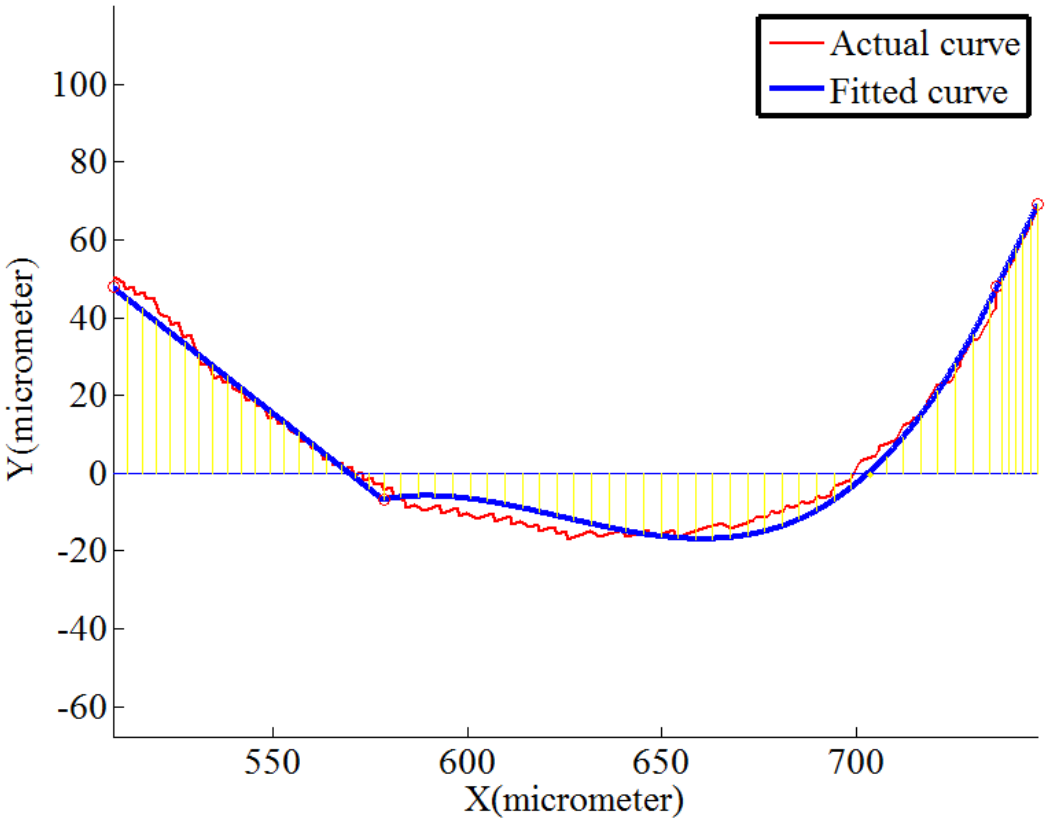

Figure 5-6: An example of fitted curve using 3-piece third degree polynomial and GA for the surface angle of 90° and layer thickness of 250 microns

5.5 Three Piece Curve Fitting Including Second degree Polynomial Curve and Genetic Algorithm

The fitted curves using the second degree polynomial, 2 pieces of lines and genetic algorithm are shown in Figure 5-7 and Figure 5-8.

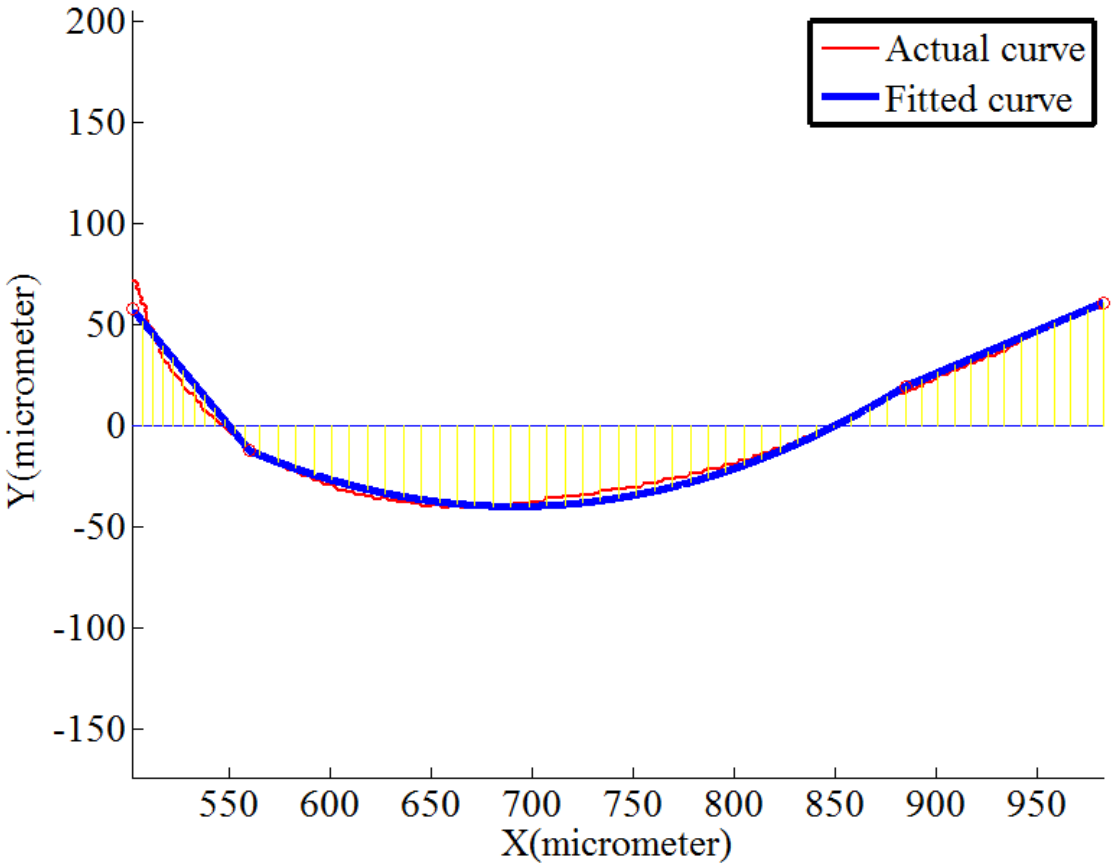

Figure 5-7: An example of fitted curve using 3-piece second degree polynomial and GA for the surface angle of 25° and layer thickness of 250 microns

5.5.1 Case Study For Three Piece Curve Fitting Including second degree Polynomial Curve and Genetic Algorithm

The Final curve fitted to the points of a cusp using degree 3 polynomial and 2 line segments and GA at surface angle of 25° and layer thickness of 250 microns is like 5-3 and the coefficients are as follows:

$$\begin{bmatrix} x_1 & 1 & 0 & 0 & 0 & 0 & 0 \\ x_2 & 1 & 0 & 0 & 0 & 0 & 0 \\ 0 & 0 & x_2^2 & x_2 & 1 & 0 & 0 \\ 0 & 0 & x_3^2 & x_3 & 1 & 0 & 0 \\ -1 & 0 & 2x_2 & 0 & 1 & 0 & 0 \\ 0 & 0 & 2x_3 & 1 & 0 & -1 & 0 \\ 0 & 0 & 0 & 0 & 0 & x_3 & 1 \\ 0 & 0 & 0 & 0 & 0 & x_4 & 1 \end{bmatrix} \begin{bmatrix} a \\ b \\ c \\ d \\ e \\ f \\ g \end{bmatrix} = \begin{bmatrix} y_1 \\ y_2 \\ y_2 \\ \emptyset \\ \emptyset \\ y_3 \\ y_3 \\ y_4 \end{bmatrix} \qquad 5\text{-}3$$

Where $a = 0.2511, b = 181.6707, c = 7.96e-05, d = 0.19068, e = 152.0931, f = 40414.9$ g =772.645 for the specific surface angle of 20°

And layer thickness of 250 microns.

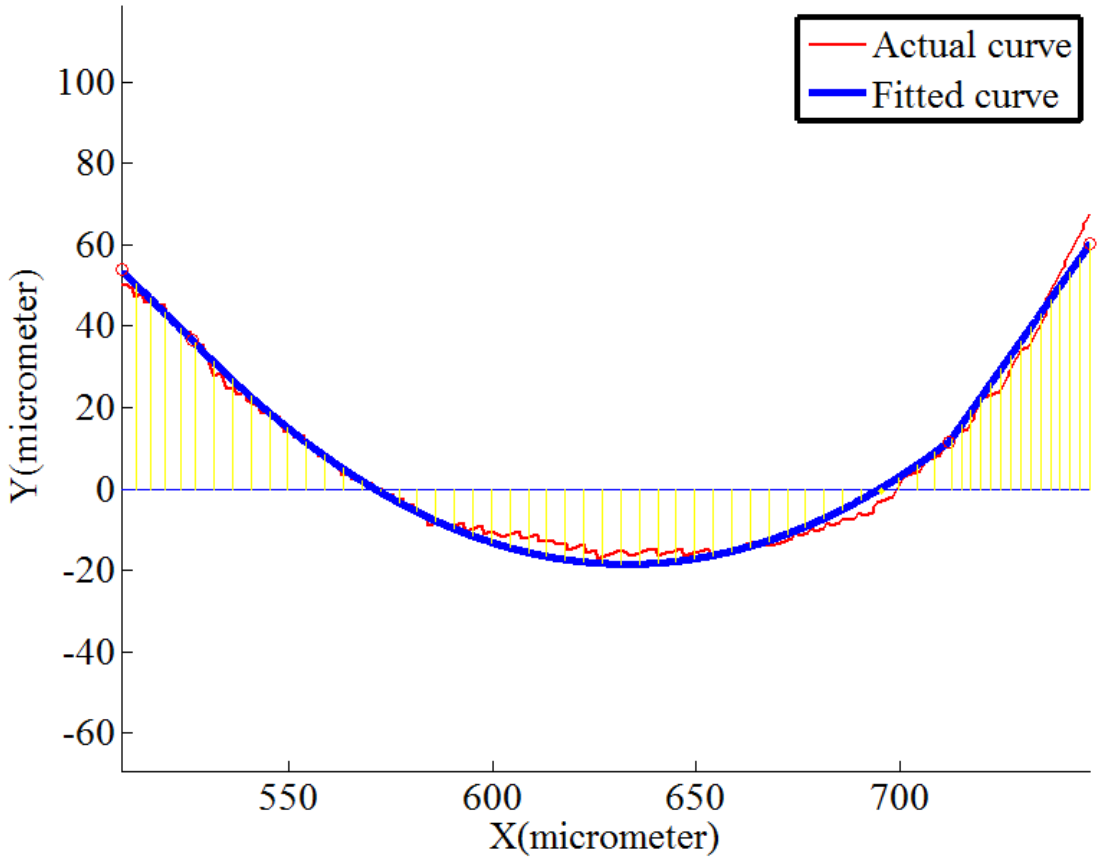

Figure 5-8: An example of fitted curve using 3-piece second degreepolynomial and GA for the surface angle of 90° and layer thickness of 250 microns

5.6 Surface Roughness Prediction

For all experimented fabrication layer thicknesses it is observed that increasing the surface angle corresponding to the vertical surface reduces the surface roughness and the surface becomes gradually smoother, as shown in Figure 5-9, Figure 5-11 and Figure 5-13. The best fitted models that express the relationship between the surface angle and the surface roughness are also presented in these Figures. For each cusp in every surface angle, the method that resulted in the minimum residual error for the fitting has been chose to predict the surface roughness for that specific cusp and surface angle. Figure 5-10 shows the general cusp shape by increasing the

surface angle from 5° to 90° by increment of 5° for the layer thickness of 125 microns. It can be observed that the length of the line segments at low surface angles is more than when the surface angle approaches 90 degrees.

Actual surface roughness is the value of roughness at each surface angle which is measured using 3*D* surface topography device and the predicted value is the value of surface roughness at each surface angle measured using the experimental method.

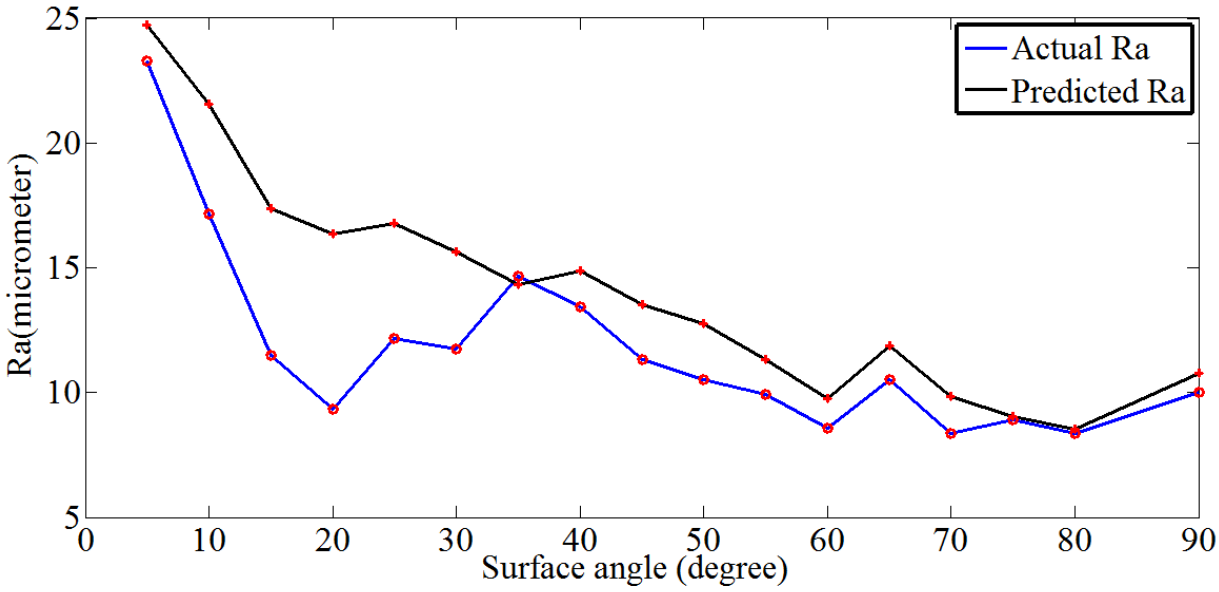

Figure 5-9: Distribution of the predicted and actual surface roughness and by variation of the surface angle – 125 micron Layer thickness

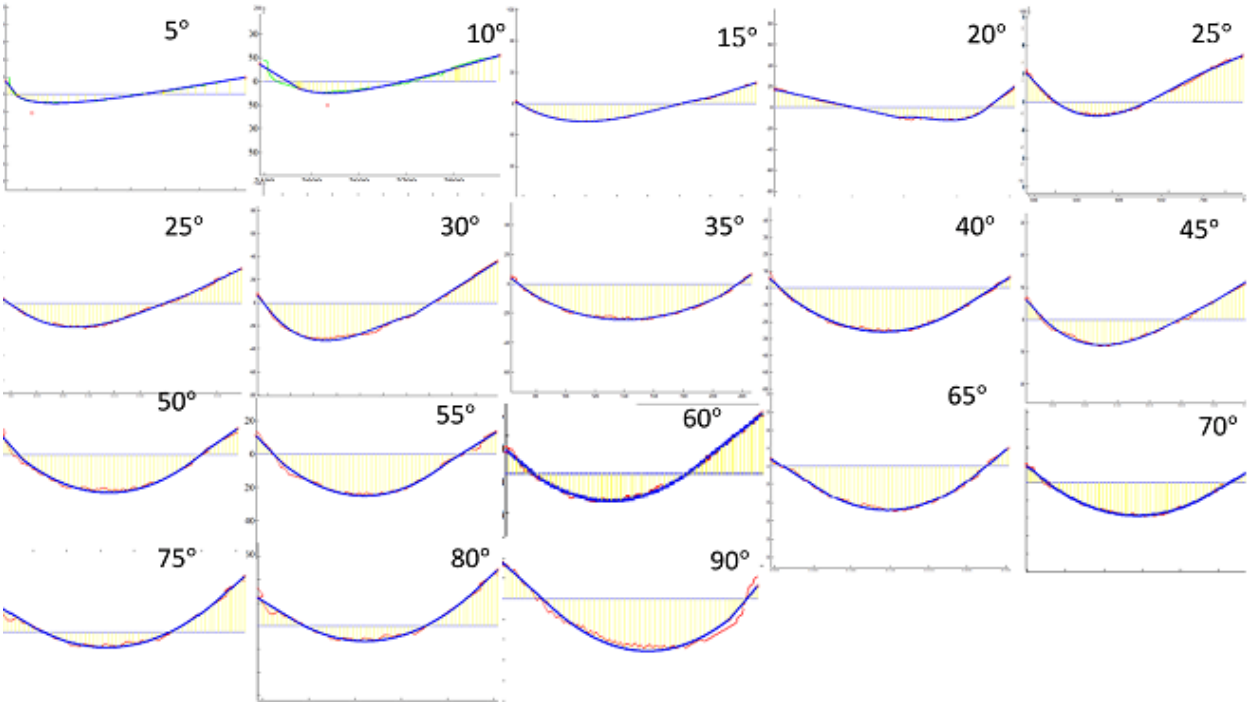

Figure 5-10: General shape of the cusp for surface angle from 5° to 90° and layer thickness of 125 microns

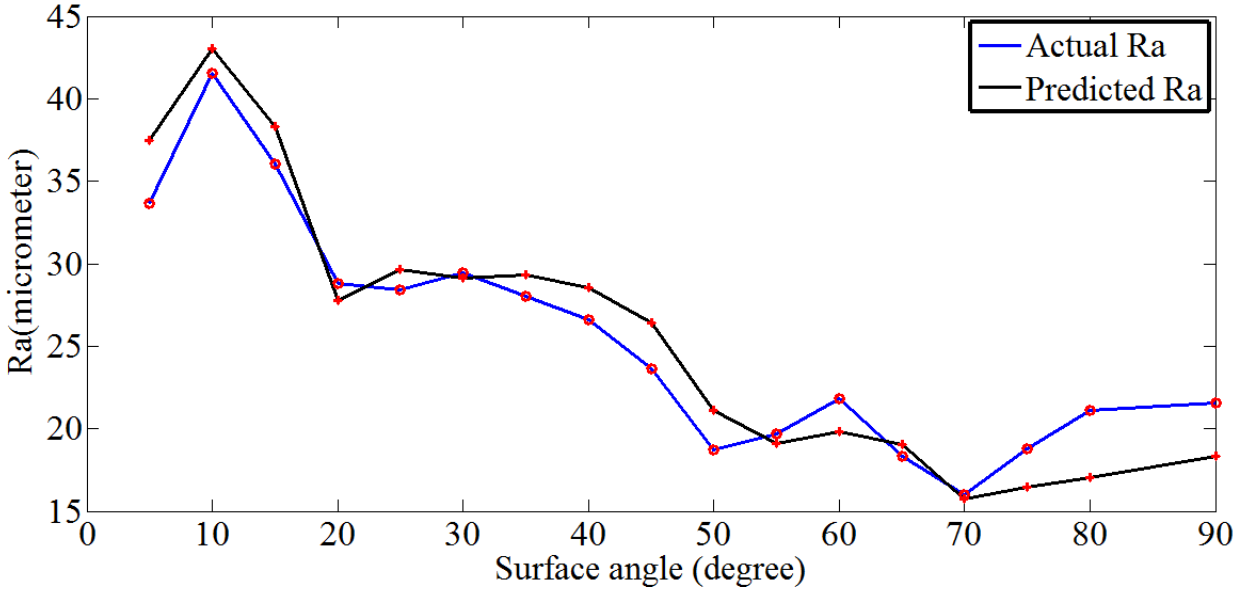

Figure 5-11: Distribution of the predicted and actual surface roughness by variation of the surface angle – 250 micron Layer thickness

Figure 5-12 shows the general cusp shape by increasing the surface angle from 5° to 90° by increment of 5° for layer thickness of 250 microns.

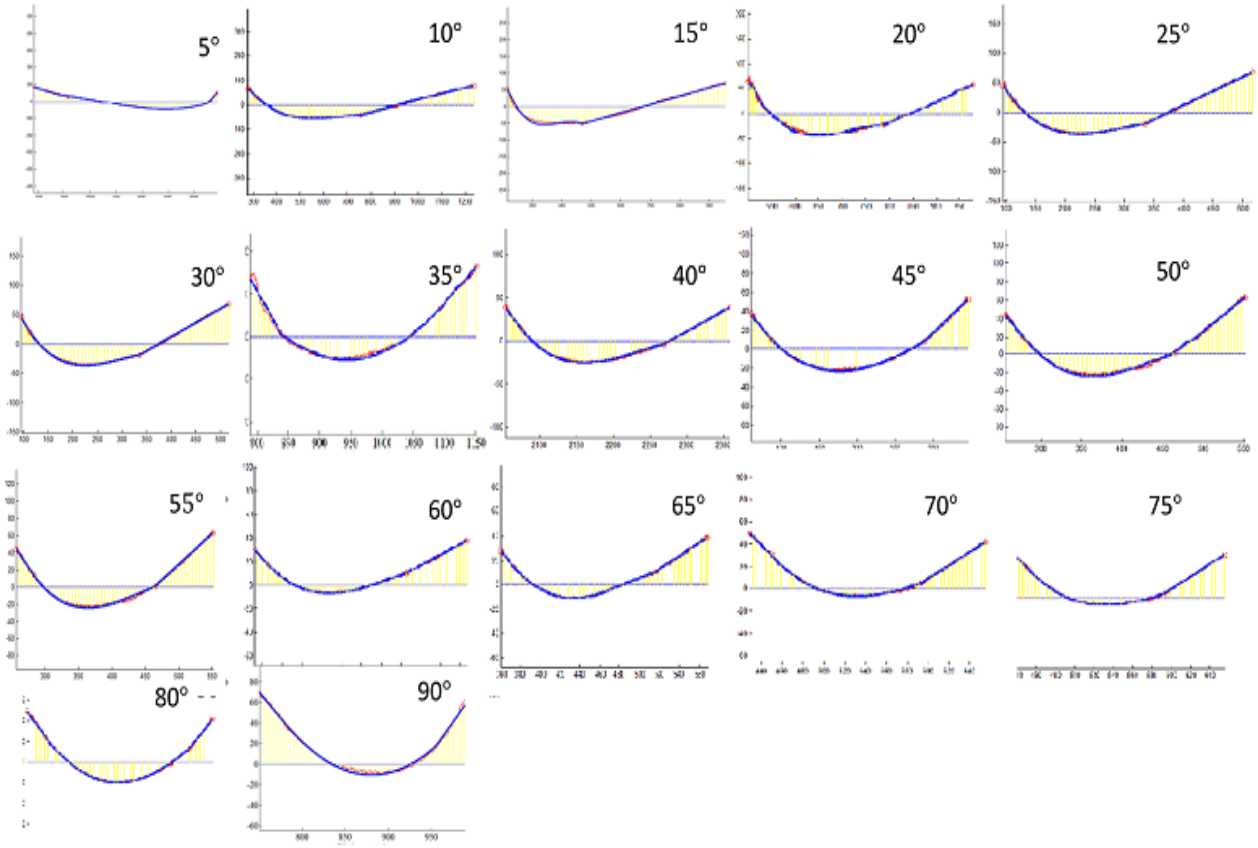

Figure 5-12: General shape of the cusp for surface angle from 5° to 90° and layer thickness of 250 microns

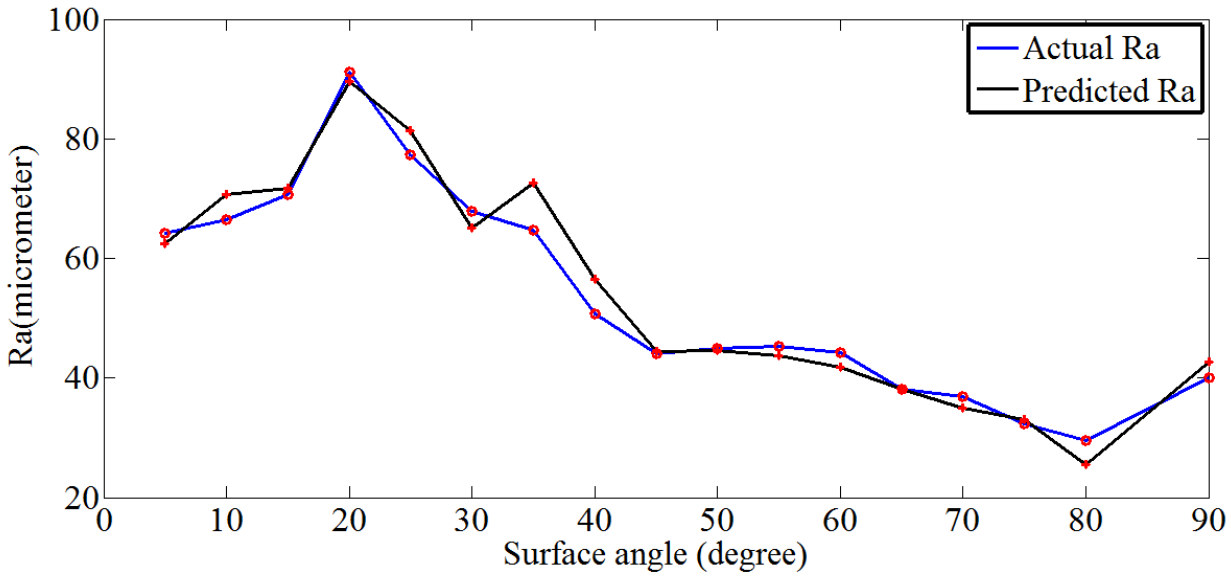

Figure 5-13: Distribution of the predicted and actual surface roughness by variation of the surface angle – 500 micron Layer thickness

Figure 5-14 shows the general cusp shape by increasing the surface angle from 5° to 90° by increment of 5° for layer thickness of 500 microns.

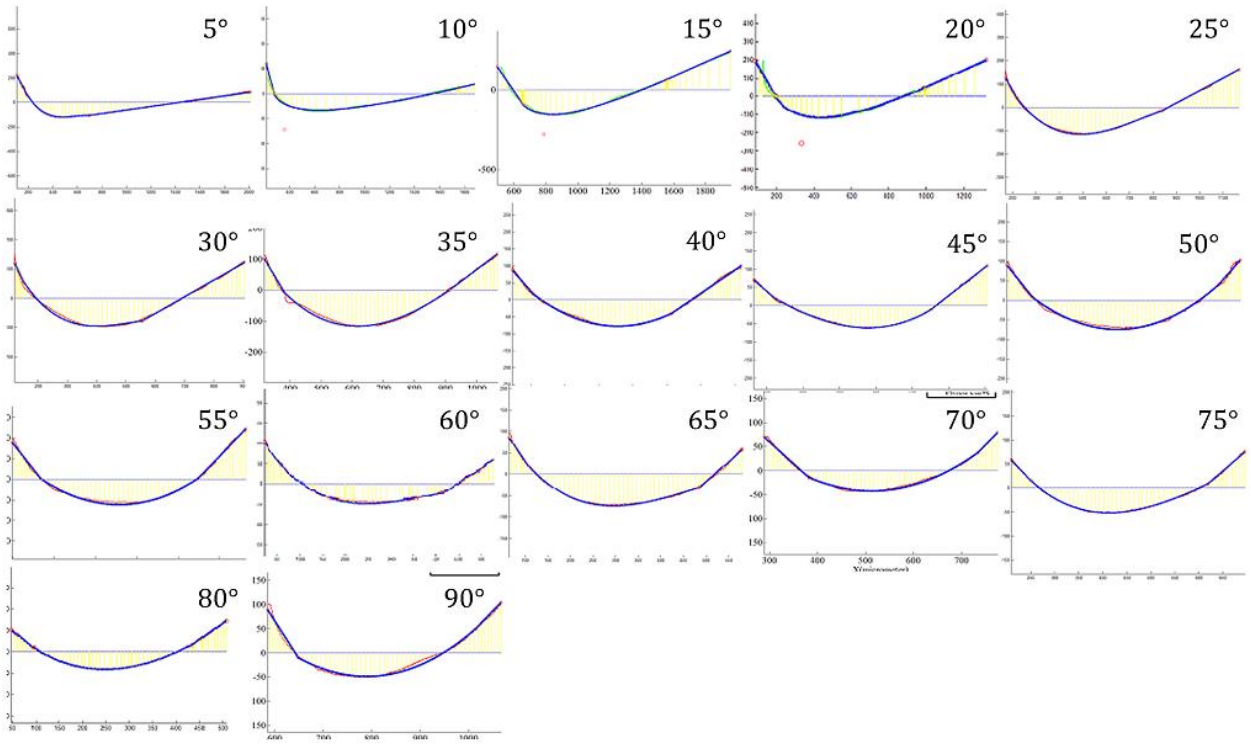

Figure 5-14: General shape of the cusp for surface angle from 5° to 90° and layer thickness of 500 microns

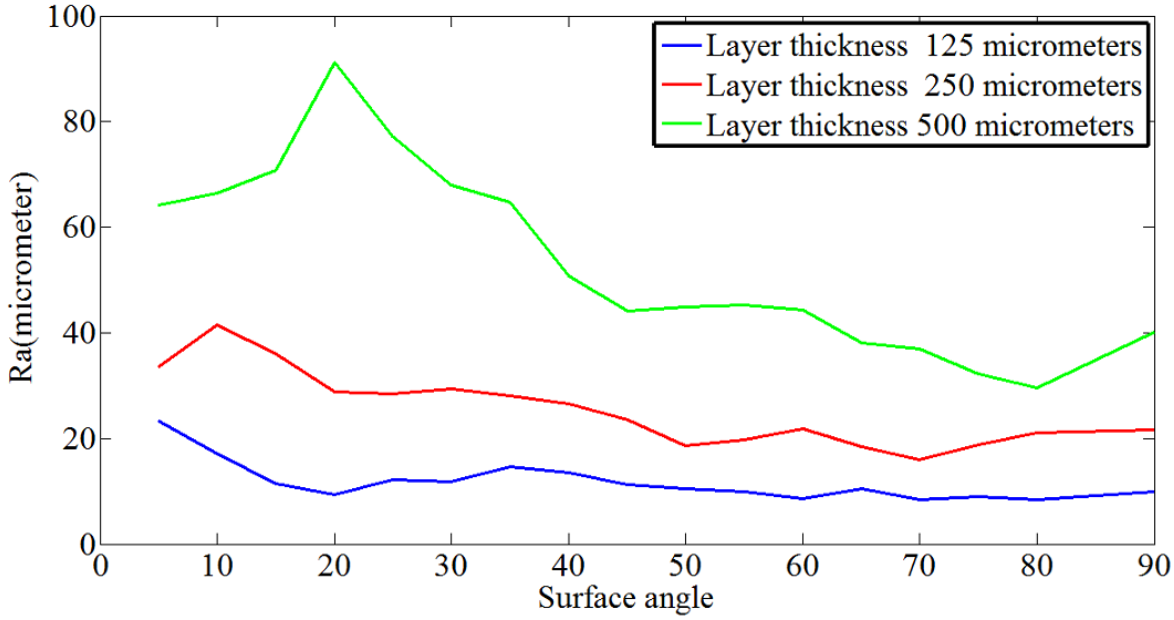

Figure 5-15: Distribution of the predicted surface roughness by variation of the surface angle

5.7 Width Calculation Results

The discussed approach in 3.9.1 was implemented in MATLAB and for each cusp, the experimental width was calculated. It was observed that in surface angles close to 0° up to critical surface angle, the predicted width using Equation 3-53 is far from the nominal width. As the surface angle approaches to the critical surface angle, experimental width gets closer to the nominal width which means at critical surface angle, the extruded filaments are touching each other and the air gap introduced as undetermined region is disappeared. The negative width means that the value of S_1 and S_2 are highly greater than the measured profile consists more than one single extruded path.

5.8 Comparison of Four Fitting Methods

It was mentioned in previous sections that for modelling f the surface roughness, the fitting method corresponding to minimum residual error is chosen. It's useful to compare the robustness and the degree of the success in each algorithm. Figure 5-16 to Figure 5-19 shows the average residual error for each method of fitting for layer thickness of 250 microns. Figure 5-20 shows the distribution of normalized fitting error for each method for layer thickness of 250 microns. It can be observed that the third degree polynomial fitting gives the best answer for the layer thickness of 250 microns. Table 5-1 shows the average and standard deviation of fitting errors for each fitting method for layer thickness of 250 microns.

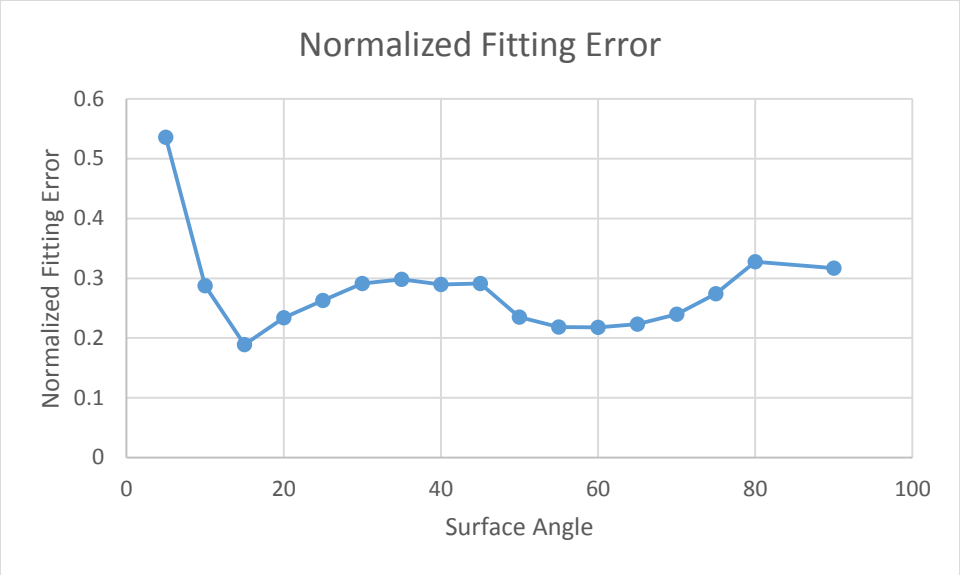

Figure 5-16: Distribution of fitting error using TLS method for layer thickness of 250 microns

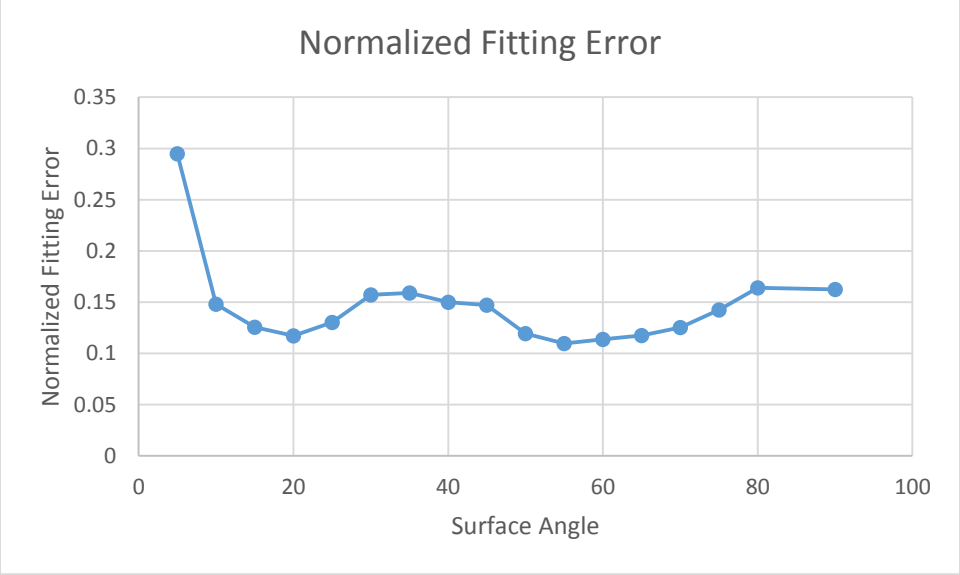

Figure 5-17: Distribution of fitting error using TLS and genetic algorithm method for layer thickness of 250 microns

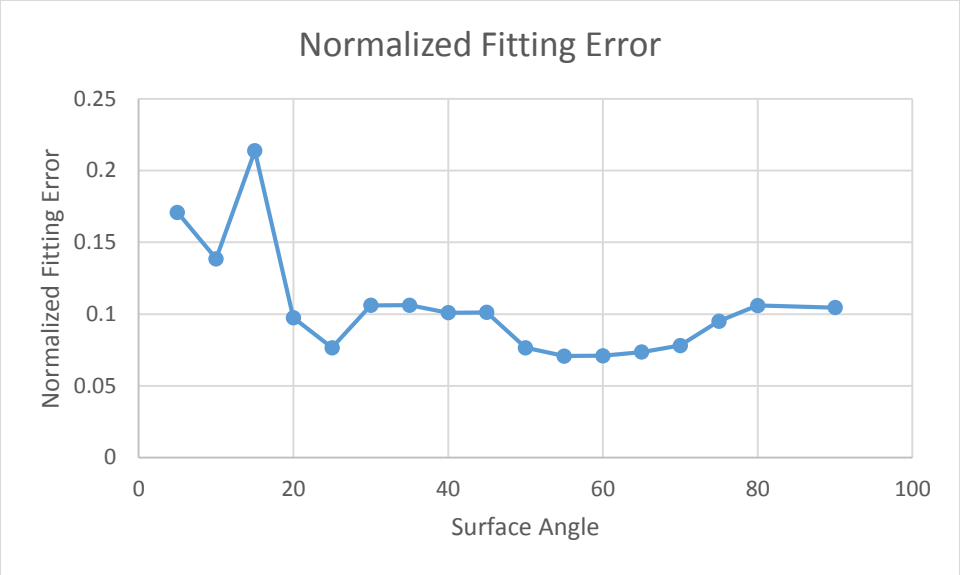

Figure 5-18: Distribution of fitting error using third degree polynomial and genetic algorithm method for layer thickness of 250 microns

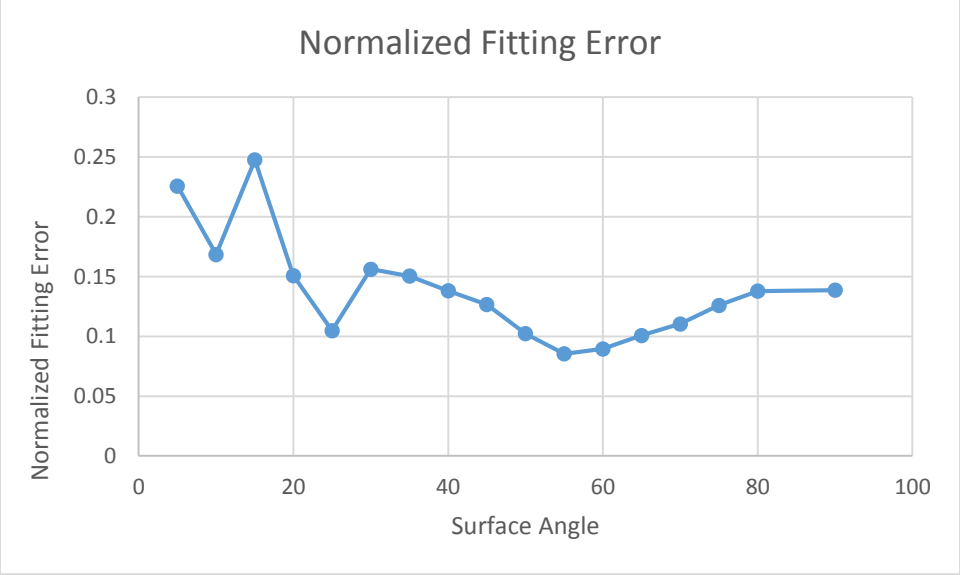

Figure 5-19: Distribution of fitting error using second degree polynomial and genetic algorithm method for layer thickness of 250 microns

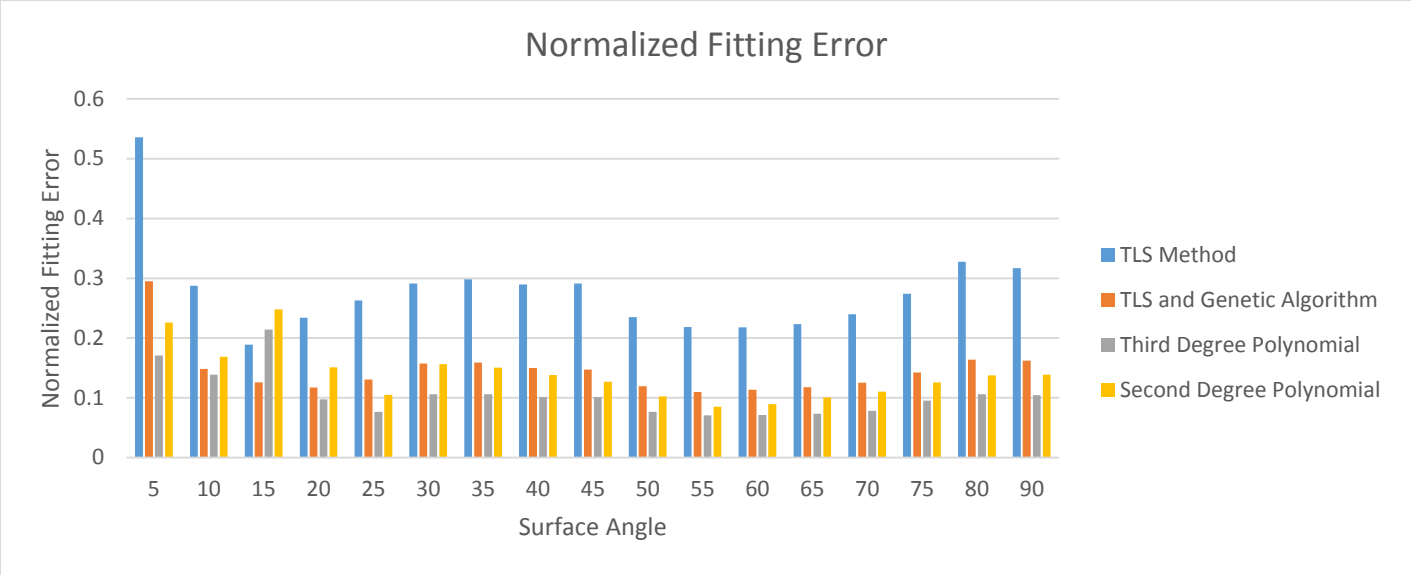

Figure 5-20: Comparison of fitting error using all developed fitting models

Table 5-1: Average Fitting Error and Standard Deviation of Fitting Models for Layer thickness of 250 microns

Method	TLS Method	TLS and GA	Third Degree Polynomial	Second Degree Polynomial
Standard Deviation of Errors	0.077	0.042	0.038	0.044
Average of Fitting Errors	0.278	0.146	0.105	0.139

Figure 5-21 to Figure 5-24 shows the average residual error for each method of fitting for layer thickness of 250 microns. Figure 5-25: Comparison of fitting error using all developed fitting models shows the distribution of normalized fitting error for each method for layer thickness of 125 microns. It can be observed that the for surface angles up to 35 °, third degree polynomial fitting gives the best answer but

for higher surface angle Degree 2 polynomial finds the best fit. Table 5-2 shows the average and standard deviation of fitting errors for each fitting method for layer thickness of 125 microns.

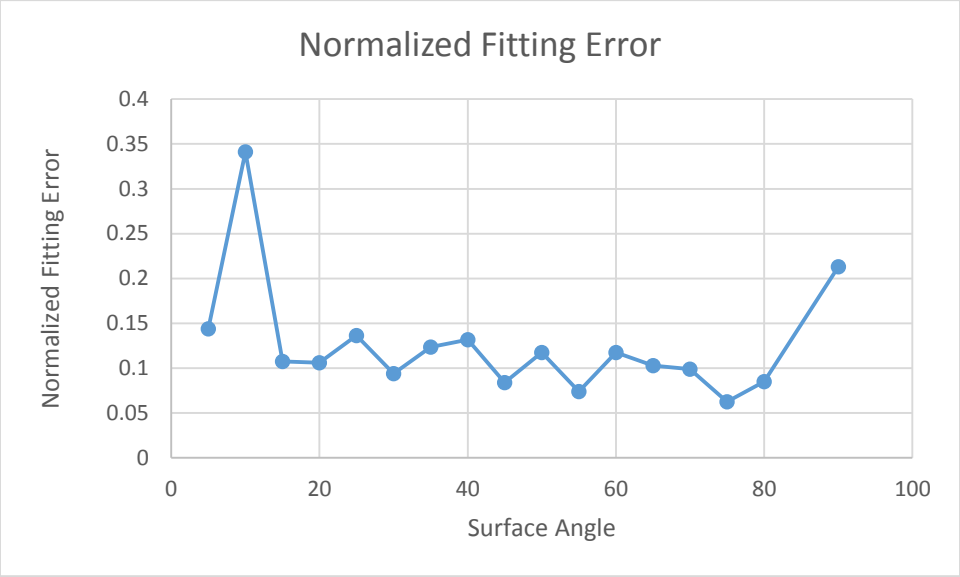

Figure 5-21: Distribution of fitting error using TLS method for layer thickness of 125 microns

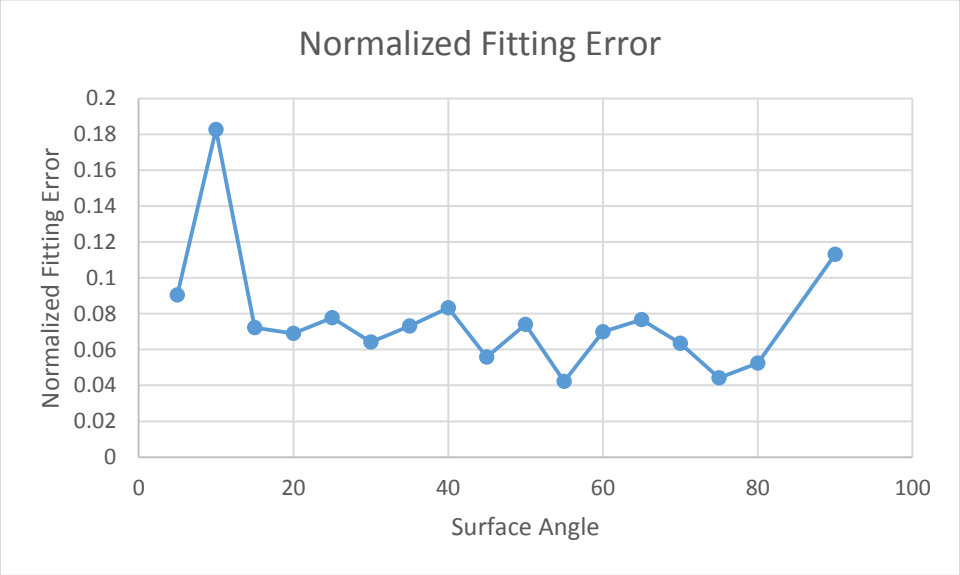

Figure 5-22: Distribution of fitting error using TLS and genetic algorithm method for layer thickness of 125 microns

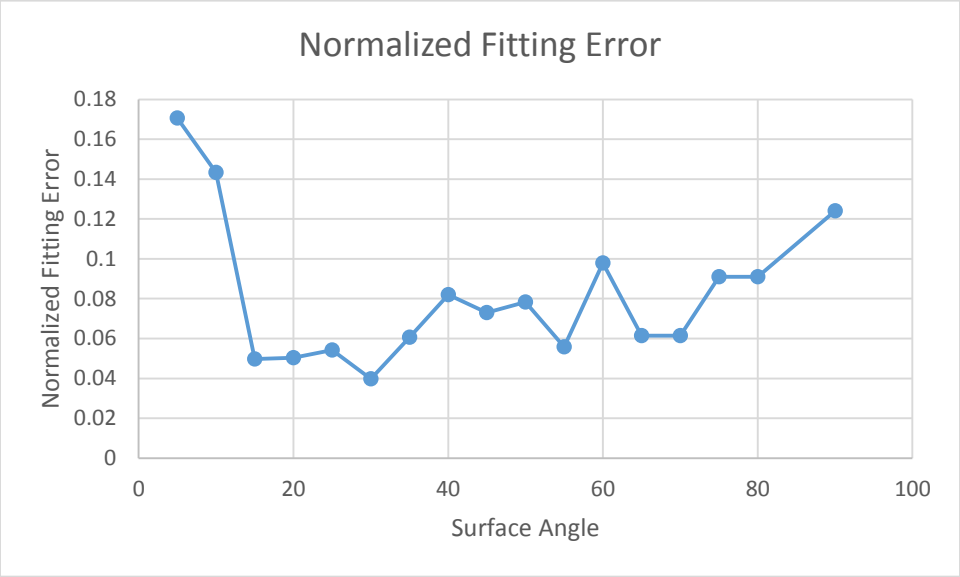

Figure 5-23: Distribution of fitting error using third degree polynomial and genetic algorithm method for layer thickness of 125 microns

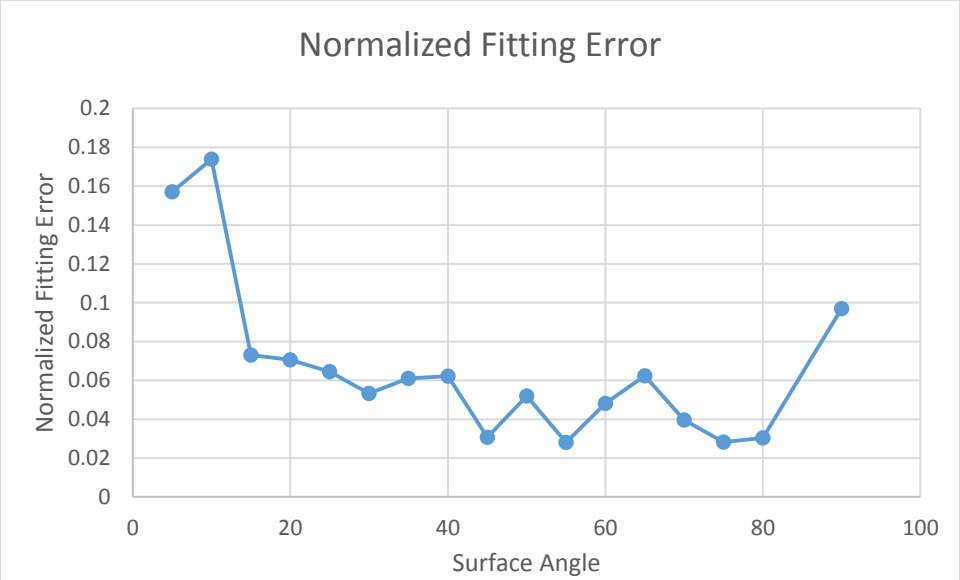

Figure 5-24: Distribution of fitting error using second degree polynomial and genetic algorithm method for layer thickness of 125 microns

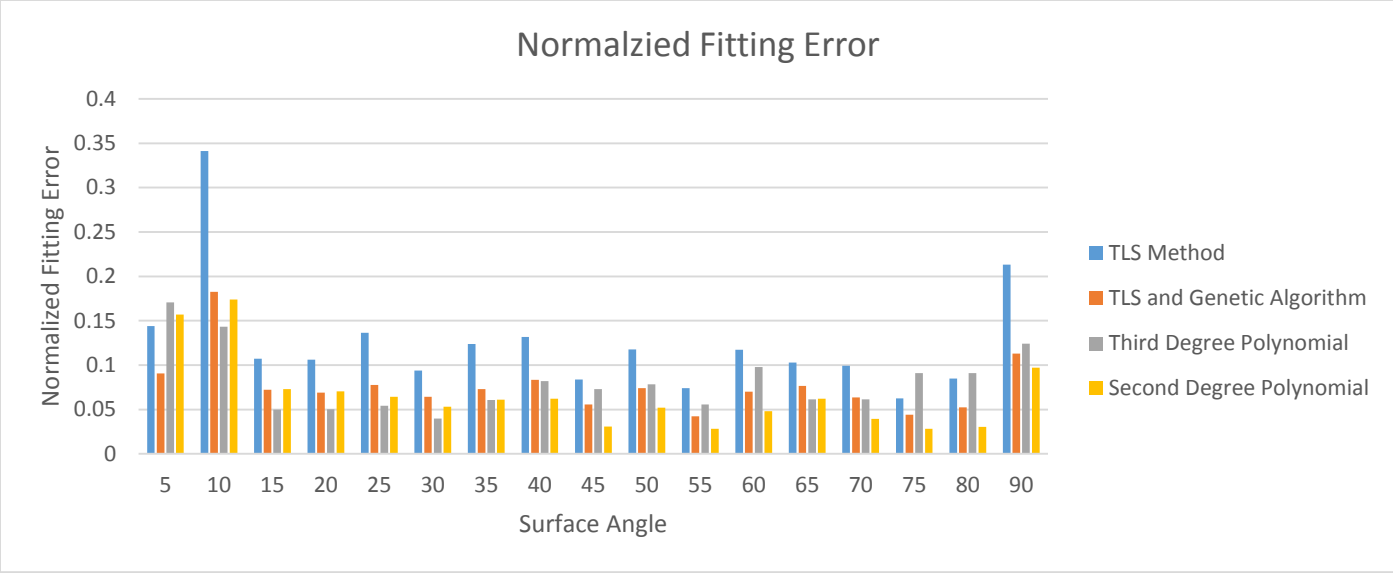

Figure 5-25: Comparison of fitting error using all developed fitting models for layer thickness of 125 microns

Table 5-2: Average Fitting Error and Standard Deviation of Fitting Models for Layer thickness of 125 microns

Method	TLS Method	TLS and GA	Third Degree Polynomial	Second Degree Polynomial
Standard Deviation of Errors	0.065	0.032	0.035	0.041
Average of Fitting Errors	0.125	0.076	0.081	0.066

Figure 5-26:Figure 5-29: show the average residual error for each method of fitting for layer thickness of 500 microns. Figure 5-30 shows the distribution of normalized fitting error for each method for layer thickness of 500 microns. It can be observed that the for surface angles up to 25 °, TLS and genetic algorithm method gives the

best answer but for higher surface angle, second degree and third degree polynomials find the best fit. Table 5-3 shows the average and standard deviation of fitting errors for each fitting method for layer thickness of 500 microns.

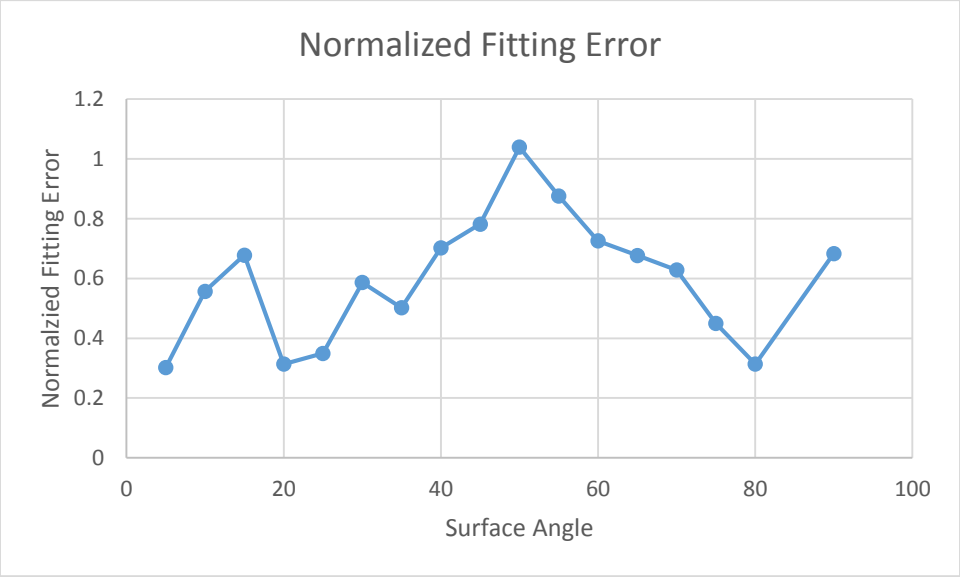

Figure 5-26: Distribution of fitting error using TLS method for layer thickness of 500 microns

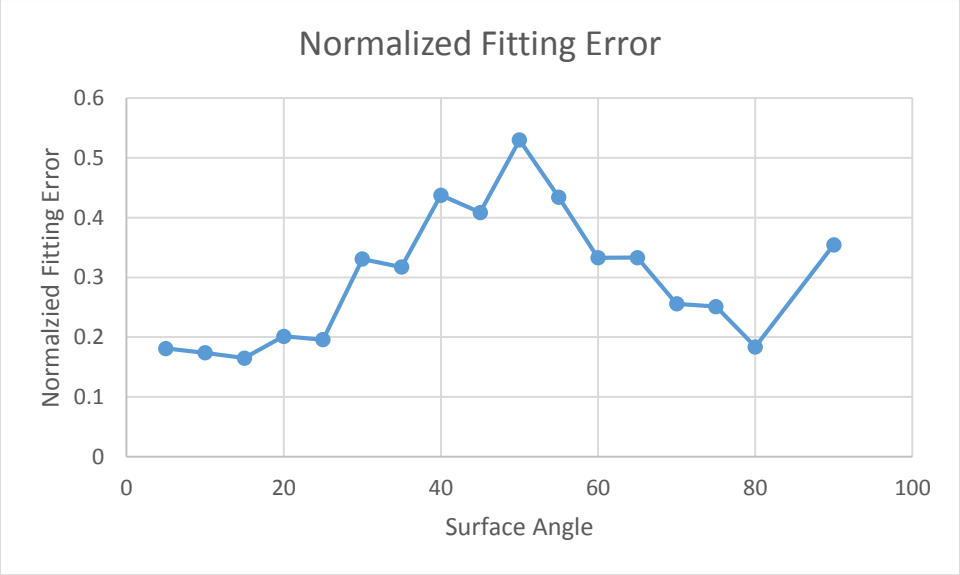

Figure 5-27: Distribution of fitting error using TLS and genetic algorithm method for layer thickness of 500 microns

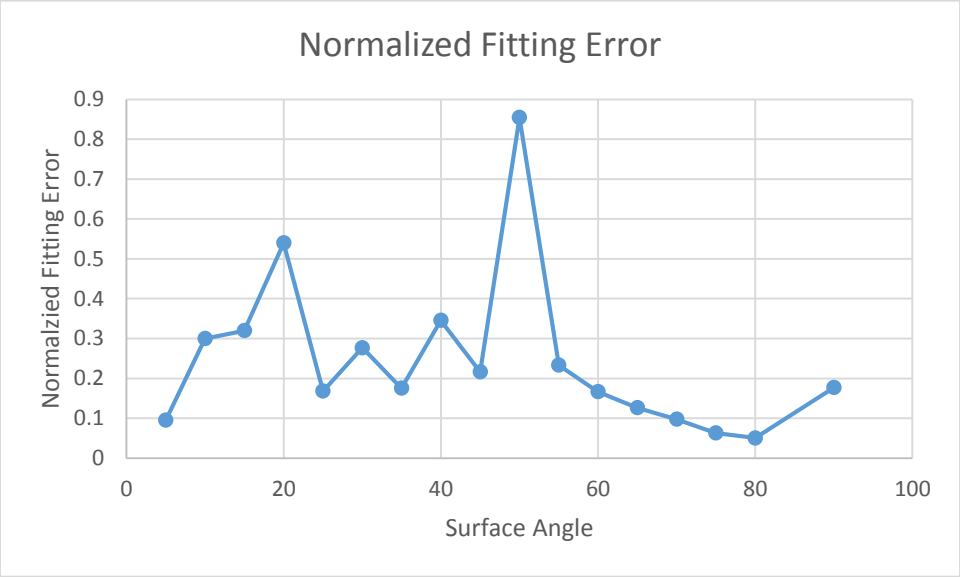

Figure 5-28: Distribution of fitting error using third degree polynomial method for layer thickness of 500 microns

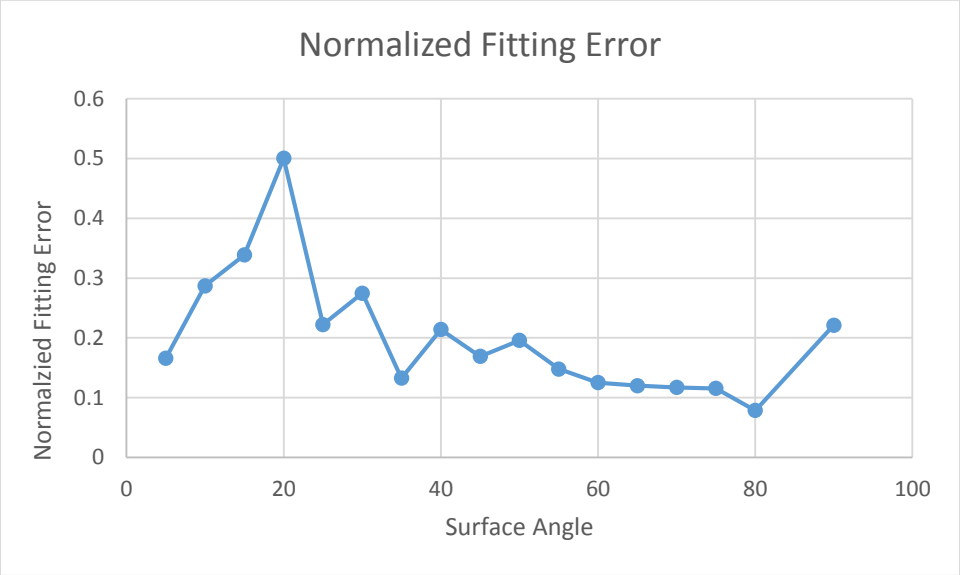

Figure 5-29: Distribution of fitting error using second degree polynomial method for layer thickness of 500 microns

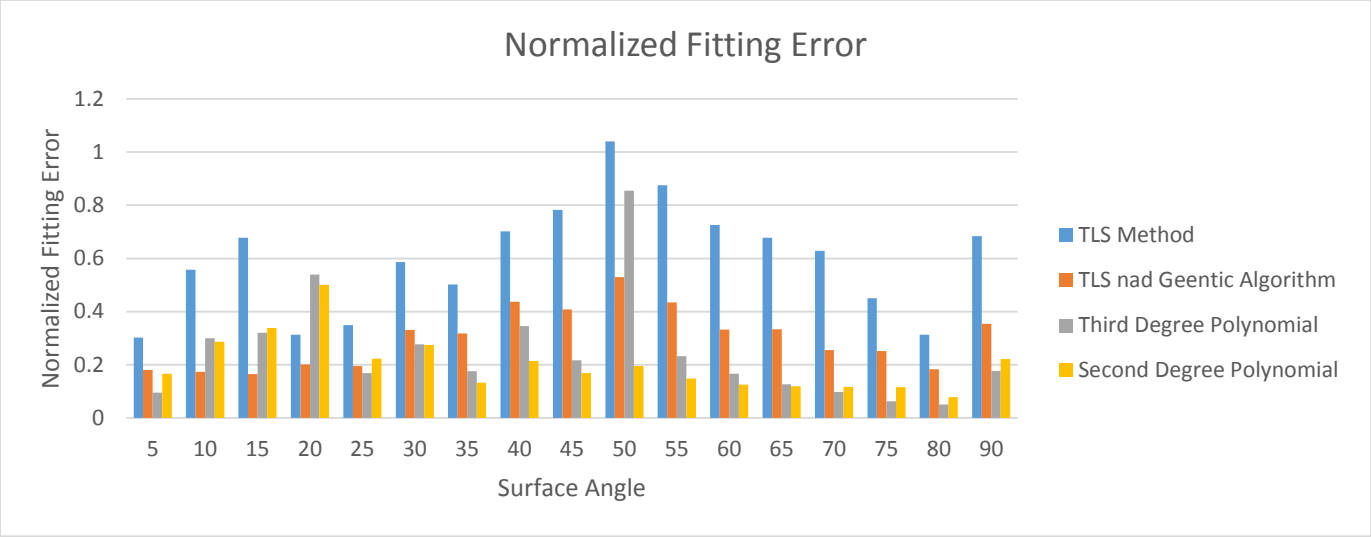

Figure 5-30: Comparison of fitting error using all developed fitting models for layer thickness of 500 microns

Table 5-3: Average Fitting Error and Standard Deviation of Fitting Models for Layer thickness of 500 microns

Method	TLS Method	TLS and GA	Third Degree Polynomial	Second Degree Polynomial
Standard Deviation of Errors	0.208	0.11	0.198	0.104
Average of Fitting Errors	0.598	0.299	0.247	0.201

5.9 Discussion

5.9.1 Effect of Layer Thickness on Surface Roughness

The layer thickness generally has a deep effect on the surface roughness. Figure 5-15 shows the computed roughness value for layer thicknesses of 125 μm, 250 μm and

500 μm. As the layer thickness increases the surface quality becomes poor at a given surface angles. Figure 5-15 also shows that the dependency of surface roughness to the surface angle is higher in the larger layer thicknesses.

5.9.2 Effect of Surface Angle on Surface Roughness

Figure 5-9, Figure 5-11 and Figure 5-13 show that the roughness value is increasing. By increasing the surface angle up to the critical surface angle, and as the surface angle approaches the 90° the surface roughness is decreasing significantly.

5.9.3 Surface Roughness of Surface Angles Less Than Critical Surface Angle

As shown in Figure 5-9, Figure 5-11 and Figure 5-13, the value of surface roughness from 5° up to almost critical surface angle for each layer thickness is increasing and after critical surface angle, it's decreasing and the surface becomes smoother as the surface angle approaches 90°. In layer thickness of 125 microns, the increasing pattern in the smaller surface angles is not observed due to small value of critical angle for this layer thickness, but for layer thickness of 250 and 500 microns, in surface angles close to the critical surface angle, the surface roughness reaches its maximum value in a range of 0° to 90° due to increasing in depth of undetermined region that happens in cusp geometry in the range of critical surface angle.

6 Conclusion and Recommendations

6.1 Conclusion

A methodology is developed to predict the surface roughness of FDM products based on the thickness of the fabricate layer and the desired slope of the surface. The experiments and implementations are conducted for a variety of upward surface angles and also for 3 different layer thicknesses. Considering the comprehensiveness of the experiments, the developed diagrams that relate the layer thickness and surface angle to the surface roughness can be interpolated for other combinations of layer thickness/surface angle. Using the developed results one can predict the roughness values for a given set of surface angle and layer thickness. . As another application, the surface roughness relation with layer thickness and surface angle can be used to estimate the required layer thickness and surface angle to reach the certain surface roughness. The developed models can be used to optimize the amount of time and cost spent on post-processing and surface finishing in industrial applications.

The model is validated using a set of experiments using 3D surface topography microscope and the experimental results are in a very good agreement with the actual surface roughness measured by the microscope. This shows the predicted roughness is an accurate prediction which potentially can be used by the industries and companies to predict the final product's surface roughness.

A major contribution of this research is the developed models for the cusp profile geometries. The cusp profile not only affect the surface roughness but also it defines the dimensional and geometric uncertainties for the final product. Having the geometry of the cusp profiles known creates opportunities to improve the overall accuracy in the product and the process.

Modeling of the cusp profiles is done by the developed inspection procedure which is a combination of the experimental measurements and analytical processes. The approach demonstrates a good compatibility of the experimental data and the conceptual theories.

Although the methodology is implemented for the FDM process in this thesis, but it doesn't harm the generality of the approach and methodology. The methodology and the approach presented in this work, can be used in many other AM processes including SLS and SLA to model the cusp profile and to predict the surface roughness.

6.2 Using B-spline and NURBS to Represent The Cusp Geometry

Using B-spline and NURBS to represent the cusp geometry is a novel approach which was not practiced before. Cusp has a continuous geometry and this continuity can be fully maintained using the NURBS approach developed in this work.

6.3 Recommendation

Future work can be done to model the cusp profile using the presented experimental and theoretical approach for the downward surface angles (Parts with support material). This will help to predict the surface roughness for all the possible surface angles and inside the holes and structures in FDM parts.

It also can be considered to model the cusp profile of the other AM processes using the methodology developed in this research. The developed approach can be used widely for predicating the surface roughness of AM parts.

7 References

[1] K. V. Wong and A. Hernandez, "A review of additive manufacturing," *ISRN Mechanical Engineering*, vol. 2012, 2012.

[2] J.-P. Kruth, M.-C. Leu, and T. Nakagawa, "Progress in additive manufacturing and rapid prototyping," *CIRP Annals-Manufacturing Technology*, vol. 47, pp. 525-540, 1998.

[3] D. Pham and R. Gault, "A comparison of rapid prototyping technologies," *International Journal of Machine Tools and Manufacture*, vol. 38, pp. 1257-1287, 1998.

[4] B. Bidanda, V. Narayanan, and R. Billo, "Reverse engineering and rapid prototyping," *Handbook of Design, Manufacturing and Automation*, pp. 977-990, 2007.

[5] E. Sachs, M. Cima, J. Cornie, D. Brancazio, J. Bredt, A. Curodeau, *et al.*, "Three-dimensional printing: the physics and implications of additive manufacturing," *CIRP Annals-Manufacturing Technology*, vol. 42, pp. 257-260, 1993.

[6] A. Simchi, F. Petzoldt, and H. Pohl, "On the development of direct metal laser sintering for rapid tooling," *Journal of Materials Processing Technology*, vol. 141, pp. 319-328, 2003.

[7] E. C. Santos, M. Shiomi, K. Osakada, and T. Laoui, "Rapid manufacturing of metal components by laser forming," *International Journal of Machine Tools and Manufacture*, vol. 46, pp. 1459-1468, 2006.
[8] G. N. Levy, R. Schindel, and J.-P. Kruth, "Rapid manufacturing and rapid tooling with layer manufacturing (LM) technologies, state of the art and future perspectives," *CIRP Annals-Manufacturing Technology*, vol. 52, pp. 589-609, 2003.
[9] M. McGurk, A. Amis, P. Potamianos, and N. Goodger, "Rapid prototyping techniques for anatomical modelling in medicine," *Annals of the Royal College of Surgeons of England*, vol. 79, p. 169, 1997.
[10] C. Cheah, C. Chua, C. Lee, C. Feng, and K. Totong, "Rapid prototyping and tooling techniques: a review of applications for rapid investment casting," *The International Journal of Advanced Manufacturing Technology*, vol. 25, pp. 308-320, 2005.
[11] D. Klosterman, R. Chartoff, G. Graves, N. Osborne, and B. Priore, "Interfacial characteristics of composites fabricated by laminated object manufacturing," *Composites Part A: Applied Science and Manufacturing*, vol. 29, pp. 1165-1174, 1998.
[12] D. Pham and S. Dimov, "Rapid prototyping processes," in *Rapid Manufacturing*, ed: Springer, 2001, pp. 19-42.
[13] G. Chryssolouris, J. Kechagias, J. Kotselis, D. Mourtzis, and S. Zannis, "Surface Roughness Modeling of the Helisys Laminated Object Manufacturing Process," in *8th European Conference on Rapid Prototyping and Manufacturing*, 1999.
[14] B. Vasudevarao, D. P. Natarajan, M. Henderson, and A. Razdan, "Sensitivity of RP surface finish to process parameter variation," in *Solid Freeform Fabrication Proceedings*, 2000, pp. 251-258.
[15] R. Anitha, S. Arunachalam, and P. Radhakrishnan, "Critical parameters influencing the quality of prototypes in fused deposition modelling," *Journal of Materials Processing Technology*, vol. 118, pp. 385-388, 2001.
[16] P. Bacchewar, S. Singhal, and P. Pandey, "Statistical modelling and optimization of surface roughness in the selective laser sintering process," *Proceedings of the Institution of Mechanical Engineers, Part B: Journal of Engineering Manufacture*, vol. 221, pp. 35-52, 2007.
[17] L. Galantucci, F. Lavecchia, and G. Percoco, "Experimental study aiming to enhance the surface finish of fused deposition modeled parts," *CIRP Annals-Manufacturing Technology*, vol. 58, pp. 189-192, 2009.
[18] S. Sikder, A. Barari, and H. Kishawy, "Effect of Adaptive Slicing on Surface Integrity in Additive Manufacturing," in *ASME 2014 International Design*

Engineering Technical Conferences and Computers and Information in Engineering Conference, 2014, pp. V01AT02A052-V01AT02A052.

[19] S. Jamiolahmadi and A. Barari, "Surface Topography of Additive Manufacturing Parts Using a Finite Difference Approach," *Journal of Manufacturing Science and Engineering*, vol. 136, p. 061009, 2014.

[20] S. Sikder, A. Barari, and H. Kishawy, "Control of Nurbs-Based Surface Error Factor Using a Manufacturing Cost Optimization in Rapid Prototyping Process," in *Manufacturing Modelling, Management, and Control*, 2013, pp. 1560-1565.

[21] P. E. Reeves and R. C. Cobb, "Reducing the surface deviation of stereolithography using in-process techniques," *Rapid Prototyping Journal*, vol. 3, pp. 20-31, 1997.

[22] B. K. Paul and V. Voorakarnam, "Effect of layer thickness and orientation angle on surface roughness in laminated object manufacturing," *Journal of manufacturing processes*, vol. 3, pp. 94-101, 2001.

[23] C. L. Pérez, J. V. Calvet, and M. S. Pérez, "Geometric roughness analysis in solid free-form manufacturing processes," *Journal of Materials Processing Technology*, vol. 119, pp. 52-57, 2001.

[24] P. M. Pandey, N. V. Reddy, and S. G. Dhande, "Improvement of surface finish by staircase machining in fused deposition modeling," *Journal of materials processing technology*, vol. 132, pp. 323-331, 2003.

[25] P. Pandey, N. Reddy, and S. Dhande, "Surface roughness simulation for FDM processed parts," in *Proceedings of 18th International Conference on Computer Aided Production Engineering*, 2003, pp. 413-421.

[26] P. Pandey, N. V. Reddy, and S. Dhande, "Real time adaptive slicing for fused deposition modelling," *International Journal of Machine Tools and Manufacture*, vol. 43, pp. 61-71, 2003.

[27] D. Ahn, H. Kim, and S. Lee, "Surface roughness prediction using measured data and interpolation in layered manufacturing," *Journal of materials processing technology*, vol. 209, pp. 664-671, 2009.

[28] D. Ahn, J.-H. Kweon, S. Kwon, J. Song, and S. Lee, "Representation of surface roughness in fused deposition modeling," *Journal of Materials Processing Technology*, vol. 209, pp. 5593-5600, 2009.

[29] R. I. Campbell, M. Martorelli, and H. S. Lee, "Surface roughness visualisation for rapid prototyping models," *Computer-Aided Design*, vol. 34, pp. 717-725, 2002.

[30] D. Ahn, J.-H. Kweon, J. Choi, and S. Lee, "Quantification of surface roughness of parts processed by laminated object manufacturing," *Journal of Materials Processing Technology*, vol. 212, pp. 339-346, 2012.

[31] J. Kechagias, "An experimental investigation of the surface roughness of parts produced by LOM process," *Rapid Prototyping Journal,* vol. 13, pp. 17-22, 2007.
[32] H.-S. Byun and K. H. Lee*, "Determination of the optimal part orientation in layered manufacturing using a genetic algorithm," *International journal of production research,* vol. 43, pp. 2709-2724, 2005.
[33] A. Boschetto, V. Giordano, and F. Veniali, "Modelling micro geometrical profiles in fused deposition process," *The International Journal of Advanced Manufacturing Technology,* vol. 61, pp. 945-956, 2012.
[34] F. Ali, B. V. Chowder, and J. Maharaja, "Influence of Some Process Parameters on Build Time, Material Consumption, and Surface Roughness of FDM Processed Parts: Inferences Based on the Taguchi Design of Experiments."
[35] A. Boschetto and L. Bottini, "Roughness prediction in coupled operations of Fused Deposition Modeling and Barrel Finishing," *Journal of Materials Processing Technology,* 2015.
[36] Y.-z. Jin, J.-f. Zhang, Y. Wang, and Z.-c. Zhu, "Filament geometrical model and nozzle trajectory analysis in the fused deposition modeling process," *Journal of Zhejiang University SCIENCE A,* vol. 10, pp. 370-376, 2009.
[37] P. Sreedhar, C. MathikumarManikandan, and G. Jothi, "Experimental Investigation of Surface Roughness for Fused Deposition Modeled Part with Different Angular Orientation," *Technology,* vol. 5, pp. 21-28, 2012.
[38] A. Boschetto, V. Giordano, and F. Veniali, "3D roughness profile model in fused deposition modelling," *Rapid Prototyping Journal,* vol. 19, pp. 240-252, 2013.
[39] L. A. Piegl and W. Tiller, "The NURBS book (Monographs in visual communication)," 1996.
[40] G. H. Golub and C. F. Van Loan, *Matrix computations* vol. 3: JHU Press, 2012.
[41] G. H. Golub and C. F. Van Loan, "An analysis of the total least squares problem," *SIAM Journal on Numerical Analysis,* vol. 17, pp. 883-893, 1980.
[42] I. Markovsky and S. Van Huffel, "Overview of total least-squares methods," *Signal processing,* vol. 87, pp. 2283-2302, 2007.
[43] Y. Saad, *Numerical methods for large eigenvalue problems* vol. 158: SIAM, 1992.
[44] C. Ding, D. Zhou, X. He, and H. Zha, "R 1-PCA: rotational invariant L 1-norm principal component analysis for robust subspace factorization," in *Proceedings of the 23rd international conference on Machine learning*, 2006, pp. 281-288.

[45] S. Van Huffel and J. Vandewalle, *The total least squares problem: computational aspects and analysis* vol. 9: Siam, 1991.
[46] I. Standard and B. ISO, "4287/1997," *Geometrical product specifications (GPS)–Surface texture: Profile method–Terms, definitions and surface texture parameters*, 1997.